



OECD Environment Working Papers No. 201

Monitoring exposure  
to climate-related hazards:  
Indicator methodology and  
key results

**Mikaël J.A. Maes,**  
**Abel Gonzales-**  
**Hishinuma,**  
**Ivan Haščič,**  
**Claire Hoffmann,**  
**Alexandre Banquet,**  
**Paolo Veneri,**  
**Alexandre Bizeul,**  
**Arnau Risquez Martin,**  
**Roberta Quadrelli**

<https://dx.doi.org/10.1787/da074cb6-en>

**ENVIRONMENT DIRECTORATE**

**MONITORING EXPOSURE TO CLIMATE-RELATED HAZARDS: INDICATOR  
METHODOLOGY AND KEY RESULTS**

**Environment Working Paper No. 201**

by Mikaël J.A. Maes (1), Abel Gonzales-Hishinuma (1), Ivan Haščič (1), Claire Hoffmann (2), Alexandre Banquet (2), Paolo Veneri (2), Alexandre Bizeul (3), Arnau Risquez Martin (3) and Roberta Quadrelli (3)

- (1) OECD Environment Directorate
- (2) OECD Centre for Entrepreneurship, SMEs, Regions and Cities
- (3) IEA Energy Data Centre

OECD Working Papers should not be reported as representing the official views of the OECD or its member countries. The opinions expressed and arguments employed are those of the authors.

Authorised for publication by Jo Tyndall, Director, Environment Directorate.

Keywords: adaptation, climate change, climate-related hazards, earth observation, exposure, geospatial, natural hazards, resilience

JEL Codes: Q15, Q2, Q54, R11

Contacts:

Mikaël Maes ([Mikael.MAES@oecd.org](mailto:Mikael.MAES@oecd.org))

Ivan Haščič ([Ivan.HASCIC@oecd.org](mailto:Ivan.HASCIC@oecd.org))

**JT03503552**

## OECD ENVIRONMENT WORKING PAPERS

Working Papers should not be reported as representing the official views of the OECD or of its member countries. The opinions expressed and arguments employed are those of the author(s). Working Papers describe preliminary results or research in progress by the author(s) and are published to stimulate discussion on a broad range of issues on which the OECD works.

This series is designed to make available to a wider readership selected studies on environmental issues prepared for use within the OECD. Authorship is usually collective, but principal author(s) are named. The papers are generally available only in their original language – English or French – with a summary in the other language. Comments on Working Papers are welcomed, and may be sent to:

OECD Environment Directorate

2 rue André-Pascal, 75775 Paris Cedex 16, France

or by email: [env.contact@oecd.org](mailto:env.contact@oecd.org)

-----  
OECD Environment Working Papers are published on [www.oecd.org/environment/workingpapers.htm](http://www.oecd.org/environment/workingpapers.htm) as well as on the OECD iLibrary ([www.oecdilibrary.org](http://www.oecdilibrary.org))

-----  
The statistical data for Israel are supplied by and under the responsibility of the relevant Israeli authorities. The use of such data by the OECD is without prejudice to the status of the Golan Heights, East Jerusalem and Israeli settlements in the West Bank under the terms of international law.

Note by Republic of Türkiye: The information in this document with reference to “Cyprus” relates to the southern part of the Island. There is no single authority representing both Turkish and Greek Cypriot people on the Island. Türkiye recognises the Turkish Republic of Northern Cyprus (TRNC). Until a lasting and equitable solution is found within the context of the United Nations, Türkiye shall preserve its position concerning the “Cyprus issue”.

Note by all the European Union Member States of the OECD and the European Union: The Republic of Cyprus is recognised by all members of the United Nations with the exception of Türkiye. The information in this document relates to the area under the effective control of the Government of the Republic of Cyprus.

### © OECD (2022)

You can copy, download or print OECD content for your own use, and you can include excerpts from OECD publications, databases and multimedia products in your own documents, presentations, blogs, websites and teaching materials, provided that suitable acknowledgment of OECD as source and copyright owner is given. All requests for commercial use and translation rights should be submitted to [rights@oecd.org](mailto:rights@oecd.org).

# Abstract

This paper supports countries in understanding the potential impact of climate-related natural hazards by assessing the exposure of people and assets to these hazards. It develops indicators of climate-related hazards and exposures for seven hazard types (extreme temperature, extreme precipitation, drought, wildfire, wind threats, river flooding and coastal flooding) and four exposure variables (cropland, forests, urban areas and population density). The paper presents the associated methodologies and discusses the global geospatial datasets used to construct the indicators. It shows that it is possible to develop exposure indicators for climate-related hazards with a global geographic coverage at the national and subnational levels. The results, presented for 52 IPAC countries, suggest that all countries are exposed to one or more climate-related natural hazards, but with significant differences in the occurrence and intensity of such hazards. The empirical evidence presented here points to the urgency to take strong climate change mitigation measures. It also highlights the need to accelerate efforts towards the global goal on adaptation to strengthen resilience and reduce vulnerability to climate change in the context of the Paris Agreement.

**Keywords:** adaptation, climate change, climate-related hazards, earth observation, exposure, geospatial, natural hazards, resilience

**JEL Classification:** Q15, Q2, Q54, R11

# Résumé

Le présent document vise à aider les pays à mesurer les effets potentiels des aléas climatiques naturels en évaluant l'exposition des personnes et des ressources à ces aléas. Sept types d'aléa climatique naturel (températures extrêmes, précipitations extrêmes, sécheresses, incendies incontrôlés, vents violents, inondations fluviales et submersions marines) et quatre variables d'exposition (terres labourables, forêts, zones bâties et densité de population) permettent de développer les indicateurs idoines. Les principes méthodologiques et les ensembles de données géo-spatiales mondiales qui ont servi à leur élaboration sont également exposés. Il est donc possible de mettre au point des indicateurs d'exposition aux aléas climatiques couvrant une échelle mondiale au niveau national et infranational. Les résultats ainsi obtenus pour 52 pays participants au Programme international pour l'action sur le climat (IPAC) montrent que tous les pays sont exposés à un ou plusieurs aléas naturels climatiques, mais l'intensité et la fréquence sont très variables. Les données empiriques présentées ici soulignent l'urgence de prendre des mesures drastiques pour atténuer les effets du dérèglement climatique, de même que la nécessité d'accélérer le pas vers l'objectif mondial en matière d'adaptation, de façon à renforcer la résilience et à réduire la vulnérabilité au changement climatique dans le contexte de l'Accord de Paris.

**Mots-clés :** adaptation, changement climatique, aléas climatiques, observation de la Terre, exposition, géo-spatial, aléas naturels, risques naturels, résilience

**Classification JEL :** Q15, Q2, Q54, R11

# Acknowledgements

This paper is part of the OECD Horizontal Project on “Building Climate and Economic Resilience in the Transition to a Low-Carbon Economy” and its International Programme for Action on Climate (IPAC). This work contributes to the development of the IPAC Climate Action Dashboard (indicator on exposure of people and assets to climate-related hazards), and the broader set of IPAC indicators (the OECD set of indicators to monitor progress towards climate objectives). It further contributes to the OECD work programme on environmental information and indicators.

This paper has been reviewed by the OECD Environmental Policy Committee (EPOC). It benefitted from helpful comments by members of the IPAC Technical Expert Group (TEG) and the Task Force on Climate Change Adaptation (TFCCA) as well as by Delegates to the Working Party on Environmental Information (WPEI), the Working Party on Climate, Investment and Development (WPCID) and the Working Party on Territorial Indicators (WPTI). Written comments by experts from Australia, Chile, the European Environment Agency, France, Germany, Greece, Ireland, Latvia, the Netherlands, New Zealand, Norway, Sweden, Switzerland, the United Nations Statistics Division and the United States of America have been considered in this version. Through the TFCCA, expert advice was received from wildfire experts, including Emilio Chuvieco from Alcalá University, Cristina Santin Nuno and Stefan Doerr from Swansea University and Jesus San-Miguel from the Joint Research Centre of the European Commission.

The paper has been authored by Mikaël J.A. Maes, Abel Gonzales-Hishinuma, Ivan Haščič (OECD-ENV), Claire Hoffmann, Alexandre Banquet, Paolo Veneri (OECD-CFE), Alexandre Bizeul, Arnau Risquez Martin and Roberta Quadrelli (IEA-EDC). The work was carried out under the supervision of Nathalie Girouard, Head of the Environmental Performance and Information Division at the OECD Environment Directorate, Rüdiger Ahrend, Head of the Economic Analysis, Data and Statistics Division at the OECD Centre for Entrepreneurship, SMEs, Regions and Cities, and Nick Johnstone, Chief Statistician and Head of the IEA Energy Data Centre.

The authors would like to thank OECD Secretariat colleagues for their helpful comments on a previous version of this paper, including Marta Arbinolo, Amy Cano Prentice, Daniel Clarke, Catherine Gamper, Guillaume Gruère, Maïke Kirsch, Myriam Linster, Roger Martini, Mauro Migotto, Jerome Mounsey, Daniel Nachtigall, Rodrigo Pizarro, Mikaela Rambali, Nathan Rueche, Simon Touboul and Hugo Valin.

The authors also gratefully acknowledge financial support for this paper and other IPAC outputs from Australia, Belgium, Bulgaria, Colombia, Estonia, Finland, France, Ireland, Italy, Japan, Korea, Latvia, Lithuania, Luxembourg, Malta, the Netherlands, New Zealand, Spain, Türkiye, Romania, the Russian Federation, the United Kingdom and the United States of America.

# Executive summary

This paper develops indicators that support countries in understanding the impact of climate-related hazards by assessing the exposure of people and assets to these hazards. It focuses on seven hazard types: (1) extreme temperature, (2) extreme precipitation, (3) drought, (4) wildfire, (5) wind threats, (6) river flooding and (7) coastal flooding. These are key natural hazards, influenced by climate change, with important impacts on people and assets. They are chosen for their relevance after an extensive qualitative review of available data sources. Four exposure variables are selected, including (1) built-up areas, (2) croplands, (3) forests and (4) population density, to assess the impact of each climate-related hazard on one or more of these variables. Indicators are calculated for all countries with time series from 1979 to 2021 depending on data availability (Table 1). For ease of presentation, empirical results in this paper are restricted to the 52 countries covered by the International Programme for Action on Climate (IPAC). The full dataset including all countries in the world will be available on [OECD.Stat](#) for public access. A selection of indicators will be visualised on the [IPAC Climate Action Dashboard](#) and the [IEA Weather for Energy Tracker](#).








The contributions of this paper are twofold. First, despite a growing availability of data from earth observation on climate-related hazards there is a dearth of readily available indicators at the national and subnational levels. This paper responds to demands for internationally comparable indicators suitable for analyses with a global geographic coverage, over long time periods, and with timely updates. Second, the underlying geospatial datasets are often complex, requiring specific expertise for meaningful analysis, and involve large volumes of data that require long processing times. This paper facilitates the use of such data by summarising the underlying information into indicators accessible to non-expert audiences and suitable to support policy analyses and government decision making.

The 2020 technical report developed by the European Environment Agency on compiling climate-related hazard indices was used as a starting point. Based on this, and other key resources, such as the 2020 technical report from the United Nations Office for Disaster Risk Reduction on hazard definition and classification, it examines in detail data sources to construct national and subnational exposure indicators for climate-related natural hazards, each with a risk-specific methodology. The methodologies are informed by standards from the World Meteorological Organization, the US National Oceanic and Atmospheric Administration, latest research and standards developed by well-recognised organisations, and builds on international frameworks for assessing climate-related hazards. This paper ensures, to the extent possible, coherence with national and international data sources and guidelines for assessing climate-related hazards.

The paper shows that it is possible to develop national and subnational hazard and exposure indicators for common climate-related hazards. It provides evidence that across countries there is considerable exposure of built-up areas, croplands, forests and the population to climate-related hazards. For example, a high proportion of the population in most IPAC countries is exposed to serious extreme heat conditions, which is of major concern because climate change is likely to further increase unusually warm temperatures. Meanwhile, the majority of burned land area globally occurs in a subset of IPAC countries over the past five years, exposing forests and the population to wildfires. These results suggest that considerable differences exist across, and within, countries in terms of the type of climate-related hazards and of their intensities. In fact, all countries experience one or more of these hazards and the exposure varies depending on where people and assets are located. It further highlights the interconnectedness of climate-related hazards, which may reinforce or undermine one another, and may lead to over- or under-estimations of the exposure of people and assets to climate-related hazards.

This remains a work in progress. For example, data sources for river and coastal flooding are based on predicted (ex-ante) hazard maps that are not updated annually. New data sources or other techniques for analysing river or coastal flooding may allow for improvements to these indicators in the future.

**Table 1. Overview exposure indicators developed in this paper**

 <b>Extreme temperature</b>	
Why?	Temperature extremes at both ends of the spectrum can impact human health and economic activities, while they are worsening due to climate change.
Indicators	<ol style="list-style-type: none"> <li>1. Percentage of population exposed to <math>n</math> number of hot days</li> <li>2. Percentage of population exposed to <math>n</math> number of tropical nights</li> <li>3. Percentage of population exposed to <math>n</math> number of days identified as a hot day and tropical night</li> <li>4. Population-weighted average of the number of days with heat stress</li> <li>5. Percentage of population exposed to <math>n</math> number of icing days</li> </ol>
 <b>Extreme precipitation</b>	
Why?	Precipitation extremes can cause sudden flooding, impacting agriculture and leading to a loss of agricultural yield, and is expected to worsen due to climate change.
Indicators	<ol style="list-style-type: none"> <li>6. Percentage of cropland exposed to <math>n</math> number of days with above-average precipitation amounts</li> </ol>
 <b>Drought</b>	
Why?	Drought has far-reaching socio-economic impacts, particularly on agriculture, resulting in a loss of agricultural yield, and is influenced by climate change.
Indicators	<ol style="list-style-type: none"> <li>7. Average cropland soil moisture anomaly</li> </ol>
 <b>Wildfire</b>	
Why?	Wildfire threatens people's lives and wellbeing both directly and indirectly, and can also occur more frequently and intensively because of climate change.
Indicators	<ol style="list-style-type: none"> <li>8. Percentage of population located in areas at risk of burning</li> <li>9. Percentage of forested areas at risk of burning</li> </ol>
 <b>Wind threats</b>	
Why?	Wind threats are common hazards to humans directly through flying debris and falling trees or damage to built-up areas, and are expected to worsen due to climate change.
Indicators	<ol style="list-style-type: none"> <li>10. Percentage of population exposed to violent wind gusts</li> <li>11. Percentage of built-up area exposed to violent wind gusts</li> <li>12. Percentage of population exposed to cyclone wind threats with different return periods</li> <li>13. Percentage of built-up area exposed to cyclone wind threats with different return periods</li> </ol>
 <b>River flooding</b>	
Why?	River flooding can cause significant economic losses, impacting the population, built-up areas or infrastructure, and is expected to worsen due to climate change.
Indicators	<ol style="list-style-type: none"> <li>14. Percentage of population exposed to river flooding with different return periods</li> <li>15. Percentage of built-up area exposed to river flooding with different return periods</li> <li>16. Percentage of cropland exposed to river flooding with different return periods</li> </ol>
 <b>Coastal flooding</b>	
Why?	Coastal flooding threatens coastal regions and communities and is expected to worsen due to climate change.
Indicators	<ol style="list-style-type: none"> <li>17. Percentage of population exposed to coastal flooding with different return periods</li> <li>18. Percentage of built-up area exposed to coastal flooding with different return periods</li> <li>19. Percentage of cropland exposed to coastal flooding with different return periods</li> </ol>

Note: A return period is the average or estimated time that a specific climate-related hazard is likely to recur.

# Table of contents

Abstract	3
Résumé	3
Acknowledgements	4
Executive summary	5
1 Introduction	10
2 Conceptual framework for measuring climate-related risks	11
2.1. Climate-related hazards	11
2.2. Defining a hazard's risk	11
3 Data and methods	14
3.1. Identification of robust data sources	14
3.2. Impacts and measurement of climate-related hazards	17
Heat and cold	17
Wet and dry	18
Wind	20
River flooding	20
Coastal flooding	21
3.3. Selected exposure indicators for climate-related hazards	21
4 Results	24
4.1. Extreme temperature	24
Hot days and tropical nights	24
The Universal Thermal Climate Index	25
Changing extreme temperatures	30
4.2. Extreme precipitation	32
4.3. Drought	35
Soil moisture anomaly	35
4.4. Wildfire	39
Burned area extent	39
Forest exposure to wildfire danger	41
Population exposure to wildfire danger	42
4.5. Wind threats	43
Storms	43
Cyclones	44
4.6. River flooding	46
4.7. Coastal flooding	51



5 Discussion	54
6 Strengths and limitations	57
7 Conclusions and next steps	58
References	59
<b>Annex A. Methods for each exposure indicator</b>	<b>66</b>
B.1. Interpolation of population grids	66
B.2. Percentage of population exposed to extreme temperatures	66
B.3. Percentage of cropland exposed to extreme precipitation	68
B.4. Cropland soil moisture anomaly	69
B.5. Wildfires and exposure to areas at very high risk of burning	70
B.6. Percentage of population and buildings exposed to wind threats	72
B.7. River flooding	73
B.8. Coastal flooding	73
<b>Annex B. Key databases</b>	<b>75</b>
<b>Annex C. Excluded domains or subdomains</b>	<b>76</b>
C.1. Wet and dry	76
Lightning	76
Landslides	76
C.2. Snow and ice	77
Snowfall	77
Hail storm	77
C.3. Oceanic	77
<b>Annex D. Additional figures</b>	<b>78</b>
<b>Tables</b>	
Table 1. Overview exposure indicators developed in this paper	6
Table 2. Criteria to evaluate the suitability of underlying datasets	14
Table 3. Review of relevant data sources on climate-related hazards	15
Table 4. Selected indicators for climate-related hazards	22
Table A.1. Wind scales	72
Table A.2. Saffir-Simpson hurricane wind scale	73
Table B.1. Key databases for global environmental data sources on climate-related natural hazards	75
<b>Figures</b>	
Figure 1. A majority of countries have population exposed to hot summer days	24
Figure 2. A large share of population is exposed to many tropical nights	25
Figure 3. A large share of population is exposed to heat stress	26
Figure 4. Days with strong heat stress exposure are increasing across countries	27
Figure 5. Considerable subnational variation of population exposure to heat stress	28
Figure 6. Countries experience more above-average and less below-average temperature days, a clear display of a changing climate	30
Figure 7. Some countries have cropland exposed to more than one week of extreme precipitation	32
Figure 8. Some countries' GDP is more exposed to extreme precipitation than other countries	33
Figure 9. Large subnational variability in land exposure to extreme precipitation	34

Figure 10. A majority of IPAC countries experience worsening droughts on croplands	35
Figure 11. Changes in soil moisture differ widely across regions	36
Figure 12. Most countries show localised changes in soil moisture	37
Figure 13. A small subset of IPAC countries represent the majority of burned area	39
Figure 14. Substantial variation in burned area extent between countries	40
Figure 15. In a third of IPAC countries over 20% of forests are exposed to very high or extreme fire danger	41
Figure 16. In eleven IPAC countries over 10% of population lives in areas exposed to very high or extreme wildfire danger	42
Figure 17. Populations in northwestern Europe and eastern Asia are exposed to violent wind storms	43
Figure 18. Built-up areas in northwestern Europe and eastern Asia are exposed to violent wind storms	44
Figure 19. A small subset of IPAC countries is exposed to tropical cyclones	45
Figure 20. IPAC countries are exposed to river flooding to varying degrees	46
Figure 21. River flooding exposes many populations in most IPAC countries	47
Figure 22. Considerable subnational variation in population exposure to river flooding	48
Figure 23. Considerable city-level variation in population exposure to river flooding	49
Figure 24. A subset of countries has a sizeable part of built-up area potentially exposed to coastal flooding	51
Figure 25. In the absence of coastal protections, large areas of built-up area would be at risk of coastal flooding in Belgium and the Netherlands	52
Figure 26. A subset of countries has a sizeable part of the population potentially exposed to coastal flooding	53
Figure 27. Most countries experience at least one climate-related natural hazard	54
Figure A.1. Changing temperature extremes across the world	68
Figure A.2. Changing precipitation extremes across the world	69
Figure D.1. A majority of countries experience some exposure to hot days and tropical nights	78

## Boxes

Box 1. Conceptual illustration and definitions of key risk dimensions linked to climate-related impacts	12
---	----

# 1 Introduction

Climate-related natural hazards impact societies around the world and climate change poses a growing threat by influencing the intensity and, in some cases, the frequency of occurrence of such hazards (IPCC, 2021<sup>[1]</sup>). Worldwide, approximately 3.3 to 3.6 billion people live in contexts that are highly vulnerable to climate change (IPCC, 2022<sup>[2]</sup>). For example, 1.7 million deaths worldwide were linked to extreme heat and cold in 2019 alone and 356,000 of these deaths were related to heat stress (Burkart et al., 2021<sup>[3]</sup>). Meanwhile, natural disasters caused an estimated USD 280 billion of global losses in 2021, representing approximately 0.29% of global Gross Domestic Product (GDP) (Munich RE, 2022<sup>[4]</sup>). Considering the severe socio-economic losses on people's livelihoods, better understanding which countries, regions and communities are more, or less, affected by past climate-related natural hazards is important.

This paper proposes 19 national and subnational exposure indicators<sup>1</sup> for observed climate-related hazards before and after the event occurred (i.e. ex-ante and ex-post) based on a review of available and relevant data sources (Table 1). The indicators cover sudden onset climate-related hazards that are relevant around the world (e.g. extreme temperature or precipitation) and additional indicators for slow onset climate-related hazards (e.g. changes in mean temperature) when suitable global datasets could be identified. The presentation of the results covers 52 countries, corresponding to the current geographic coverage of the International Programme for Action on Climate (IPAC)<sup>2</sup> and has the following objectives:

- to provide an overview of past trends and the current situation of key representative climate-related hazards with high spatio-temporal coverage across IPAC countries;
- to support IPAC countries with the development and application of national and subnational indicators for climate-related hazards with adaptation relevance;
- to inform OECD measurement efforts and policy analyses and make information on climate-related hazards more accessible to non-specialists.

Results show that a high proportion of the population in most IPAC countries is exposed to serious extreme heat and cold conditions, and that climate change is likely to increase above-average temperatures, worsening extreme heat conditions in the future. Furthermore, only a small subset of IPAC countries is contributing to the majority of burning areas over the past five years. For example, 15% of fire events globally occurred in four IPAC countries alone, i.e. Argentina, Australia, Brazil and India. This paper confirms that it is possible to develop exposure indicators for climate-related hazards at the national and subnational levels using global data sources with high spatio-temporal resolution. This paper shows that all countries experience one or more climate-related hazards and that significant differences exist among countries in exposure to different climate-related natural hazards with varying degrees of intensities.

---

<sup>1</sup> National and subnational indicators are presented by (i) *country*, i.e. the FAO Global Administrative Unit Layer (GAUL) (2015) level 0 political boundary data source is used, and (ii) *large region*, i.e. territorial level 2 or TL2 based on the OECD territorial classification or, when unavailable, a corresponding level using FAO GAUL.

<sup>2</sup> The 52 countries include [38 OECD member countries](#), the European Union (EU27), Malta, 6 OECD accession candidates (Argentina, Brazil, Bulgaria, Croatia, Peru, Romania), 5 key partners (Brazil, People's Republic of China (hereafter 'China'), India, Indonesia, South Africa) and other G20 countries (Russian Federation, Saudi Arabia).

# 2 Conceptual framework for measuring climate-related risks

## 2.1. Climate-related hazards

Anthropogenic climate change modifies weather and climate extremes (IPCC, 2021<sup>[1]</sup>) (Spinoni, Naumann and Vogt, 2017<sup>[5]</sup>), causing an increase in property damage and loss of human life, and impacting biodiversity and ecosystems more broadly around the world (CRED, 2019<sup>[6]</sup>). Countries are faced with a growing challenge to manage the risks from climate change and increased hazard occurrence, highlighting the need to use coherent terminology across domains (OECD, 2020<sup>[7]</sup>).

Based on the definition of 'hazard' adopted by the United Nations General Assembly, this paper defines climate-related hazards as

*“a potentially damaging climate-related physical event, phenomenon, or human activity that may cause the loss of life or injury, property damage, social and economic disruption or environmental degradation” (UNDRR, 2020<sup>[8]</sup>).*

Climate-related hazards can include both sudden onset hazards (i.e. event-driven hazards such as heatwaves or cyclones) and slow onset hazards (i.e. long-term changes in the mean and variability of climate patterns such as mean precipitation or temperature). Understanding climate-related hazards can inform and support countries' efforts to mitigate and adapt to climate change. Developing a representative set of such climate-related hazard indicators is a key component to achieve this.

The Intergovernmental Panel on Climate Change (IPCC) Sixth Assessment Report (AR6) general framework on climate-related hazard indices introduces the concept of 28 Climatic Impact Drivers (CID) grouped into six categories: (i) Heat and cold, (ii) Wet and dry, (iii) Wind, (iv) Snow and ice, (v) Coastal and (vi) Oceanic (IPCC, 2021<sup>[1]</sup>). Similarly, the European Topic Centre on Climate Change Impacts, Vulnerability and Adaptation (ETC/CCA) includes the development of a compact set of 32 climate-related hazard indices for Europe, which includes the same six main categories as the overarching structure for classifying climate-related hazard indices (ETC-CCA, 2020<sup>[9]</sup>).

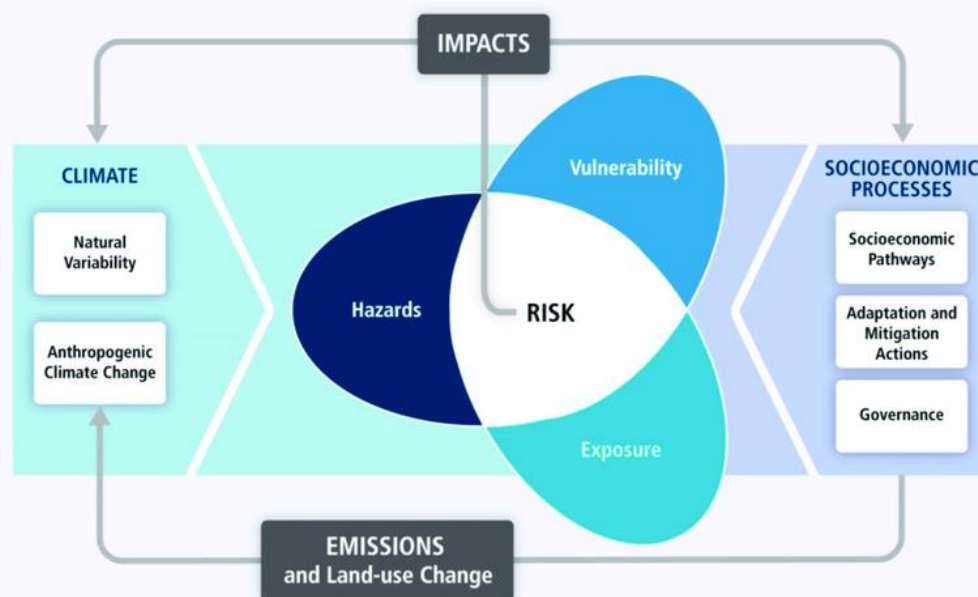
This paper develops a set of climate-related hazard indicators, drawing on relevant literature and related international work. It prioritises the development of exposure indicators in a subset of four key categories: (i) heat and cold, (ii) wet and dry, (iii) wind and (iv) coastal.

## 2.2. Defining a hazard's risk

Natural climate variability and anthropogenic climate change increase risks attributed to climate-related hazards, influencing the frequency, intensity, extent and duration of extreme weather and climate events (IPCC, 2022<sup>[2]</sup>). Different conceptual models for defining risk have been reviewed. The IPCC considers the climate-related hazard, exposure and vulnerability as the key dimensions of disaster risk (see Box 1) (IPCC, 2022<sup>[2]</sup>), while the Index for Risk Management (INFORM) model from the European Commission expands on this with a fourth dimension on coping capacity (Marin-Ferrer, Vernaccini and Poljansek, 2017<sup>[10]</sup>). The

coping capacity is defined as the ability of exposed individuals, systems or institutions to adjust or cope with potential impacts from climate change (Marin-Ferrer, Vernaccini and Poljansek, 2017<sup>[10]</sup>). For example, specific policies can result in a potential positive or negative outcome to climate-related hazards independent from a population's vulnerability to these hazards (Simpson et al., 2021<sup>[11]</sup>). Similarly to the INFORM model, the Sendai Framework for Disaster Risk Reduction considers that disaster risk management should include all dimensions of vulnerability, capacity, exposure and hazard (UNDRR, 2015<sup>[12]</sup>).

### Box 1. Conceptual illustration and definitions of key risk dimensions linked to climate-related impacts



Source: (IPCC, 2014<sup>[13]</sup>). A more elaborate version of this figure is available in AR6 Working Group II (IPCC, 2022<sup>[2]</sup>).

**Hazard:** the potential occurrence of a natural or human-induced physical event or trend or physical impact that may cause loss of life, injury, or other health impacts, as well as damage and loss to property, infrastructure, livelihoods, service provision, ecosystems, and environmental resources.

**Exposure:** the presence of people or assets in areas prone to climate-related hazards (e.g. population density, valuable ecosystems).

**Vulnerability:** the conditions determined by physical, social, economic and environmental factors or processes, which increase the susceptibility of a community to the impact of climate-related hazards (e.g. an individual's or household's socio-economic status, particular vulnerable groups in society) (ISDR, 2005<sup>[14]</sup>).

All of these conceptual models imply integrating the physical and socio-economic drivers that influence the risk from climate-related hazards. Making meaningful predictions of the risks associated with climate-related hazards requires accounting for as many, if not all, key dimensions possible depending on data availability (see Box 1). However, the hazard and exposure dimensions are often treated differently from the vulnerability dimension. While components within the hazard and exposure dimensions are considered hazard-dependent factors, the vulnerability dimension is considered hazard-independent (Marin-Ferrer, Vernaccini and Poljansek, 2017<sup>[10]</sup>).

This paper focuses on hazard-dependent factors (i.e. the hazard and exposure) to develop national and subnational exposure indicators for climate-related hazards. Measuring all dimensions that encompass risk is difficult because of data limitations, particularly on a global scale. For example, there are no commonly used data sources for assessing vulnerability globally. The Notre Dame-Global Adaptation Index (ND-GAIN) shows a country's current vulnerability to climate disruptions (Chen et al., 2015<sup>[15]</sup>). However, the ND-GAIN has no subnational spatial resolution, making it difficult to use in combination with data sources with high spatio-temporal resolution. Similarly, the Global Human Settlement Layer (GHSL) population grids, developed by the European Commission Joint Research Centre, provide population counts with a 250 m spatial resolution. However, the GHSL population grids do not have demographic data to identify, for example, vulnerable groups such as elderly. Due to the lack of global data sources to assess vulnerability with a high spatio-temporal resolution, this paper focuses on identifying the hazard and exposure dimension.

# 3 Data and methods

## 3.1. Identification of robust data sources

This paper identifies data sources for developing national and subnational hazard and exposure indicators for climate-related hazards by searching variables, indices, indicators and larger databases from a variety of organisations such as the Copernicus Climate Data Store (CDS), the National Aeronautics and Space Administration (NASA) and the Japan Aerospace Exploration Agency (JAXA), among others. Annex B provides a description of the main data sources reviewed.

A quality review was conducted to prioritise the most suitable data sources, based on a set of criteria, including assessing the geographic and temporal resolution of a data source, its feasibility for computational analysis and its relevance for the purpose of this work (Table 2).

**Table 2. Criteria to evaluate the suitability of underlying datasets**

Criterion	High	Medium	Low
<b>Computational efficiency</b>	No computation needed	Automated computations needed	Heavy computations needed
<b>Computational feasibility</b>	Essential climate variable requiring simple calculations	Multiple input variables required	Many input variables required or heavy statistical computing
<b>Geographic coverage</b>	Complete global data coverage	Data available for most countries	Data available only for certain countries
<b>Geographic resolution</b>	Gridded data	Station data or country-level data	Point data
<b>Temporal coverage</b>	Complete data coverage for the period 2018-2020, incl. historical data where relevant	Data coverage for all countries but missing most recent year	Data coverage missing for multiple years
<b>Temporal resolution</b>	Daily data	Monthly data	No daily or monthly data

The paper identifies good quality data sources and classifies these within four broad categories: (i) heat and cold, (ii) wet and dry, (iii) wind and (iv) coastal, based on the suitability of data sources (Table 3). A variety of other data sources of lower quality were not retained such as lightning or snowfall because (i) the domain or subdomain does not have any global data sources relevant to this analysis or (ii) the identified data sources for this domain or subdomain are not considered appropriate for developing a national exposure indicator for the respective climate-related hazard. However, the paper does not exclude the possibility to add climate-related hazards to follow-up OECD work in other broad categories such as snow and ice or oceanic. Annex C provides more details on the excluded domains or subdomains.

**Table 3. Review of relevant data sources on climate-related hazards**

Greyed-out rows are data sources selected for developing national and subnational exposure indicators

<i>Data source</i>	<i>Description</i>	<i>Geographic resolution</i>	<i>Temporal resolution</i>	<i>Update frequency</i>
<b>Temperature</b>				
Copernicus Climate Data Store (CDS) ERA5 hourly data on single levels (ERA5)	Mean, minimum, maximum temperature	0.25° resolution (~27.75 km) per grid cell	Daily: 1979 to present	Quarterly updates (every three months)
Thermal comfort indices derived from ERA5 reanalysis ERA5-HEAT	Universal Thermal Comfort Index (UTCI)	0.25° (~27.75 km)	Hourly: 1979 to present	Near real time (2.5 months lag)
Berkeley Earth Surface Temperatures (BEST)	Mean, minimum and maximum temperature	1.0° resolution (~111 km) per grid cell	Daily: 1880 – 2019	NA
<b>Precipitation</b>				
Copernicus CDS ERA5 hourly data on single levels (ERA5)	Total precipitation	0.25° resolution (~27.75 km) per grid cell	Daily: 1979 to present	Quarterly updates (every three months)
NASA/JAXA Global Satellite Mapping of Precipitation (GPM) IMERG	Precipitation estimates (mm h-1)	0.1° resolution (~11 km)	Hourly: 2014 to present 3-hourly: 2000 to present Daily: 2000 to present	Late run: ~14 hours Final run: ~3.5 months
JAXA/NASA Global Satellite Mapping of Precipitation (GSMaP)	Precipitation estimates (mm h-1)	0.1° resolution (~11 km)	Hourly, 3-hourly and daily: 2014 to present	Standard product: 3 days Near-real-time product: 4 hours
Copernicus Global Precipitation Climatology Project (GPCP)	Mean precipitation (mm day-1)	1.0° resolution (~111 km)	Daily: 1996 to present Monthly: 1979 to present	Quarterly
NOAA CMORPH Climate Data Record	Precipitation estimates	8 km resolution (30-min data), 0.25° resolution (hourly and daily data) (~27.75 km)	30-min, hourly and daily: 2002 to present	18 hours past real-time
<b>Drought</b>				
Copernicus CDS ERA5-Land monthly averaged data	Volume of water in soil layer 0-7 cm	0.1° resolution (~11 km)	Monthly: 1950 to present	Near real time
Soil moisture gridded data (Copernicus CDS)	Volumetric surface soil moisture	0.25° resolution (~27.75 km)	Monthly: 1978 to present	Near real time
NOAA	CMORPH Daily Standardised Precipitation Index (SPI)	0.25° resolution (~27.75 km)	Half-hourly and daily: 2002 to present	18 hours past real-time
	GPCC Precipitation anomalies	5.0° resolution (~555 km)	Monthly: 1900 to present Base period: 1961 – 1990	Same as above
	MERRA2 Evaporative Demand Drought Index (EDDI)	0.125° resolution (~15km)	Daily: 1980 to present	5 days past real-time
European Commission Joint Research Centre (JRC)	Risk of Drought Impacts for Agriculture (RDrl-Agri)	1.0° resolution (~111 km)	Yearly: 2013 to present	~14 days past real-time
Global Precipitation Climatology Centre	Global Drought Index	1.0° resolution (~111 km)	Monthly: 2013 to present Base period: 1961 – 1990	Updated to the most recent full month
Climatology and Climate Services Laboratory	Standardised Precipitation and Evapotranspiration Index (SPEI)	0.5° resolution (~55 km)	Monthly: 1901 - 2018	No updates after December 2018
<b>Wildfire</b>				
Global Fire Emissions database	Burned area Fire events	Vector shapefiles (underlying data: 500 m)	Monthly: 1997 to 2021	Updated annually
MODIS/Terra and Aqua MCD64A1 product	Burned area	500 m	Monthly: 2000 to present	Updated monthly



Copernicus	Danger rating Fire danger index	0.25° resolution (~27.75 km)	Daily: 1979 to present	Updated monthly
NASA	Active fire data	MODIS: 1 km VIIRS: 250 m	MODIS: daily, 2000 to present VIIRS: half-daily, 2012 to present	Available usually after 2 to 3 months
<b>Wind</b>				
Cyclone wind hazard maps (GAR 2015)	Maps of cyclone-prone areas expressed in terms of wind gust (km/h) for different return periods (50 to 1000 years)	0.27° (~27.75 km)	No time coverage	Unknown
Copernicus CDS ERA5 hourly data on single levels	Maximum 10 m wind gust	0.25° (~27.75 km)	1979 to present	Updated daily (7-day lag)
Copernicus CDS Agrometeorological indicators AgERA5	Mean wind speed at a height of 10 m above the surface (m s <sup>-1</sup> )	0.1° resolution (~11 km)	1979 to present	Updated daily (7-day lag)
Copernicus CDS ERA5 hourly data on single levels (ERA5)	Mean wind speed at a height of 10 / 100 m above the surface (m s <sup>-1</sup> )	0.25° resolution (~27.75 km)	1979 to present	Quarterly updates (every three months)
Global wind atlas	Mean wind speed at 10 / 50 / 100 / 150 / 200 m above the surface (m s <sup>-1</sup> )	250 m	No time coverage	Unknown
NOAA	Tropical cyclone track data	0.1° resolution (~11 km)	1841 to present	Updated twice weekly
	Pacific hurricane catalog	Point and line vector data	1851 to 2020 (Atlantic) 1949 to 2020 (Pacific)	Unknown
<b>River flooding</b>				
JRC flood hazard maps at European and global scale	Maps of flood prone areas in Europe and the Mediterranean Basin for river flood events of different magnitude (from 1-in-10-year to 1-in-500-year)	100 m (European and Mediterranean Basin), 1 km (Global)	No time coverage	Unknown
WRI Aqueduct flood hazard maps	Flood prone areas for river and coastal floods of different magnitude under current baseline and for different future projections	1 km	Baseline, 2030, 2050, 2080	Unknown
<b>Coastal flooding</b>				
Global coastal flood hazard maps	Global reanalysis of storm surges and extreme sea levels	1 km	No time coverage	Unknown
WRI Aqueduct Water Risk Atlas – Coastal flood risk	Expected percentage of population to be affected by coastal flooding in an average year, accounting for existing flood protection standards	30 arc minutes (~55 km)	No time coverage, coastal flooding measured in an average year	Unknown
WRI Aqueduct flood hazard maps	Flood prone areas for river and coastal floods of different magnitude under current baseline and for different future projections	1 km	Baseline, 2030, 2050, 2080	Unknown
Coastal flooding and sea level rise maps by Climate Central	Areas that will likely be flooded at different amounts of rising water due to a combination of sea level rise, tides and storm surges	USA and Hawaii (~5m); Areas where NOAA coastal lidar is unavailable (~1/3 arcsec resolution or 10m); Alaska (~60 m)	No time coverage	Unknown

## 3.2. Impacts and measurement of climate-related hazards

### Heat and cold

#### *Frequency of extreme temperature events*

Extreme heat and cold are important climate-related hazards for many human activities, including human health, agriculture, transport and energy. Temperature extremes at both ends of the temperature spectrum are considered global health risk factors (The Lancet, 2021<sup>[16]</sup>). In 2019, for example, 1.7 million deaths worldwide were linked to non-optimal temperatures and 356 000 of these deaths were related to high temperatures (Burkart et al., 2021<sup>[3]</sup>). Extreme heat and cold can increase or decrease morbidity and mortality, exacerbate pre-existing health conditions, impact agricultural output and result in lower economic output, amongst other effects (Burke, Hsiang and Miguel, 2015<sup>[17]</sup>). Recent studies found that extreme heat and cold are associated with a diverse set of death causes, including a variety of cardiorespiratory and metabolic diseases but also external causes of mortality such as suicide and several types of injury (Burkart et al., 2021<sup>[3]</sup>). Considering that climate change increases extreme heat-related health risks (Limaye et al., 2018<sup>[18]</sup>), accounting for extreme temperatures is considered a key climate-related hazard in this paper.

Population exposure to extremely hot or cold days can be measured through a variety of commonly used indices. For example, the IPCC AR6 measures hot summer days ( $TMAX_{ij} > 35^{\circ}C$ ) where  $TMAX_{ij}$  is the daily maximum temperature on day  $i$  in year  $j$  (IPCC, 2021, p. 1522<sup>[11]</sup>). According to the European Environment Agency (EEA) report on climate-related hazard indices, another index of high priority is the number of tropical nights ( $TMIN_{ij} > 20^{\circ}C$ ) where  $TMIN_{ij}$  is the minimum temperature on day  $i$  in year  $j$  (ETC-CCA, 2020<sup>[9]</sup>). This index allows to measure days when people are unable to cool down at night. Other measures of heat stress, such as the Universal Thermal Climate Index (UTCI), describe how the human body experiences atmospheric conditions, and includes other contributing factors beyond air temperature such as humidity, wind speed and solar radiation. Meanwhile, measurements of cold stress focus on indices such as the number of icing days ( $TMAX_{ij} < 0^{\circ}C$ ) where  $TMAX_{ij}$  is the maximum temperature on day  $i$  in year  $j$ .

Extreme temperature events can also be measured based on the exceedance of the daily minimum or maximum temperature above or below a certain percentile value over the base period<sup>3</sup> (Head et al., 2018<sup>[19]</sup>) (Perkins and Alexander, 2013<sup>[20]</sup>). For example, above-average temperatures ( $TMAX_{95p}$ ) can be measured when  $TMAX_{ij} > 95^{\text{th}}$  percentile of the base period where  $TMAX_{ij}$  is the maximum temperature on day  $i$  in period  $j$  (Karl, Nicholls and Ghazi, 1999<sup>[21]</sup>). Similarly, below-average temperatures ( $TMIN_{5p}$ ) can be measured when  $TMIN_{ij} < 5^{\text{th}}$  percentile of the base period where  $TMIN_{ij}$  is the daily minimum temperature on day  $i$  in period  $j$ . These indices allow identifying changes in extreme temperature conditions over time.

A variety of data sources estimates daily minimum, mean and maximum temperature. For example, the Copernicus CDS ERA5 hourly data on single levels dataset from the European Centre for Medium-Range Weather Forecasts (ECMWF) provides data with 0.25 degrees resolution (~27.75 km) from 1979 to present (Hersbach et al., 2018<sup>[22]</sup>). In addition, the thermal comfort indices such as the UTCI derived from ERA5 reanalysis (ERA5-HEAT) is available on the Copernicus CDS and provides hourly UTCI at a 0.25° spatial resolution. Alternatively, the Berkeley Earth provides global surface temperature data, which includes minimum and maximum temperature. However, this data source has a coarser spatial resolution and does not appear to be updated with temperature data after 2019 (Table 3), making it less suitable for estimating extreme temperatures in this paper.

---

<sup>3</sup> A base period is a standard reference period to calculate average climate normals that represent what can be considered a typical climate for a given period. These climate normals are used to compare shorter-term data at local, national or global level.

## **Wet and dry**

### ***Frequency of extreme precipitation days***

Extreme precipitation is a common climate-related hazard around the world. Annual and seasonal precipitation patterns influence a wide range of human, social and economic activities. Extreme precipitation predominantly triggers flooding events, which can lead to casualties, displacement of people, damage to infrastructure, and losses in agricultural productivity (Kirchmeier-Young and Zhang, 2020<sup>[23]</sup>). Recent studies suggest that excessive precipitation can affect crop yield as much as excessive heat and drought, including through direct physical damage, delayed planting and harvesting, restricted root growth, oxygen deficiency and nutrient loss (Li et al., 2019<sup>[24]</sup>). Identifying specific areas at risk of extreme precipitation is thus important to protect individuals, households, communities and the broader society.

The WMO-mandated Expert Team on Sector-specific Climate Indices (ET-SCI) developed indices describing the frequency of extreme precipitation (i.e. the number of events with an intensity above a given threshold) (Karl, Nicholls and Ghazi, 1999<sup>[21]</sup>). For example, the number of very heavy precipitation days (*R20mm*), is a count of the number of days, within a given time period of interest, in which daily precipitation amounted to more than 20mm and is formulated as  $R20mm = \sum R_{ij} > 20 \text{ mm}$  where  $R_{ij}$  is the daily precipitation amount on day  $i$  in period  $j$  (Petroliagkis and Alessandrini, 2021<sup>[25]</sup>). Extreme precipitation events can also be measured based on the exceedance of the daily precipitation amount above and below a certain percentile value over the reference period. For example, the frequency of extreme precipitation events is often measured when the daily precipitation amount  $> 99^{\text{th}}$  percentile of the reference period to identify days with particularly heavy precipitation and is consistent with the EEA's methodology for assessing the frequency of extreme precipitation event (EEA, 2021<sup>[26]</sup>).

A variety of data sources are available to estimate precipitation on an hourly, daily or monthly basis and enable the observation of changes in annual and seasonal precipitation (Table 3). For example, the IMERG data provided by NASA estimates hourly and daily precipitation over the majority of the Earth's surface since 2000 through the Global Precipitation Measurement (GPM) satellite constellation with a high pixel resolution. Similarly, the ERA5 hourly data on single levels for the daily precipitation amount with a 0.25 degrees resolution (~27.75 km) from 1979 to present (Hersbach et al., 2018<sup>[22]</sup>). This data is based on hourly data from the European Centre for Medium-Range Weather Forecasts (ECMWF).

### ***Droughts***

Droughts are an important climate-related hazard that can result in serious impacts on agriculture, energy and water management sectors, and the society as a whole. Droughts are typically categorised into three types: (1) meteorological, (2) agricultural or (3) hydrological droughts (Ziese et al., 2014<sup>[27]</sup>) (Wang et al., 2016<sup>[28]</sup>). Generally, meteorological droughts are based on the interplay between precipitation and evapotranspiration due to changes in temperature. Agricultural and hydrological droughts usually start from meteorological droughts, but are different. For example, changes to the hydrological cycle result in soil moisture depletion which can impact crops (i.e. agricultural drought) and eventually lead to changes in hydrological features such as rivers or lakes (i.e. hydrological drought). Droughts can also have a socioeconomic origin, resulting from the mismanagement of water but this type of drought is more likely to affect specific people and regions (OECD, 2016<sup>[29]</sup>).

A variety of indices have been developed over the years to estimate past droughts. This includes a variety of water stress indicators to assess water stress impacts on agriculture, even though these often do not have the geospatial component needed to develop a drought indicator with a high spatial resolution (OECD, 2017<sup>[30]</sup>). However, there are a number of geospatial data sources to estimate drought impacts. For example, the Standardised Precipitation Index (SPI) is used to estimate the wetness or dryness of an area. The SPI is an index of the probability of recording a certain amount of precipitation. This index is positive for wetter conditions and negative for drier conditions. However, the SPI does not account for temperature changes

due to climate change and therefore does not consider increased evapotranspiration, leading to misleading values in drier areas (Ziese et al., 2014<sub>[27]</sub>). Alternative drought indices have been developed to account for temperature changes such as the Standardised Precipitation Evapotranspiration Index (SPEI) and the Global Drought Index, which combines the SPI and SPEI into one global drought index (Ziese et al., 2014<sub>[27]</sub>). Further details on these data sources on global drought are in Table 3.

The agricultural sector is particularly vulnerable to climate-related hazards due to its heavy reliance on weather and climate (FAO, 2021<sub>[31]</sub>), and this is why agricultural droughts are studied in more detail in this paper. Agricultural droughts can also be measured using volumetric surface soil moisture, which corresponds to the water content in a 0 to 7 cm-depth layer of soil. Water content in the superficial layer of soil is important for water supply and for vegetation health. Soil moisture anomaly is a suitable indicator for monitoring the intensity of droughts, and shows similar performances in identifying droughts to the Standardized Precipitation Index (Zeri et al., 2021<sub>[32]</sub>). Additionally, the Copernicus CDS provides different data sources on soil moisture, which are both satellite and in-situ based. ERA5-Land is more accurate and available at a higher resolution than other identified data sources, which allows to capture more variations in drought conditions at the local level (Dorigo et al., 2017<sub>[33]</sub>) (Gruber et al., 2019<sub>[34]</sub>).

### **Wildfires**

Wildfires are an important natural hazard with impacts on forestry, agriculture, tourism, transport, infrastructure, water supply, biodiversity, wildlife and human health. Proximate causes of wildfire encompass lightning or human activities such as agricultural burning, arson, electric sparks or cigarette discarding. Fire activity is conditioned by environmental variables such as weather, fuel availability (i.e. accumulation of biomass) and topography (Balch et al., 2017<sub>[35]</sub>) (Bowman et al., 2020<sub>[36]</sub>). Generally, persistent dry periods characterized by high evaporation and low precipitation combined with the presence of strong winds increase the risk of wildfires to spread.

In developed countries, wildfires are a growing threat to the expanding population living nearby or within forested areas. On the other hand, wildfires remain a direct threat to vulnerable minority communities such as the elderly, disadvantaged persons or indigenous populations, exacerbating existing inequalities (Davies et al., 2018<sub>[37]</sub>).

Wildfires are influenced both by climate and non-climate drivers and distinguishing between these drivers can be challenging not only at a global level but also nationally and locally (Butry, Prestemon and Thomas, 2014<sub>[38]</sub>). Non-climate drivers of wildfires are mostly human activities, such as prescribed burning, agricultural activity and land use change, amongst others. Meanwhile, climate change can further exacerbate the suitable hot and dry conditions for wildfires, influence wildfire frequency, duration, intensity and spread rate (see OECD, forthcoming publication, *Adapting to climate change in the management of wildfires*).

Interlinkages between climate change, forests, wildfires and the financial sector are increasingly acknowledged to strengthen adaptation measures. Forests represent about 45% of the offset credits issued to help fight the changing climate, implying that wildfires have growing implications for financial markets because they can burn the forests and release the carbon designed to be permanently stored (So, Haya and Elias, 2022<sub>[39]</sub>). In addition, forest offset programmes should account for wildfire risks to avoid developing a landscape that is more flammable or dangerous (Leverkus et al., 2022<sub>[40]</sub>). Wildfires are thus a risk to the environmental integrity of forest offset programmes (Badgley et al., 2022<sub>[41]</sub>).

At the global level, data and indices are available to identify (a) wildfire occurrence and extent, and (b) wildfire risk.

- a) For example, the Global Wildfire Information System (GWIS), a joint initiative of the Group on Earth Observations (GEO), the NASA Applied Research and the EU Copernicus work programmes, developed the GlobFire Database, which provides information on the occurrence of wildfires (i.e. fire events) during a month or a year based on NASA MODIS Terra and Aqua satellite data. Due to

technical constraints, GlobFire data omits small fire events (< 25 ha), which indirectly removes most controlled fires such as prescribed burnings (Felipe Galizia et al., 2021<sup>[42]</sup>). It also excludes small wildfires that are part of the natural system and that can benefit fire-adapted ecosystems through vegetation renewing.

- b) To assess the fire danger of the risk of wildfires to occur, the Fire Weather Index (FWI) System is a meteorologically based index used worldwide for most jurisdictions around the world (Goldammer et al., 2018<sup>[43]</sup>) (Field, 2020<sup>[44]</sup>). The FWI System was developed in Canada and is composed of three moisture codes, and three fire behaviour indices. The moisture codes capture the moisture content of three generalised fuel classes and the behaviour indices reflect the spread rate, fuel consumption and intensity of a starting fire. Overall, these indices do not detect actual wildfires but rather the likelihood for a wildfire to occur if there is an ignition (Table 3).

## **Wind**

Wind threats or windstorms are an important climate-related hazard with direct impacts on humans, ecosystems and economic infrastructures. For example, the force of windstorms can create flying debris and falling trees, which can either strike humans directly or damage built structures. For this reason, identifying wind threats is an important part of assessing the risk of climate-related hazards. A common way of measuring wind threats is through wind speed, which refers to the horizontal speed of the wind or movement of air. Several global data sources identify daily and monthly mean wind speeds at varying heights (e.g. 10, 50, 150, 200 m) above the Earth's surface such as the Copernicus Climate Data Store (Table 3). However, most damages of windstorms are due to the extreme wind speeds during gusts. Therefore, gust speeds, defined as the maximum value of the 3-second running average wind speed, can be used to assess wind-related hazards.

Other global data sources to assess the occurrence of windstorms are limited. For example, the NOAA provides data on tropical cyclones (hurricanes, typhoons) through the International Best Track Archive for Climate Stewardship (IBTrACS) and the HURDAT2 database. This includes information on the maximum sustained wind speed, minimum central pressure and storm centre for circulation. However, these data sources would require substantial data manipulation and are region-specific, making it unclear how to assess windstorms in areas that are not affected by tropical cyclones. Alternatively, the Emergency Events Database (EM-DAT) from the Centre for Research on the Epidemiology of Disasters' (CRED) records windstorms as part of the category 'convective storm', which contains several subcategories relevant to windstorms (i.e. tornado, wind, severe storm, etc.). Although this database has information on the country and region, it is not georeferenced, making it difficult to assess the risk of wind threats to populations and infrastructure.

## **River flooding**

Flooding can cause economic losses through its impacts on energy and transport infrastructures, human settlements and agricultural land. Flooding is considered the second gravest hazard for the agriculture sector, responsible for an estimated loss of USD 21 billion of crop and livestock production between 2008 and 2018 in Least Developed and Low-to-Middle-Income countries (Global Network Against Food Crises, 2022<sup>[45]</sup>). With changing climate and without appropriate adaptation measures, flood events are projected to rise in all continents, especially in Asia, America and Europe (Alfieri et al., 2017<sup>[46]</sup>).

Different types of floods can be distinguished by the source and the mechanism of flooding. River flooding occurs when excessive rainfall results in the river exceeding the channel capacity and spilling into the adjacent areas. Pluvial floods occur when the absorption capacity of the soil or the drainage capacity in urban areas is exceeded. River flooding can be caused by heavy rainfalls or snowmelt runoffs. River flooding is consequently interrelated to pluvial flooding, but different.

Various data sources and variables exist to assess river flooding hazard. The World Resources Institute (WRI) developed the Aqueduct Floods online platform that measures riverine and coastal flood risks under both current baseline conditions and future projections in 2030, 2050 and 2080. The Joint Research Centre (JRC) also provides River Flood Hazard Maps for the whole world, and for Europe and the Mediterranean Basin region at a more granular spatial resolution (Dottori et al., 2021<sup>[47]</sup>). The Global Flood Awareness System (GloFAS) provides data on daily river discharge in the last 24 hours ( $\text{m}^3 \text{s}^{-1}$ ) informing on the amount of water that flows through a river section. GloFAS is part of the Copernicus Emergency Management Service (CEMS) and provides a forecasting tool to develop a flood summary based on 2-, 5- and 20-year exceedance probability of rivers.

### **Coastal flooding**

Coastal areas experience a variety of climate-related hazards and climate change is expected to exacerbate existing impacts even more (OECD, 2021<sup>[48]</sup>). This includes sea level rise, coastal storm surges, ocean warming and acidification, and changes to the hydrological cycle (OECD, 2019<sup>[49]</sup>) (OECD, 2021<sup>[48]</sup>). The IPCC AR6 provides, for example, sea level rise simulations between 2020 and 2150 (IPCC, 2021<sup>[1]</sup>). Including sea level rise into existing data sources for coastal flooding is complicated. It requires accounting for a variety of climate scenarios, and it is unclear what relative contribution sea level rise has to present-day coastal flooding considering other contributing events such as extreme precipitation or storm surges.

A variety of data sources exist to assess coastal flooding hazards. One data source from ResourceWatch and Surging Seas combines coastal flooding and sea level rise using a high accuracy Digital Elevation Model. However, the data source is not publicly accessible (Climate Central and Surging Seas, 2018<sup>[50]</sup>). The Water Risk Atlas provides data on coastal flood risk by measuring the percentage of population expected to be affected by coastal flooding, accounting for existing flood protection standards (Hofste et al., 2019<sup>[51]</sup>). The downside of using this data source for assessing coastal flooding is that it does not allow assessing the estimated impact of coastal flooding on other exposed assets (such as urban areas). The Global Tide and Surge Reanalysis (GTSR) data source provides a global reanalysis of storm surges and extreme sea levels based on hydrodynamic modelling (Muis et al., 2016<sup>[52]</sup>). This data source is based on predictive modelling before the event occurred (ex-ante), providing modelled coastal flooding hazards with different return periods. A key limitation of this data source is that existing flood protection measures such as dikes and storm surge barriers are not accounted for.

### **3.3. Selected exposure indicators for climate-related hazards**

For each of the four dimensions of climate-related exposure under study, a selection of data sources were identified. These include:

- ▶ Population density: The GHSL multiannual population grid shows the distribution and density of the population at a high spatial resolution of 250 m, expressed as the number of people per cell (Freire et al., 2016<sup>[53]</sup>).
- ▶ Cropland, forest and urban area land cover: The Copernicus Global Land Cover data allows for the identification of global cropland, forest and urban area cover at a high spatial resolution of 300 m from 1992 to 2020 (Buchhorn et al., 2020<sup>[54]</sup>).

Against this background, this paper develops 19 exposure indicators for climate-related hazards that represent a risk to the economy and the society at large (Table 4). This selection remains work-in-progress and future work could add new indicators to existing hazard and exposure indicators.

Table 4. Selected indicators for climate-related hazards

Domain		Hazard indicators	Exposure indicators	Rationale	Data sources
Extreme temperature	Absolute threshold		<ul style="list-style-type: none"> <li>▶ Percentage of population exposed to <math>n</math> number of hot days (<math>T_{\max} &gt; 35^{\circ}\text{C}</math>)</li> <li>▶ Percentage of population exposed to <math>n</math> number of tropical nights (<math>T_{\min} &gt; 20^{\circ}\text{C}</math>)</li> <li>▶ Percentage of population exposed to <math>n</math> number of days identified as a hot day and a tropical night</li> <li>▶ Population-weighted average of the number of days per year with strong, very strong and extreme heat stress</li> <li>▶ Percentage of population exposed to <math>n</math> number of icing days (<math>T_{\max} &lt; 0^{\circ}\text{C}</math>)</li> </ul>	Temperature extremes on both sides of the spectrum are global risk factors. Extreme heat and cold are important climate-related hazards for many human activities, including human health, agriculture, transport and energy.	Copernicus Climate Data Store (CDS) ERA5 hourly data on single levels (ERA5), the Thermal comfort indices (ERA5-HEAT), and Global Human Settlement Layer (GHSL) population grids
	Relative threshold	<ul style="list-style-type: none"> <li>▶ Mean number of days when the daily maximum temperature is above the 95<sup>th</sup> percentile of the reference period</li> <li>▶ Mean number of days when the daily minimum temperature is below the 5<sup>th</sup> percentile of the reference period</li> </ul>			
Extreme precipitation	Absolute threshold	<ul style="list-style-type: none"> <li>▶ Percentage of land exposed to <math>n</math> number of days where the total daily precipitation is above 20 mm.</li> </ul>		Precipitation extremes are risk factors that can cause sudden flooding, impacting, for example, the agricultural sector. Accounting for precipitation extremes is vital for policymaking (e.g. disaster preparedness or investment decision-making).	Copernicus CDS ERA5 hourly data on single levels and Copernicus global land cover data
	Relative threshold	<ul style="list-style-type: none"> <li>▶ Percentage of land exposed to <math>n</math> number of days when the total daily precipitation amount is above the 99<sup>th</sup> percentile</li> </ul>	<ul style="list-style-type: none"> <li>▶ Percentage of cropland exposed to <math>n</math> number of days when the total daily precipitation amount is above the 99<sup>th</sup> percentile</li> </ul>		
Drought		<ul style="list-style-type: none"> <li>▶ Average soil moisture anomaly</li> </ul>	<ul style="list-style-type: none"> <li>▶ Average cropland soil moisture anomaly</li> </ul>	Droughts are an important indicator with far-reaching socio-economic impacts including loss of agricultural yield.	Copernicus CDS ERA5-Land monthly averaged data and Copernicus global land cover data
Wildfire		<ul style="list-style-type: none"> <li>▶ Amount of burned area</li> </ul>	<ul style="list-style-type: none"> <li>▶ Percentage of population located in areas at risk of burning</li> <li>▶ Percentage of forested areas at risk of burning</li> </ul>	Wildfires are an important natural hazard with impacts on forestry, agriculture, tourism, transport, infrastructure, water supply, biodiversity, wildlife, and human health. Wildfires are expected to intensify with climate change.	Global Wildfire Information System data based on MODIS satellite imagery (NASA), GHSL population grids and Copernicus global land cover data
Wind threats	Historical data	<ul style="list-style-type: none"> <li>▶ Percentage of land exposed to violent storms per year</li> </ul>	<ul style="list-style-type: none"> <li>▶ Percentage of population exposed to violent storms per year</li> <li>▶ Percentage of built-up area exposed to violent storms per year</li> </ul>	Violent storms are defined using wind gust, as most damages occur in extreme wind speeds during gusts.	ERA5 hourly data on single levels from 1979 to present, GHSL population grids and Copernicus global land cover data
	Hazard map	<ul style="list-style-type: none"> <li>▶ Percentage of land exposed to cyclone wind threats with a 50-, 100-, 250- and 500-year return period</li> </ul>	<ul style="list-style-type: none"> <li>▶ Percentage of population exposed to cyclone wind threats with a 50-, 100-, 250- and 500-year return period</li> <li>▶ Percentage of built-up area exposed to cyclone wind threats with a 50-, 100-, 250- and 500-year return period</li> </ul>	Cyclone wind threats are risk factors to humans directly through flying debris and falling trees or damage built-up areas. The NOAA wind scale allows classification into low, moderate and high wind threats.	Cyclone wind hazard data from GAR 2015, GHSL population grids and Copernicus global land cover data

Domain		Hazard indicators	Exposure indicators	Rationale	Data sources
River flooding	Hazard map	<ul style="list-style-type: none"> <li>▶ Percentage of land exposed to river flooding with a 10-, 20-, 50- and 100-year return period</li> </ul>	<ul style="list-style-type: none"> <li>▶ Percentage of population exposed to river flooding with a 10-, 20-, 50- and 100-year return period</li> <li>▶ Percentage of built-up area exposed to river flooding with a 10-, 20-, 50- and 100-year return period</li> <li>▶ Percentage of cropland exposed to river flooding with a with a 10-, 20-, 50- and 100-year return period</li> </ul>	River flooding can cause huge economic losses, impacting the population, built-up areas, or other infrastructure.	GHSL population grids and Copernicus global land cover data
Coastal flooding	Hazard map	<ul style="list-style-type: none"> <li>▶ Percentage of land exposed to coastal flooding with a 10-, 25-, 50- and 100-year return period</li> </ul>	<ul style="list-style-type: none"> <li>▶ Percentage of population exposed to coastal flooding with a 10-, 25-, 50- and 100-year return period</li> <li>▶ Percentage of built-up area exposed to coastal flooding with a 10-, 25-, 50- and 100-year return period</li> <li>▶ Percentage of cropland exposed to coastal flooding with a 10-, 25-, 50- and 100-year return period</li> </ul>	Coastal flooding threatens coastal regions and communities and is expected to worsen due to climate change.	Global coastal flood hazard maps (Muis et al., 2016 <sup>[52]</sup> ), GHSL population grids and Copernicus global land cover data



# 4 Results

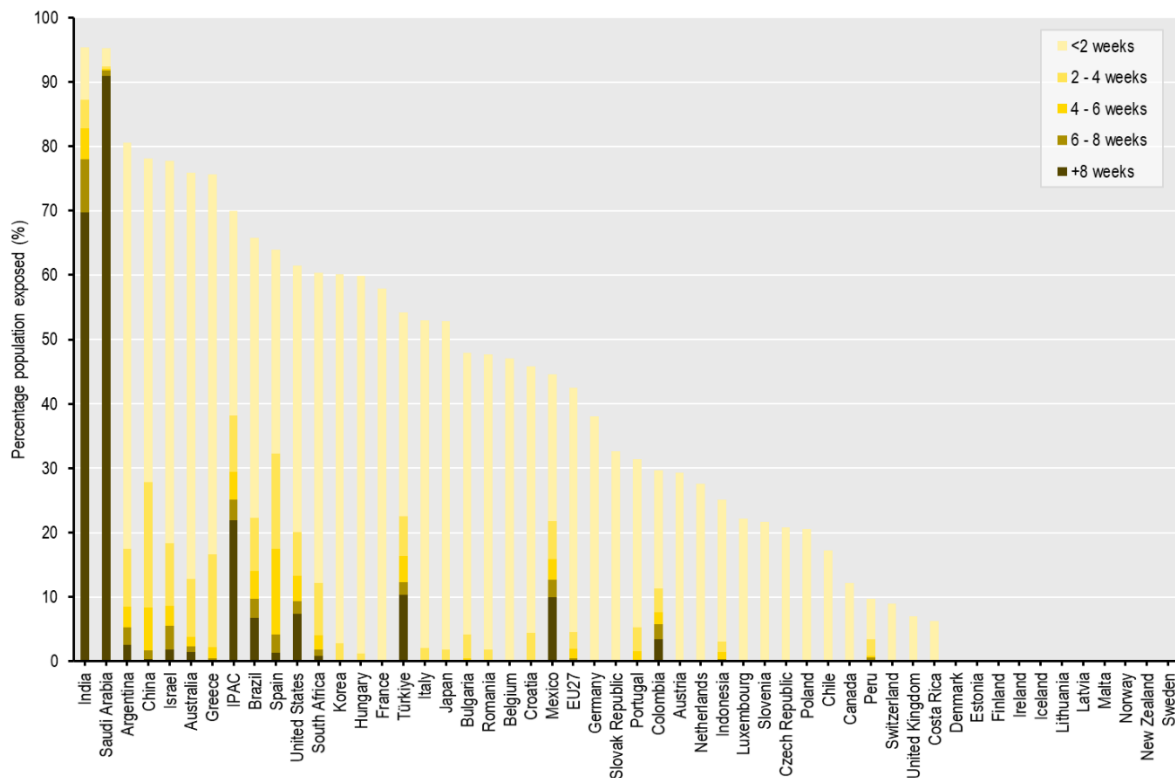
## 4.1. Extreme temperature

### Hot days and tropical nights

Most IPAC countries were affected by hot days. Hot days are defined as days where the daily maximum temperature exceeds 35°C. Countries whose population was most exposed to more than 8 weeks with hot days were Saudi Arabia, India and Türkiye, with 90.9%, 69.7% and 10.3% of the population exposed to more than 8 weeks of hot days over the period 2017-2021, respectively (Figure 1). Changes in extreme temperatures over time are discussed in more detail below in the section ‘Changing extreme temperatures’, particularly because such extremes are expected to further increase due to climate change. However, other countries such as the United States and Mexico also have a considerable proportion of their population exposed, with 7.3% (~24 million) and 10% (~13 million) of the population exposed to more than 8 weeks of hot days over the period 2017-2021, respectively.

Figure 1. A majority of countries have population exposed to hot summer days

Average percentage of population exposed to  $n$  number of hot days ( $T_{max} > 35^{\circ}C$ ) over the period 2017-2021

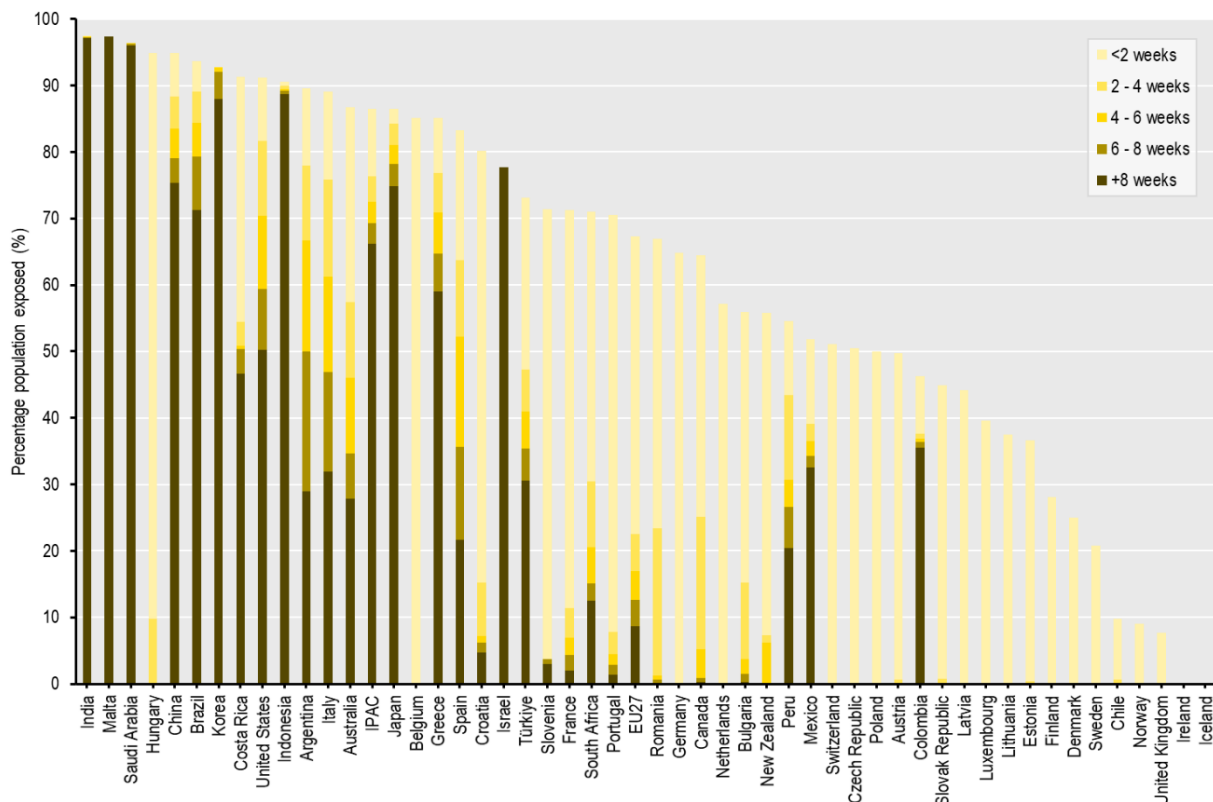


Note: Countries are ranked according to the share of population exposed to any number of hot days. For further details on methods see Annex A.

To account for the inability for human bodies to cool down at night, this paper also measures the number of tropical nights where the daily minimum temperature is above 20°C. A total of 21 countries have more than 10% of population exposed to more than 8 weeks with tropical nights over the period 2017-2021 (Figure 2). Similarly to previous results, countries such as India and Saudi Arabia have 97.1% and 95.9% of the population exposed to more than 8 weeks of tropical nights over the period 2017-2021, respectively (Figure 2). In the case of India, this represents approximately 1.35 billion people, highlighting the serious risks associated with heat stress in certain countries.

**Figure 2. A large share of population is exposed to many tropical nights**

Average percentage of population exposed to  $n$  number of tropical nights ( $T_{\min} > 20^{\circ}\text{C}$ ) over the period 2017-2021



Note: Countries are ranked according to the share of population exposed to any number of tropical nights. Further details on the methods are discussed in Annex A.

This paper also combined the indices for hot days and tropical nights to identify days that were both a hot day ( $T_{\max} > 35^{\circ}\text{C}$ ) and a tropical night ( $T_{\min} > 20^{\circ}\text{C}$ ) (Figure D.1). Results for this combined index are similar to the previous indicator assessing the number of hot days (Figure 1). This result is expected considering that days when temperatures are above 35°C likely also have night-time temperatures above 20°C.

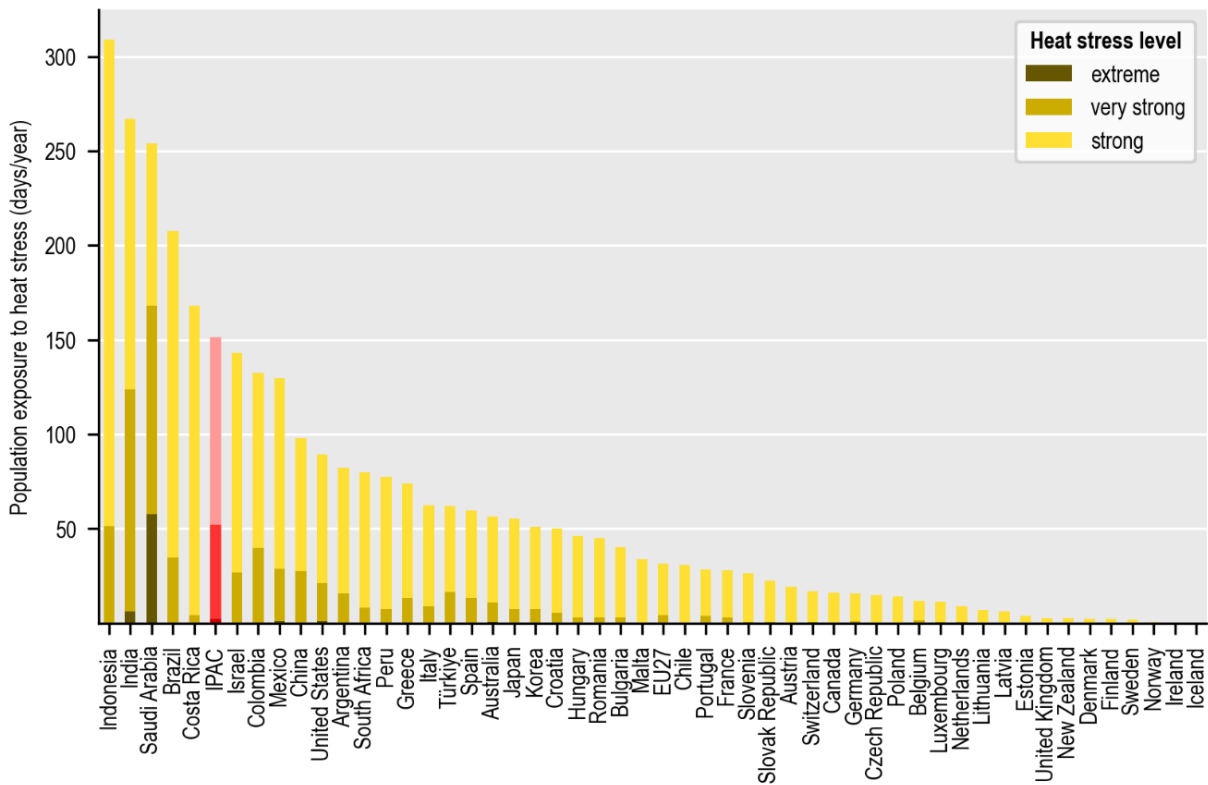
### ***The Universal Thermal Climate Index***

Another indicator included in this paper is based on the Universal Thermal Climate Index (UTCI), which accounts for other meteorological effects besides air temperature such as relative humidity, wind speed and solar radiation. Results show that over the past 5 years, population exposure to heat stress has been particularly high in Indonesia, India and Saudi Arabia, all of which experienced more than 250 days per year of strong (or worse) heat stress exposure (Figure 3). This aligns with previous indicator results on population

exposure to hot days and tropical nights (Figure 1 and Figure 2). Latin America, the Mediterranean Basin, Australia, and the United States are also particularly impacted, and this trend is increasing faster in these regions. For example, Costa Rica and Israel have been hit hard by heat stress, as population in these two countries experienced on average more than 140 days per year of strong heat stress or worse (Figure 3), and experienced more than 25 days of additional strong heat stress compared to the reference period (i.e. 1981-2010) (Figure 4).

**Figure 3. A large share of population is exposed to heat stress**

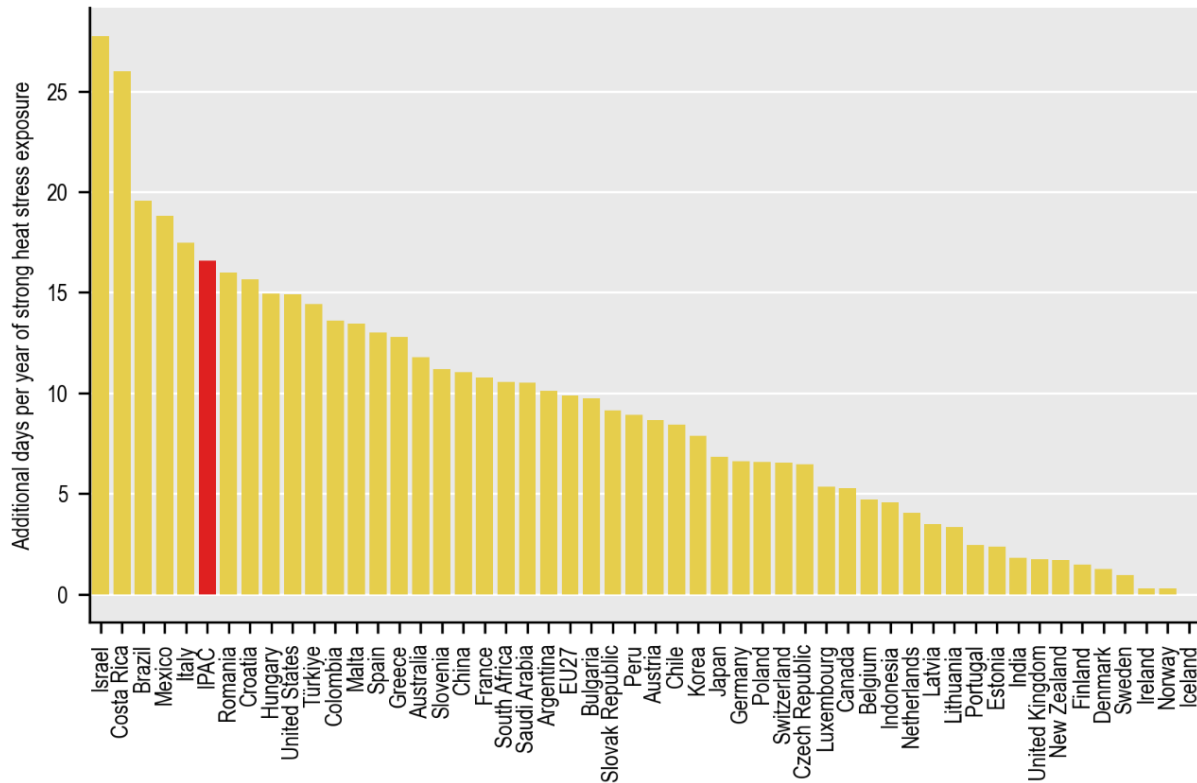
Average number of days per year of heat stress that population experienced over the period 2017-2021



Note: Further details on the methods are available in Annex A.

**Figure 4. Days with strong heat stress exposure are increasing across countries**

Additional days per year of at least strong heat stress exposure (UTCI > 32°C) over the period 2017-2021 compared to the reference period 1981-2010

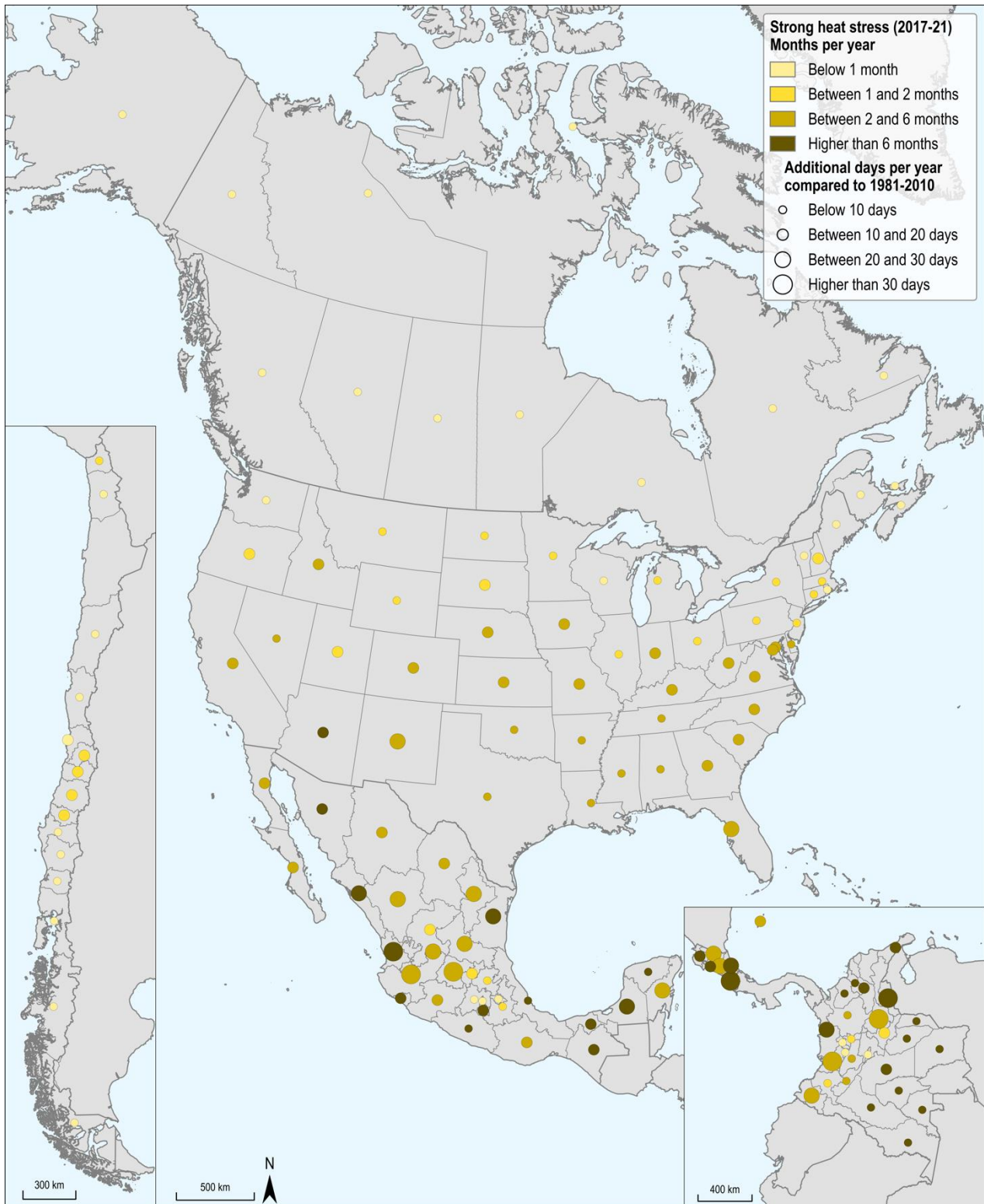


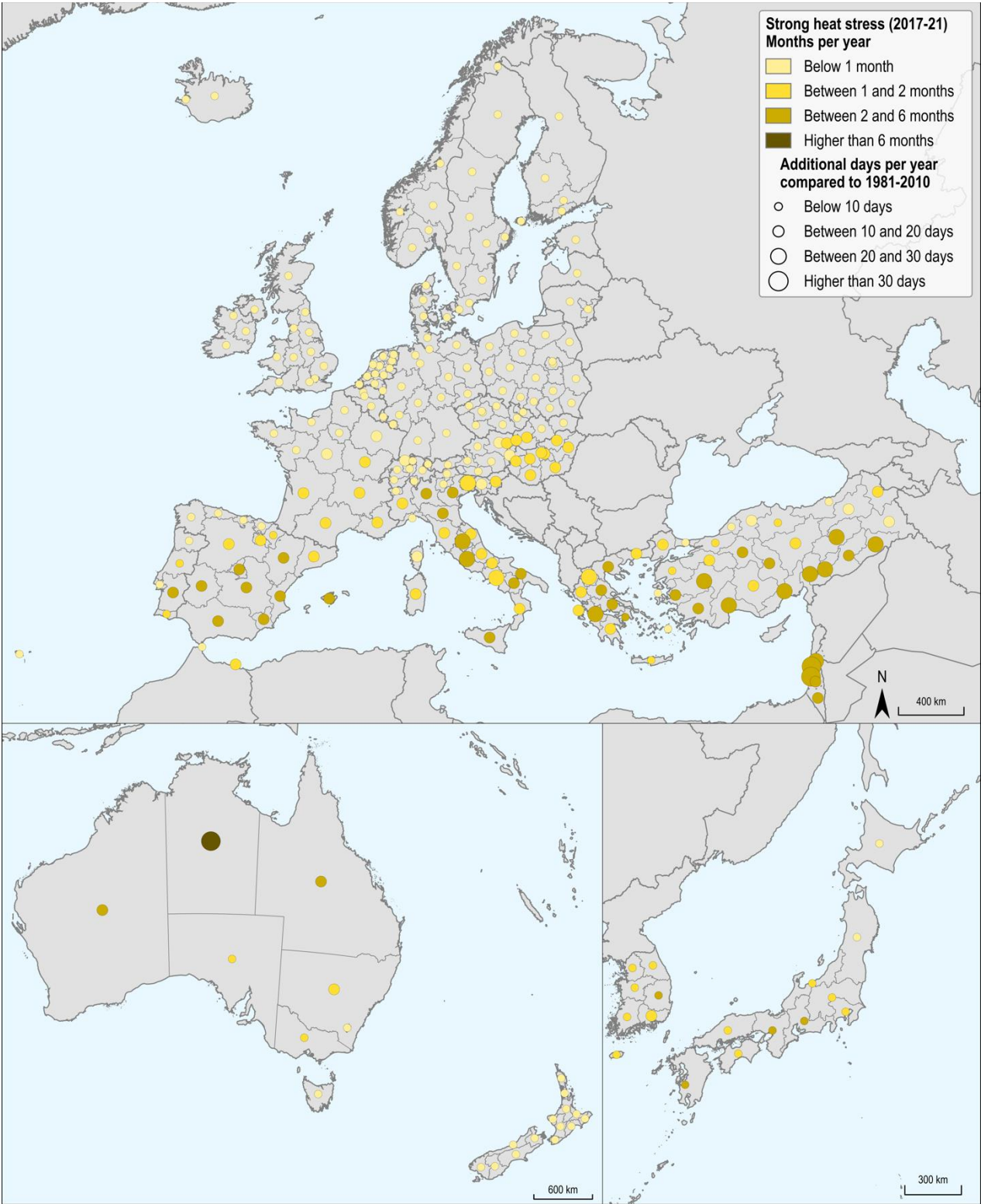
Note: Further details on the methods are available in Annex A.

Considerable subnational variation exists concerning the level and growth of population exposure to strong heat stress. Nearly all (95%) regions in OECD countries experienced an increase of exposure to heat stress over the past 5 years compared to the reference period. For example, the region of Córdoba (Colombia) experienced over the past 5 years an average of 267 days per year of very strong heat stress, a 70-day longer period compared to the reference period of 1981-2010. The districts of Haifa and Tel Aviv in Israel experienced an increase of more than a month per year in exposure to strong heat stress (UTCI > 32°C) (Figure 5). The States of Baja California Norte in Mexico and Arizona in the United States were the most impacted by extreme heat stress (UTCI > 46°C) in their respective countries during the past 5 years.

**Figure 5. Considerable subnational variation of population exposure to heat stress**

Level and growth of population exposure to strong heat stress or worse (UTCI > 32°C) over the period 2017-2021 for OECD large regions (TL2)





Note: Growth of population exposure is measured based on the reference period 1981-2010. Further details on the methods are in Annex A.

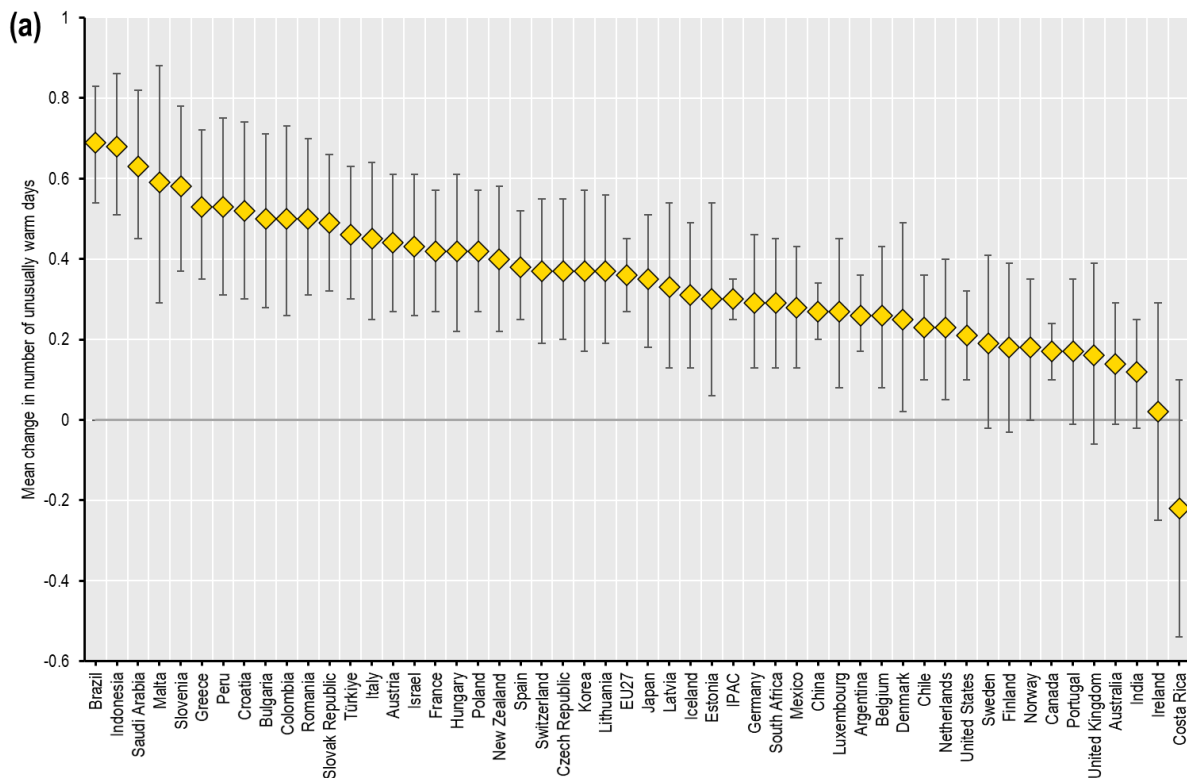


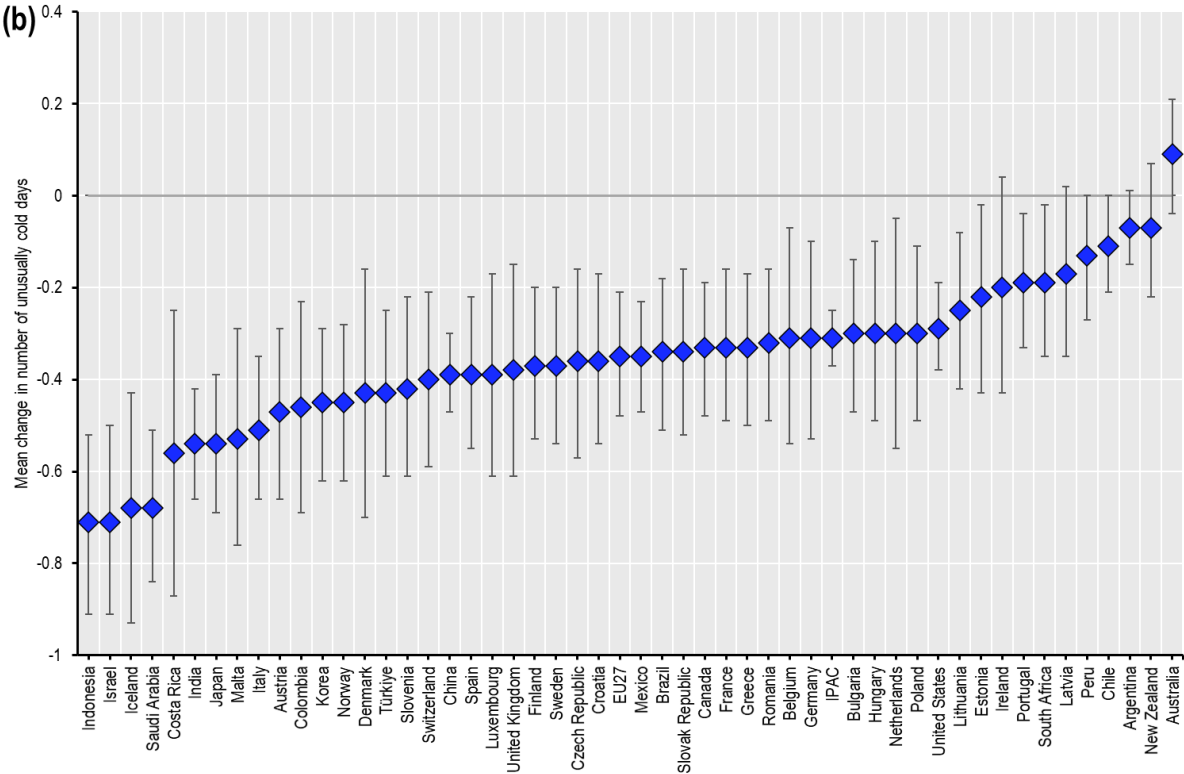
### Changing extreme temperatures

Overall, countries are experiencing more additional days with above-average temperatures compared to the reference period (1981-2010) (Figure 6a). For nine countries the overall association is unclear because the 95% confidence interval (CI) includes the reference value (i.e. 0) (Figure 6a). In addition, countries are experiencing a decreasing number of days with below-average temperatures, and only seven countries have results which are non-significant because the 95% CI includes the reference value (Figure 6b). Considering the impact of extreme temperatures on the population, these increases in above-average temperatures and decreases in below-average temperatures should be alarming, indicating that extreme temperature events may become more prevalent in the future. This highlights the urgency to adapt to climate change and mitigate its further amplification.

**Figure 6. Countries experience more above-average and less below-average temperature days, a clear display of a changing climate**

Mean annual change in the number of unusually warm and unusually cold days over the period 1979-2021 where (a)  $T_{max} > 95^{th}$  percentile and (b)  $T_{min} < 5^{th}$  percentile of the reference period (1981-2010)





Note: A linear regression model is applied on the yearly number of days when (a) the daily maximum temperature ( $T_{max}$ ) is above the 95<sup>th</sup> percentile and (b) the daily minimum temperature ( $T_{min}$ ) is below the 5<sup>th</sup> percentile of the reference period (1981-2010). This linear regression model is not adjusted for any other potentially contributing variables and is plotted with the mean and 95% confidence interval.



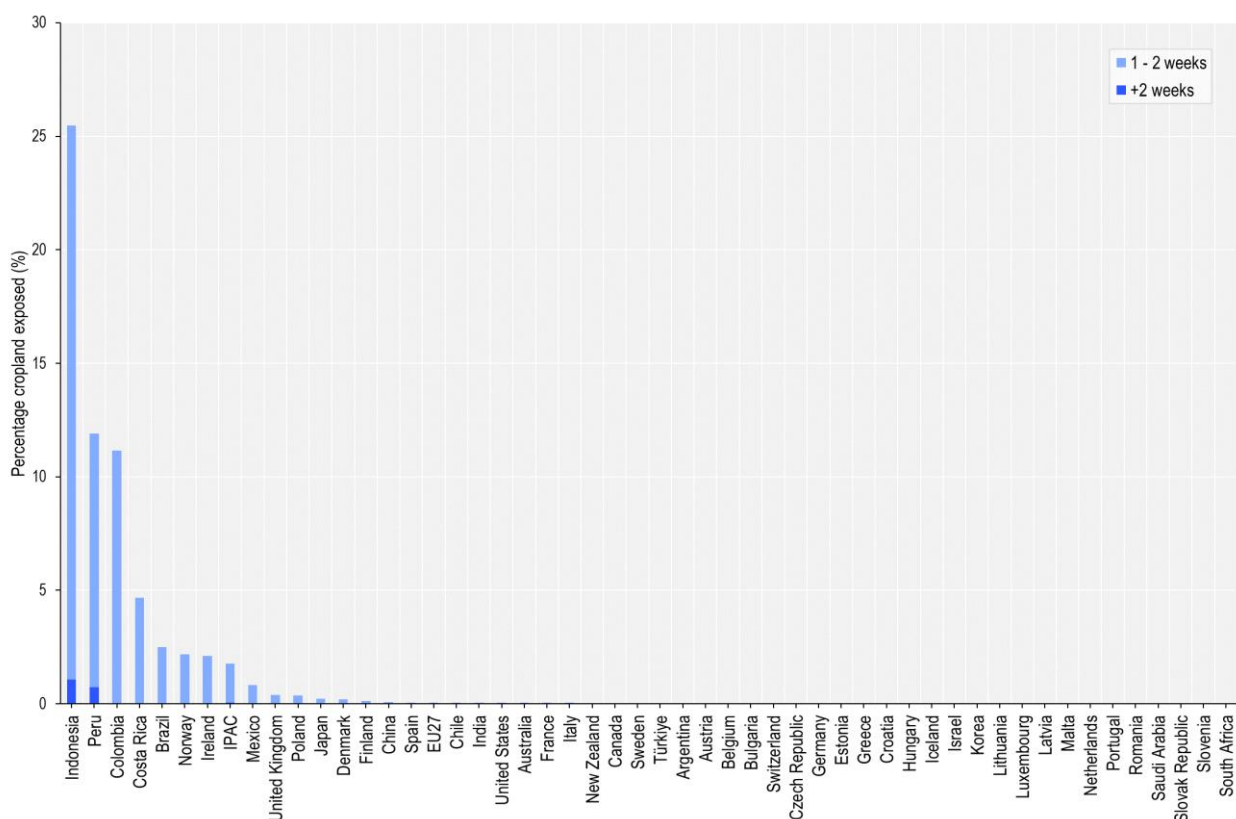
## 4.2. Extreme precipitation

This paper assesses extreme precipitation events by measuring the number of days exceeding the 99<sup>th</sup> percentile of daily precipitation values over the reference period (1981-2010). By using the 99<sup>th</sup> percentile instead of the 95<sup>th</sup> percentile, it allows identifying extreme precipitation events (ca. 4 times per year). Overall, results show that croplands in a majority of IPAC countries are experiencing a substantial number of days with extreme precipitation events compared to the reference period (1981-2010). In 2021, croplands were particularly exposed in several Western and Northern European countries such as Belgium, Latvia, the Netherlands, Sweden and Switzerland. Results show a high cropland exposure to one week or less of days with extreme precipitation events, highlighting that future analyses could identify extreme precipitation events during critical times in the year such as during seeding or harvest cycles (i.e. spring or autumn precipitation events).

On average, a small subset of IPAC countries is exposed to more than one week with extreme precipitation events over the past five years. This includes countries such as Colombia, Costa Rica, Indonesia, Norway and Peru (Figure 7). IPAC countries with the highest share of croplands exposed to extreme precipitation of more than one week include Indonesia (25.5%), Peru (11.9%) and Colombia (11.1%).

**Figure 7. Some countries have cropland exposed to more than one week of extreme precipitation**

Average percentage of cropland exposed to  $n$  number of weeks of extreme precipitation over the period 2016-2020

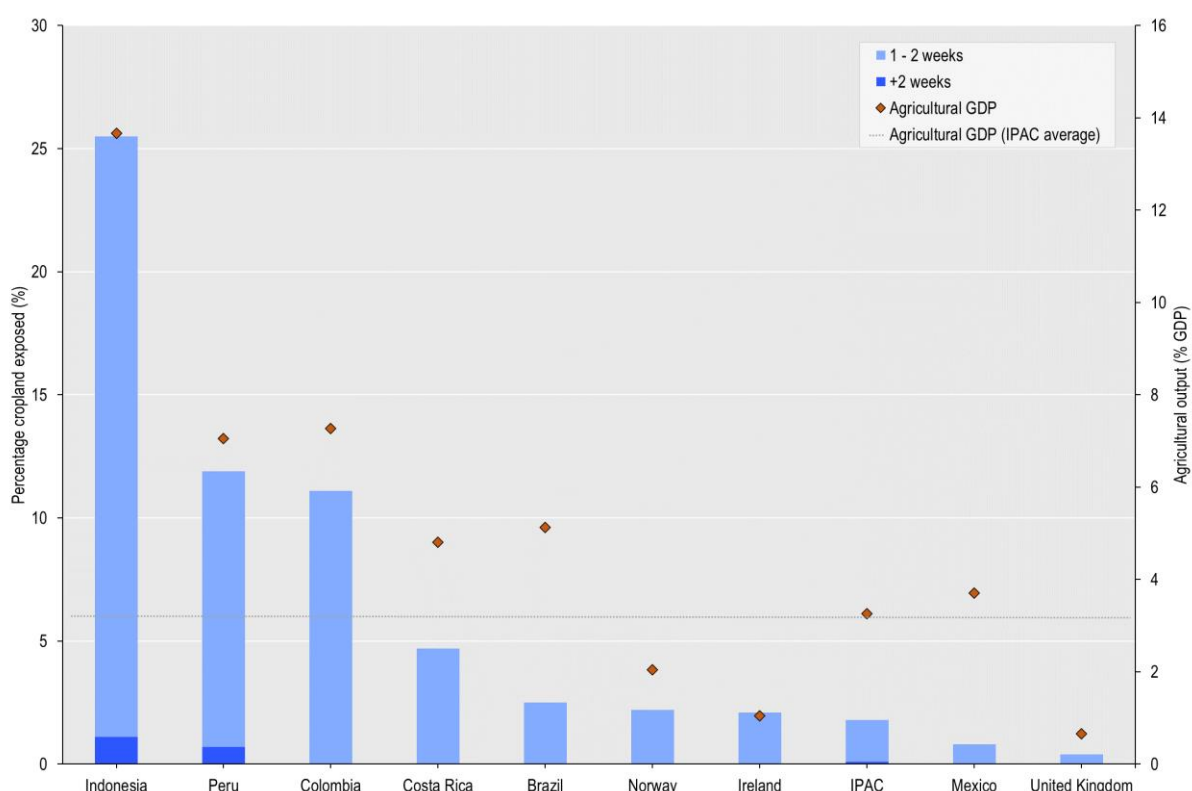


Note: Countries are ranked according to the aggregate area of cropland exposed to at least one week of extreme precipitation over the period 2016-2020. Cropland land cover data from 2020 is used and will be updated once 2021 land cover data become available. Further details on the methods are in Annex A.

For some countries where cropland was highly exposed to more than one week of extreme precipitation events in 2021, a large share of GDP is dependent on the agricultural sector. Six out of ten countries considered most dependent on the “Agriculture, forestry and fishing” sector are also among the most exposed to extreme precipitation of more than one week per year (Figure 8). For example, the GDP share of the “agriculture, forestry and fishing” sector in Indonesia and Colombia is approximately 13.3% and 7.1%, respectively, highlighting that some countries’ GDP may be more exposed to extreme precipitation events than other countries.

**Figure 8. Some countries’ GDP is more exposed to extreme precipitation than other countries**

Average annual percentage of cropland exposed to  $n$  number of weeks of extreme precipitation and share of GDP from the Agriculture, forestry and fishing sector over the period 2017-2021



Note: Countries are ranked according to the average share of cropland exposed to one week or more of extreme precipitation over the period 2017-2021. Gross Domestic Product (GDP) values represent the average GDP value from Agriculture, forestry, and fishing over the period 2017-2021 (OECD, 2022<sup>[55]</sup>). These GDP values may overestimate agricultural GDP since it includes forestry and fishing. GDP values for Peru are derived from the World Bank national accounts. Further details on the methods are available in Annex A.

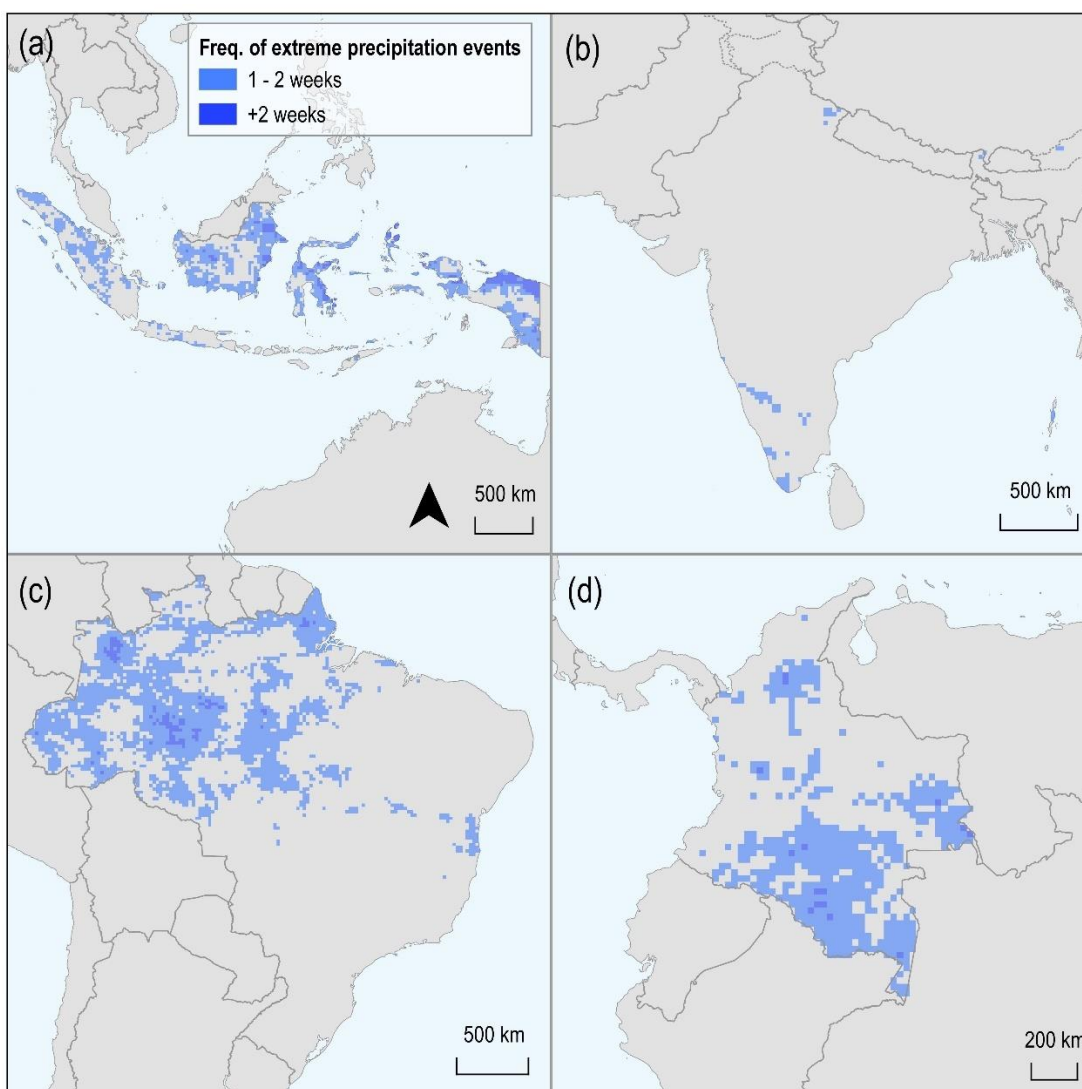
Going beyond national exposure, this indicator can also suggest potential exposure to extreme precipitation of global agricultural commodities and their supply chain. Indeed, some of the biggest producers of main primary crops are among the IPAC countries where cropland area is the most exposed to repeated extreme precipitation. For example, more than 5000 km<sup>2</sup> of cropland in Indonesia, India and Brazil was exposed to repeated extreme precipitation in 2021. According to the latest FAO data, Indonesia accounts for 59.8% of global oil palm fruit production and 7.23% of global rice production. India produces 23.5% of global rice output, 20.8% of global sugar cane output and 13.5% of global potato output. Meanwhile, Brazilian production of sugar cane and maize (corn) represents 38.6% and 8.8% of global output, respectively (FAO,

2021<sup>[56]</sup>). Some of the crops resist better to extreme precipitation events than other crops. For example, rice requires flooding to grow and therefore may not be significantly impacted by extreme precipitation events<sup>4</sup>.

In Indonesia, all provinces were exposed to repeated extreme precipitation days in 2021 (Figure 9a), while in India exposure was concentrated in the southern districts of Karnataka, Kerala, Tamil Nadu and the island of Andaman (Figure 9b). Finally, in Brazil, results show that extreme precipitation was mainly concentrated in the North and Central-West regions, including Brazilian states such as Acre, Amazonas, Mato Grosso, Rondônia, Roraima and Pará (Figure 9c).

### Figure 9. Large subnational variability in land exposure to extreme precipitation

Land exposure to more than one week of extreme precipitation events in 2021 for (a) Indonesia, (b) India, (c) Brazil and (d) Colombia



Note: Further details on the methods are available in Annex A.

<sup>4</sup> Identifying crop vulnerability to extreme precipitation events may provide a more detailed understanding of the impact on agriculture in specific countries and regions, depending on data availability.

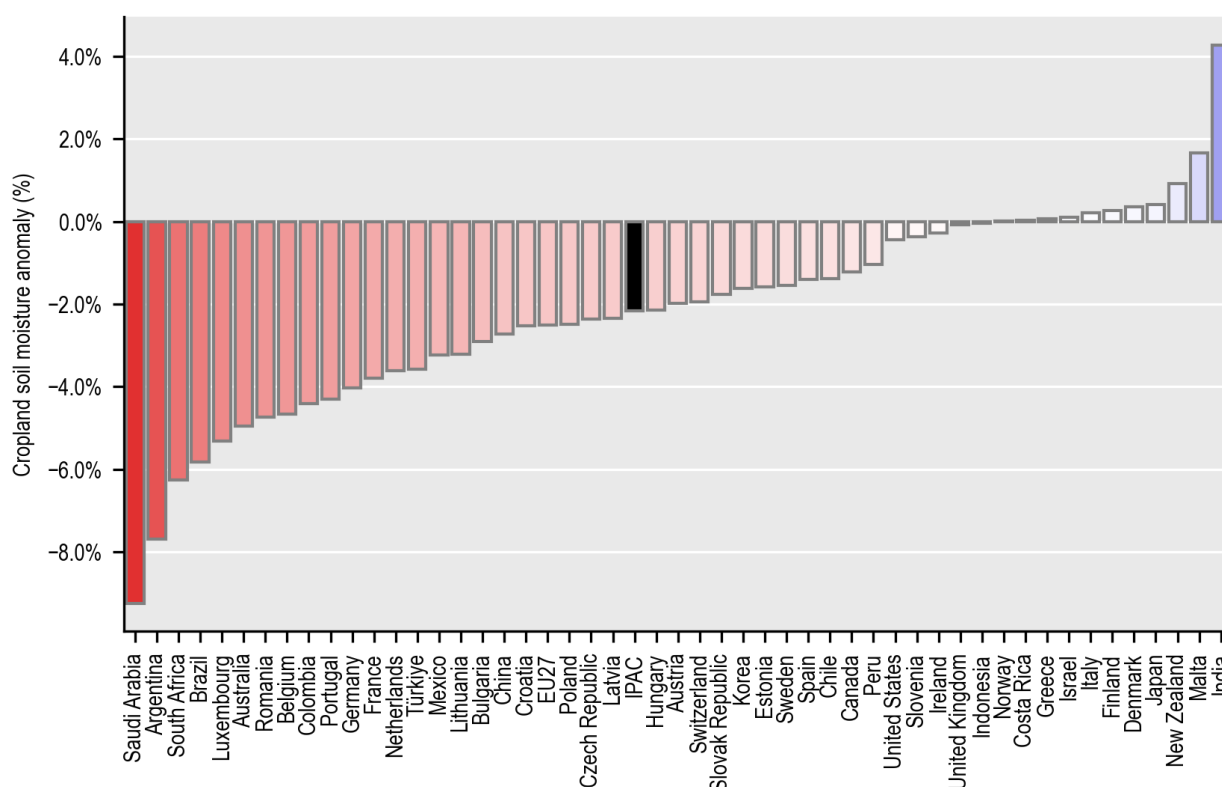
### 4.3. Drought

#### Soil moisture anomaly

Countries most affected by agricultural droughts are Saudi Arabia, Argentina and South Africa, which experienced a decline of more than 6% on average in cropland soil moisture in the past five years compared to 1981-2010 (Figure 10). However, these numbers correspond to the average soil moisture anomaly over the entire cropland area of countries, and can hide more severe local declines in soil moisture. In most countries, areas with a soil moisture anomaly below -10% are observed (Figure 12). In seven OECD countries (Australia, the United States, Canada, Spain, Mexico, Chile and Colombia) some areas recorded a drop in soil moisture of more than 30% on average over the past five years compared to 1981-2010. This paper also measures monthly soil moisture indices, which enables to detect more localised severe drought events.

**Figure 10. A majority of IPAC countries experience worsening droughts on croplands**

Soil moisture anomaly in cropland, 2017-2021 compared to the reference period 1981-2010



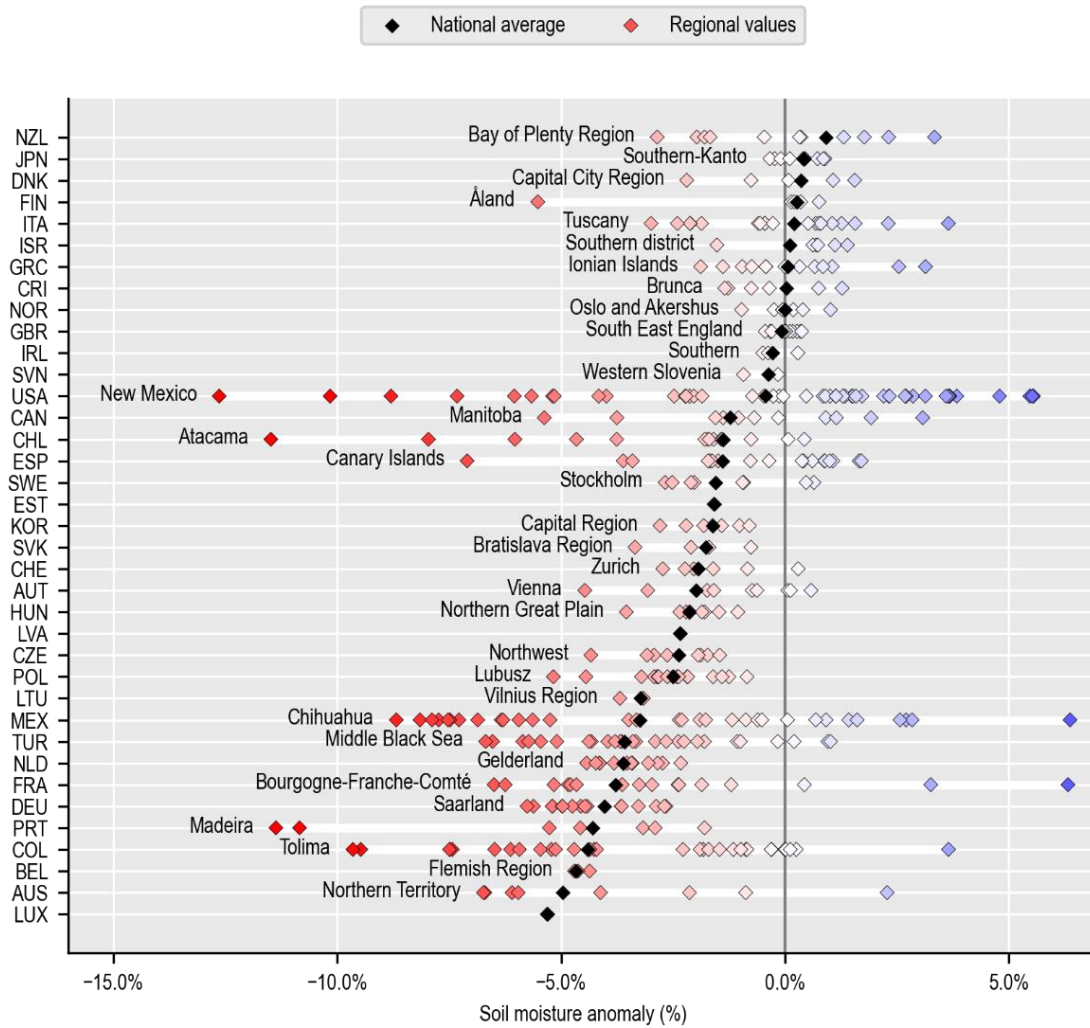
Note: Iceland is not included due to data unavailability. Further details on the methods are available in Annex A.

In almost 70% of OECD's large regions, cropland soil moisture was lower in the past 5 years than during the 1981-2010 reference period. Across and within countries, the impact of droughts on agriculture differs widely. The most impacted areas are mostly located in Australia, Western United States, Northern Mexico and Northern Chile (Figure 12). Among the most affected regions, Tolima in Colombia experienced a soil moisture decline of about 10% over the past 5 years compared to the reference period (Figure 11). In this region, Gross Value Added (GVA) in the agriculture, forestry, and fishing sector accounts for a significant

share of total GVA (more than 16%), which makes the economy of this region particularly vulnerable (OECD, 2022<sup>[57]</sup>).

**Figure 11. Changes in soil moisture differ widely across regions**

Soil moisture anomaly in cropland, 2017-21 compared to 1981-2010, OECD large regions (TL2)

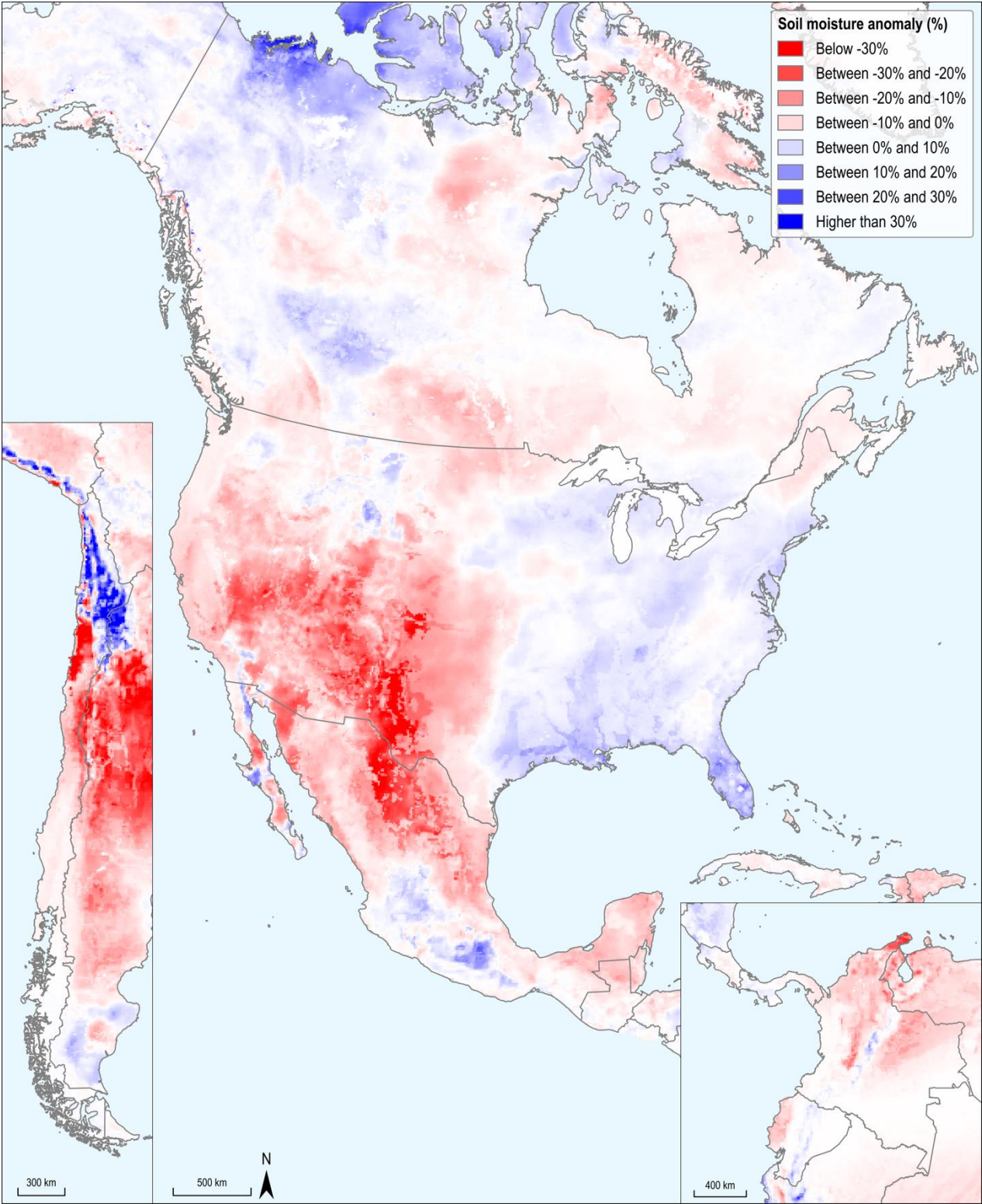


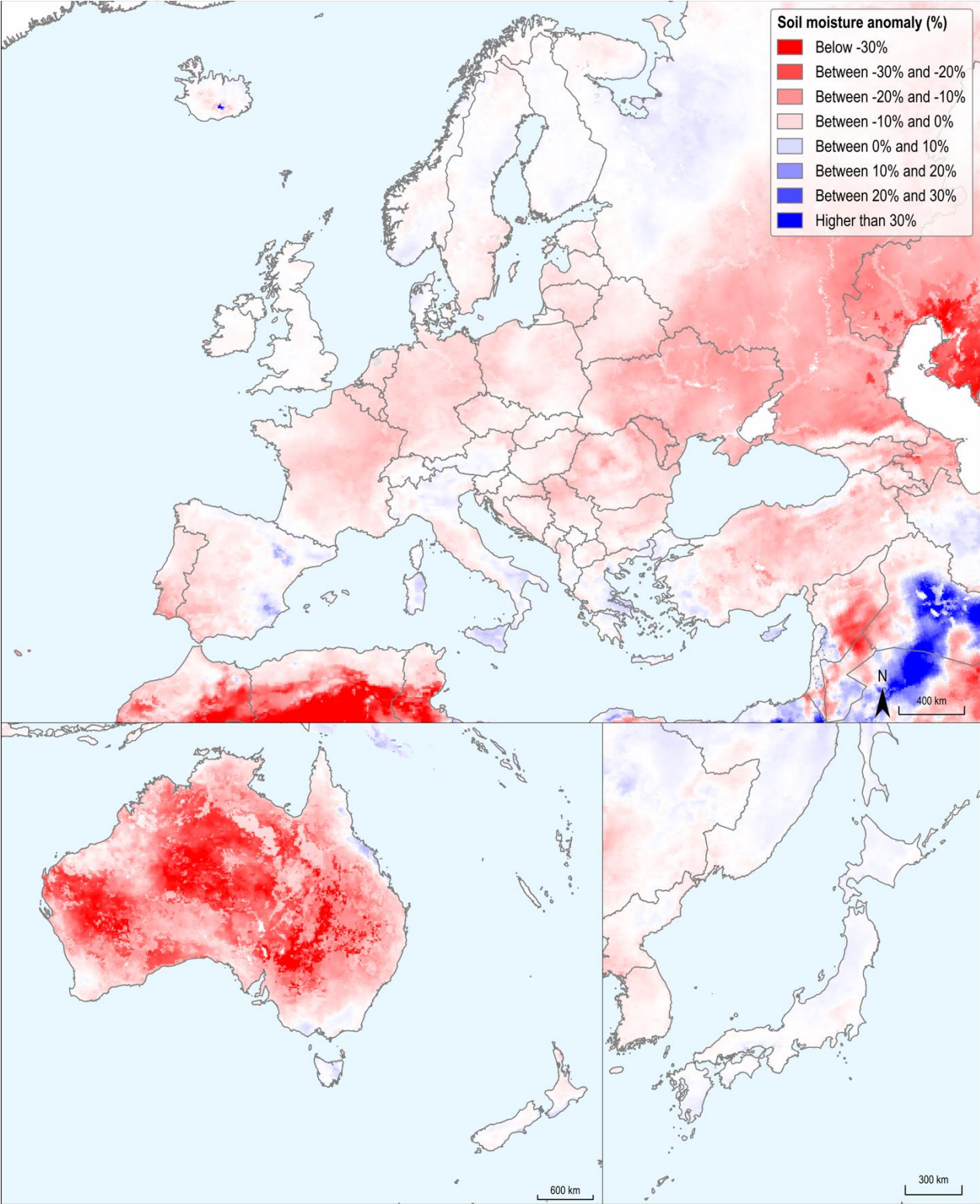
Note: Further details on the methods are available in Annex A.



Figure 12. Most countries show localised changes in soil moisture

Soil moisture anomaly 2017-21, compared to 1981-2010





## 4.4. Wildfire

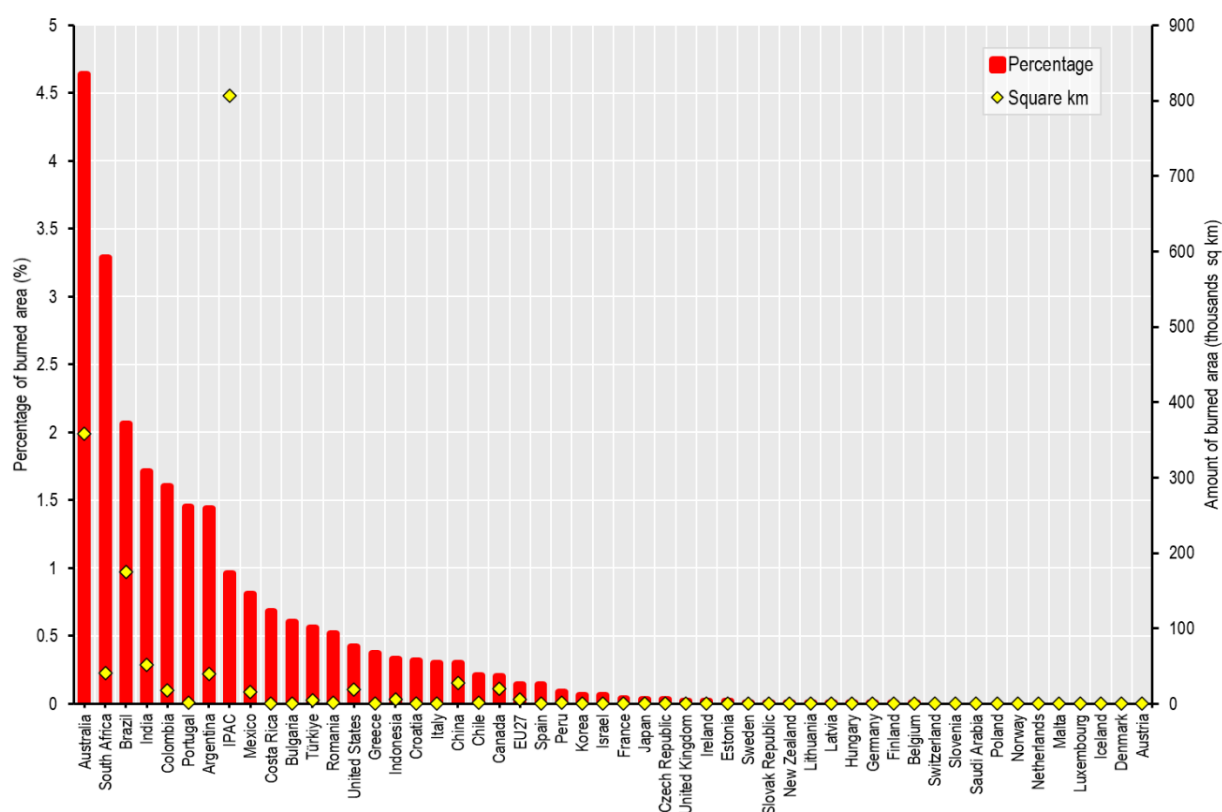
### Burned area extent

On average, more than 1% of land was burned per year over the period 2017-2021 in countries such as Argentina, Australia, Brazil, Colombia, India, Portugal and South Africa (Figure 13). In terms of the absolute amount of burned area, Australia and Brazil account for the largest share of burned land area globally (Figure 13). However, results do not differentiate between wildfire and controlled burning that is implemented to reduce the risk of severe, uncontrolled wildfires. Most of the area burnt in Australia, for example, is from controlled burning conducted for this purpose. This is further discussed in Section 6.

Overall, 20% of burned land globally in the past five years occurred in ten IPAC countries. These ten countries include three high-income economies (i.e. Australia, Canada and the United States), six upper-middle income economies (i.e. Argentina, Brazil, China, Colombia, Mexico and South Africa) and one lower-middle income economy (i.e. India), suggesting wide disparities in terms of labour-constraints, financing needs as well as fuel management wildfire policy implementation and coping capacity<sup>5</sup>.

Figure 13. A small subset of IPAC countries represent the majority of burned area

Amount and percentage of burned area, annual average over the period 2017-2021



Note: Further details on the methods are available in Annex A.

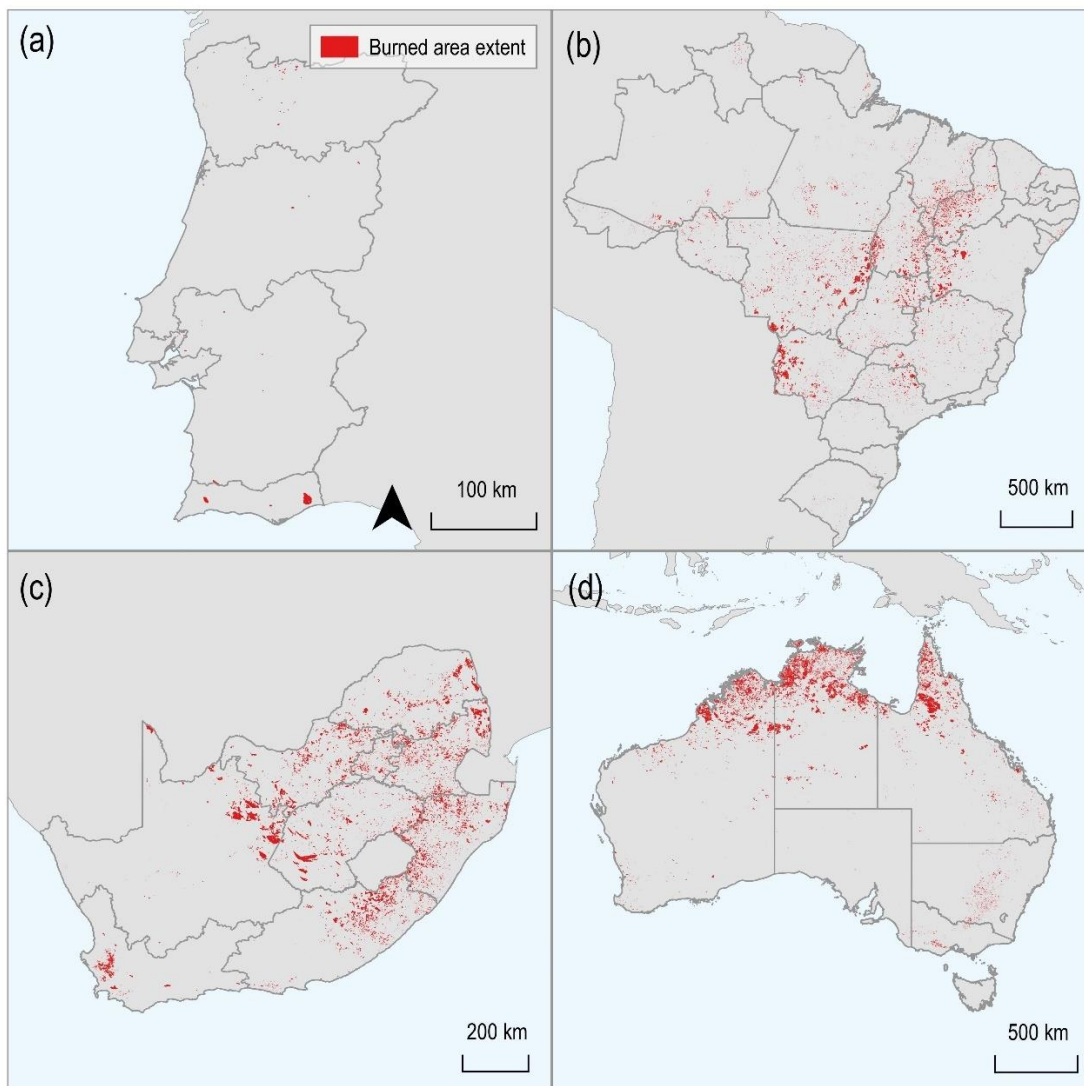
<sup>5</sup> World Bank classification of GDP per capita (2022). lower-middle income economy (USD 1,046-4,095); upper-middle income economy (USD 4,096-12,695); high-income economy (USD 12,696 or more).



The majority of burned area in Portugal was situated in the region of the Algarve (Figure 14a), while fires in Brazil span from the northeast region to the central west region. The states of Piaui, Maranhao, Tocantins, Bahia, Goias, Mato Grosso and Mato Grosso do Sul were particularly exposed to fires (Figure 14b). In South Africa, fires were mainly concentrated in the eastern provinces of Limpopo, Mpumalanga, Gauteng, North West Province, Kwazulu-Natal, Free State and Eastern Cape (Figure 14c). In Australia, some areas are burnt in managed fires to prevent large uncontrolled fires and are part of cultural practices such as in the north of Australia (Figure 14d). Therefore, not all burned areas represent a risk for humans and economic assets, having limited negative environmental and societal impacts. Nevertheless, Australia did experience extreme wildfires across many areas of the country during the summer 2019-2020, particularly in the Southeast region of the country. The number of fires, their severity and extent, and the damage caused to infrastructure and the environment were unprecedented, covering between 24 and 40 million hectares of land (Royal Commission, 2020<sup>[58]</sup>).

**Figure 14. Substantial variation in burned area extent between countries**

Burned area extent for (a) mainland Portugal, (b) Brazil, (c) South Africa and (d) Australia in 2021



Note: Results for Australia may overestimate actual wildfire events because larger 'prescribed' fires are part of the cultural practises and are increasingly re-introduced in present-day fire management techniques; this is discussed in Section 6. Further details on methods are in Annex A.

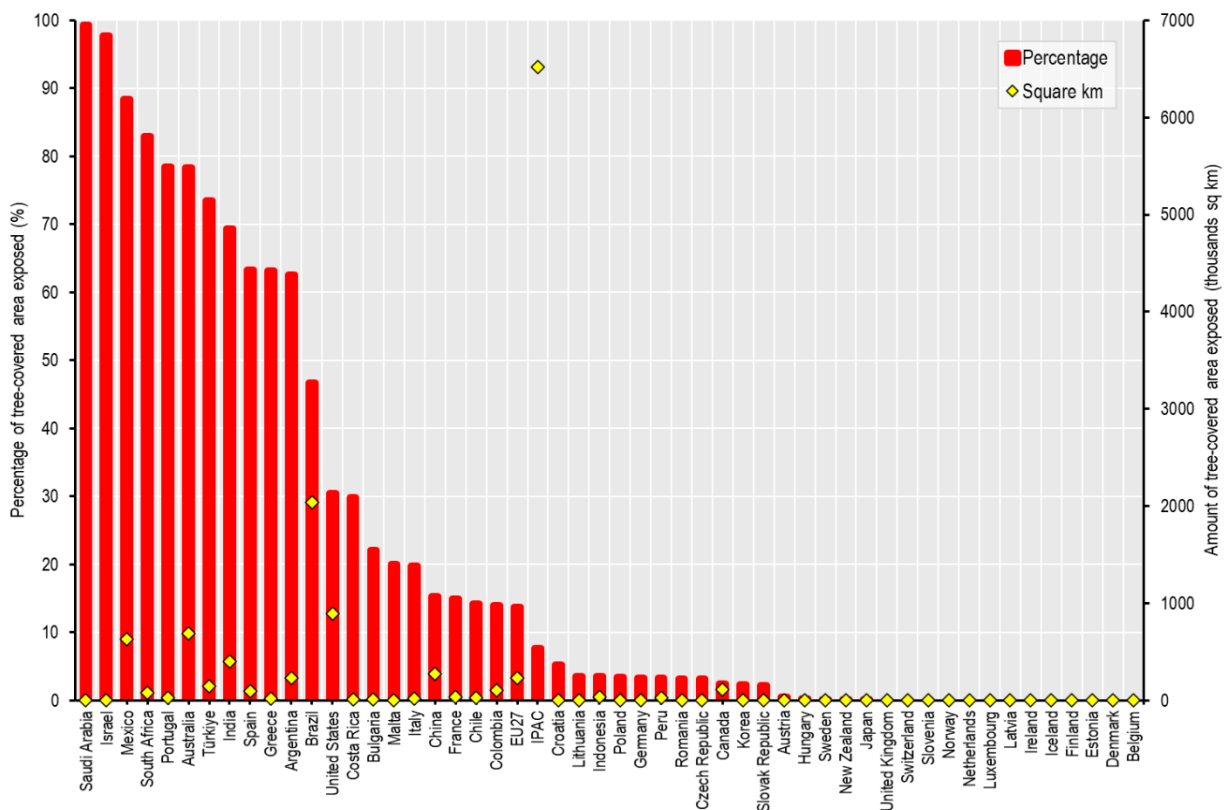
### Forest exposure to wildfire danger

Overall, forest areas exposed to more than three consecutive days of very high or extreme wildfire danger show patterns of distribution similar to previous wildfire indicators. The risk classes indicate the danger of forest fires based on numerical weather data. Over the past five years, Brazilian forests experienced the biggest absolute exposure (~2 million km<sup>2</sup>) to very high or extreme fire risk (Figure 15). Other countries such as the United States, Australia and Mexico also have considerable amounts of forest exposed, with 894 thousand km<sup>2</sup>, 701 thousand km<sup>2</sup> and 632 thousand km<sup>2</sup> of forest areas exposed to very high or extreme fire risk respectively. By mapping forest areas exposed to very high or extreme fire risk, this indicator can also indicate where and what type of forest may be at risk of fire. Forest ecosystems are a critical component of the world’s biodiversity as many forests are more biodiverse than other ecosystems (FAO, 2020<sup>[59]</sup>). For example, forests in three out of ten countries most exposed to fire risk in terms of absolute area (i.e. Brazil, Mexico and China) are amongst the forests with the biggest tree species endowment on the globe (FAO, 2020<sup>[59]</sup>).

Forests in Middle Eastern countries (e.g. Israel and Saudi Arabia) are entirely exposed to very high or extreme fire risk (Figure 15). However, Israel and Saudi Arabia are characterized by low (< 10%) and very low (< 1%) forest cover, respectively, highlighting the importance to account for both the absolute and relative extent of forest exposure to risk of burning.

**Figure 15. In a third of IPAC countries over 20% of forests are exposed to very high or extreme fire danger**

Amount and percentage of tree-covered area exposed to very high (> 5) or extreme (> 6) fire danger for more than three consecutive days, annual average over the period 2017-2021



Note: Further details on the methods are available in Annex A.

**Population exposure to wildfire danger**

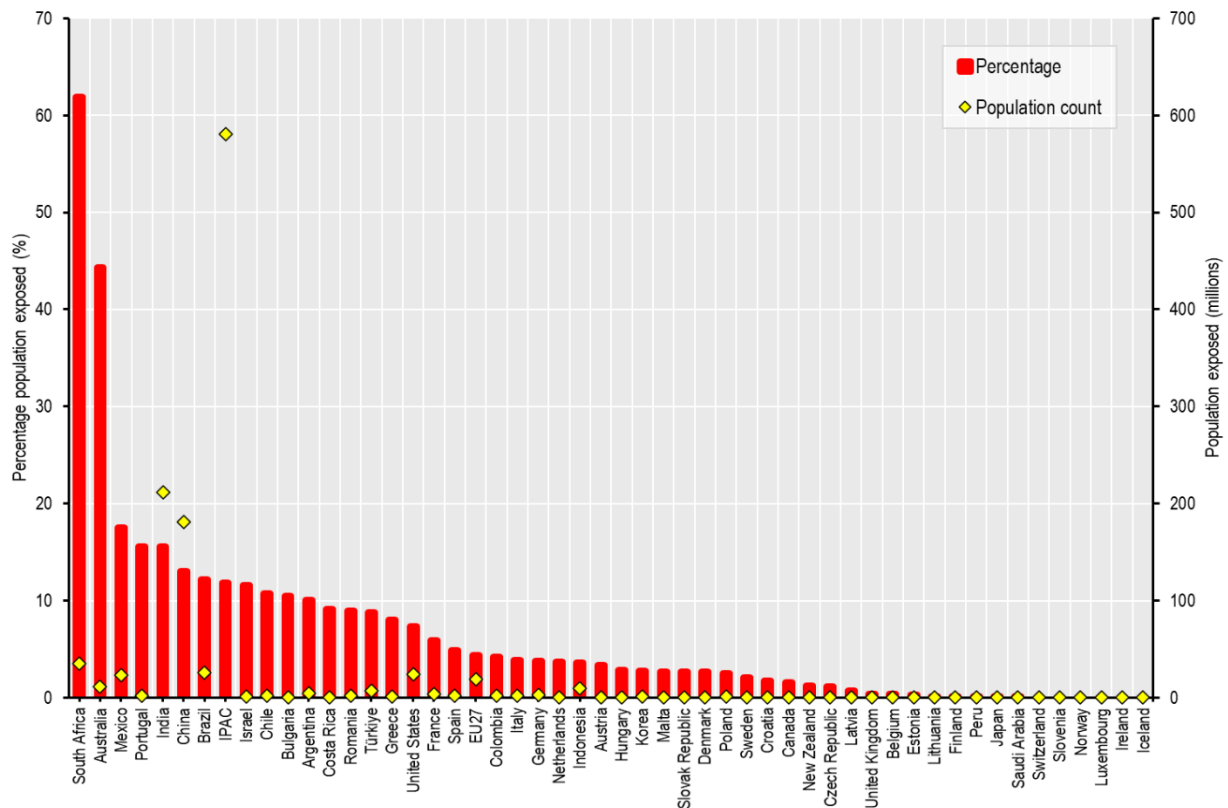
Population exposure to wildfire danger assesses locations where populations are exposed to a very high wildfire danger and accounts for vegetation biomass as well as historical fire events and burned area data. In 2021 alone, more than 25% of Australia’s population was exposed to a very high wildfire danger, while approximately 10% of the population in South Africa, India and Mexico and between 5% and 10% of population in Costa Rica, Israel and Chile lived in areas with a very high wildfire danger. However, 2021 was a La Niña year in the Pacific region, leading to cooler than average temperatures across most of mainland Australia.

Over the last five years, an annual average of 62% of the population in South Africa and 44% of the population in Australia was exposed to a very high wildfire danger (Figure 16). In other IPAC countries, more than 10% of population was exposed to a very high wildfire danger, including four countries in the Americas (i.e. Argentina, Brazil, Chile and Mexico), two European countries (i.e. Bulgaria and Portugal), two Asian countries (i.e. China and India) and one country in the Middle East (i.e. Israel).

When investigating the total amount of exposed population, India’s population is the most exposed to a very high wildfire danger. In 2021 alone, 160 million people were living in areas with a very high wildfire danger in India, and an annual average amount of 200 million people were living in areas with a very high wildfire danger in India between 2017 and 2021 (Figure 16). In addition, China and South Africa have an annual average of more than 30 million people exposed to very high wildfire danger between 2017 and 2021.

**Figure 16. In eleven IPAC countries over 10% of population lives in areas exposed to very high or extreme wildfire danger**

Amount and percentage population exposed to very high or extreme wildfire danger, annual average over 2017-2021



Note: Further details on the methods are available in Annex A.

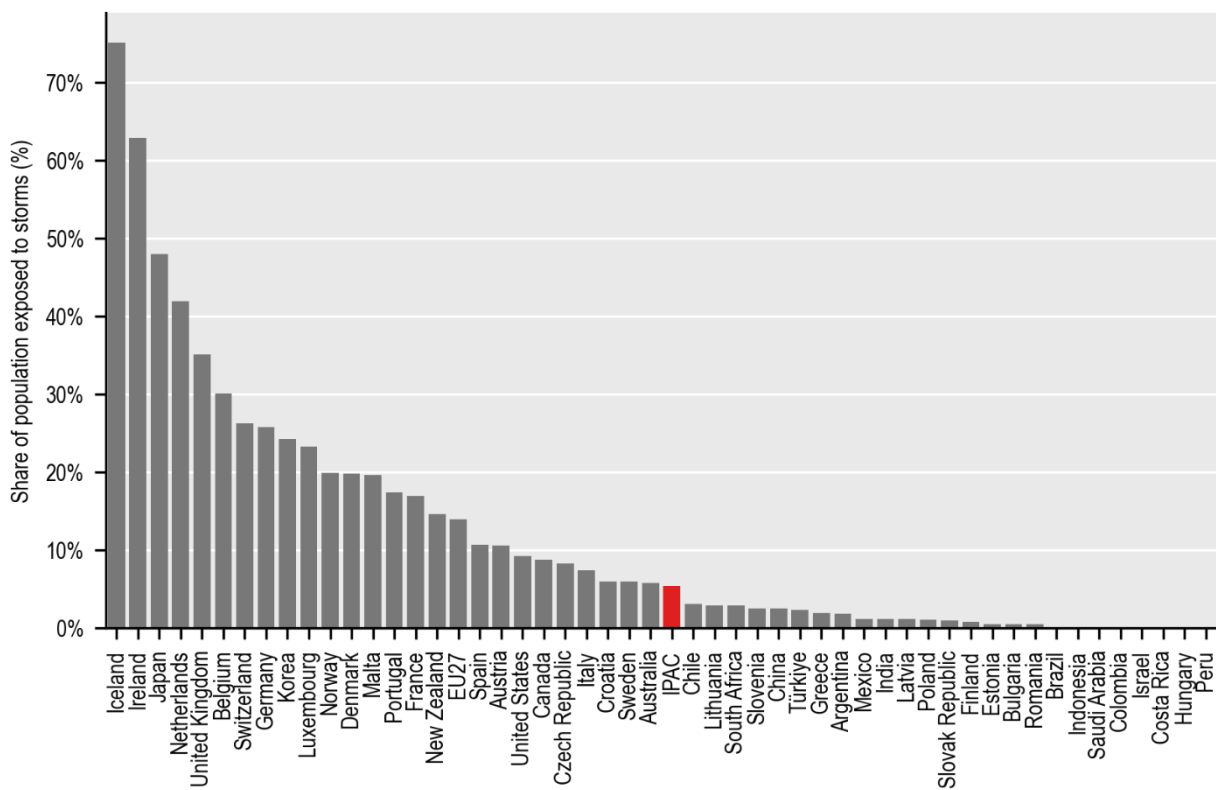
## 4.5. Wind threats

### Storms

Figure 17 and Figure 18 show respectively the share of population and built-up area exposed to violent storms in the last three years. Countries most exposed to violent storms are located mostly in north-western Europe and eastern Asia. Countries such as Iceland, Ireland, the United Kingdom, the Netherlands and Belgium had more than 80% of their population and built-up areas exposed to violent storms in 2020, highlighting the importance of accounting for wind threats as a climate-related natural hazard. Recall that this paper examines the exposure to wind-related hazards, and not the vulnerability of infrastructures or settlements to such hazards.

**Figure 17. Populations in northwestern Europe and eastern Asia are exposed to violent wind storms**

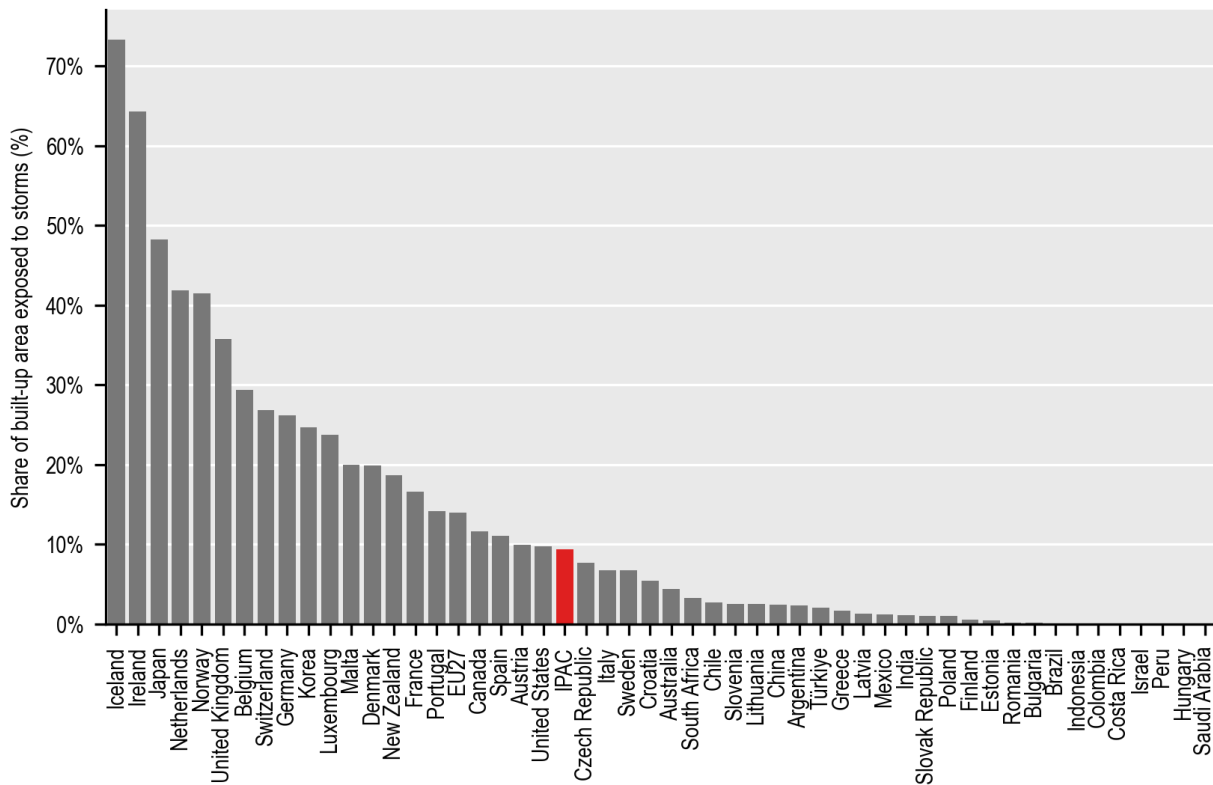
Percentage of population exposed to violent storms or worse (wind gust speed > 28.6 m/s), annual average over the period 2017-2021



Note: Further details on the methods are available in Annex A.

**Figure 18. Built-up areas in northwestern Europe and eastern Asia are exposed to violent wind storms**

Percentage of built-up area exposed to violent storms or worse (wind gust speed > 28.6 m/s), annual average over the period 2017-2021



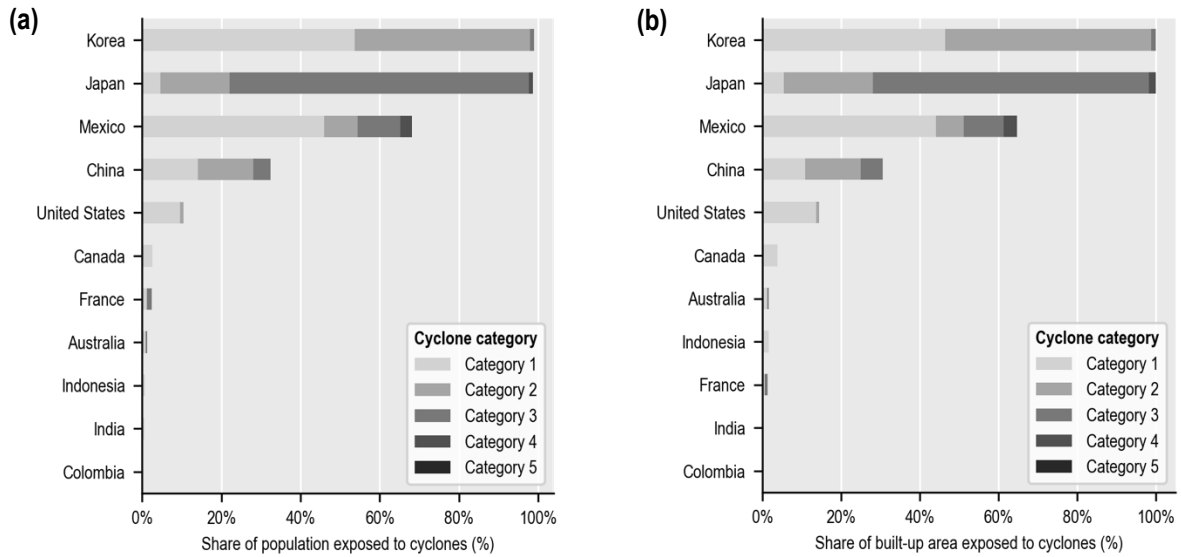
Note: Further details on the methods are available in Annex A.

### Cyclones

This paper also assesses population and built-up exposure to cyclones by looking at cyclone hazard maps, expressed in wind gusts (km/h) with a 100-year return period. To categorise the different cyclone intensities, the Saffir-Simpson hurricane scale is used, which is based on sustained wind speed. To match this wind scale, wind gust values were readjusted by considering that wind gust speed is around 30% higher than sustained wind speed. (Figure 19). The most exposed IPAC countries are Korea, Japan and Mexico where more than 60% of both their population and built-up areas are exposed to tropical cyclones (i.e. sustained wind speed higher than 119 km/h or 33 m/s) with a 100-year return period. Japan is the country most exposed to violent cyclones, as almost 80% of its population is exposed to cyclones of category 3 or higher (wind speed higher than 178 km/h) with a 100-year return period.

**Figure 19. A small subset of IPAC countries is exposed to tropical cyclones**

Percentage of (a) population and (b) built-up area exposed to cyclone categories with a 100-year return period



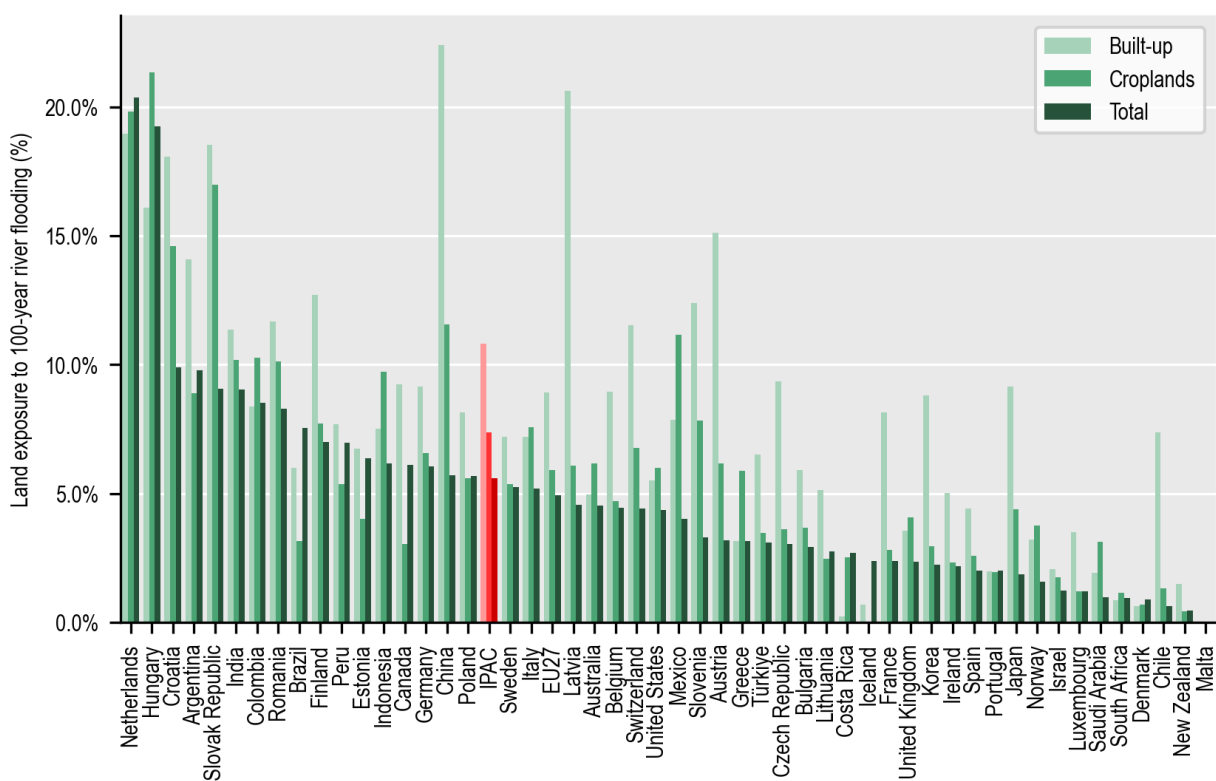
Note: Wind gust (km/h) data with a 100-year return period were first converted to sustained wind speed and separated into cyclone categories using the Saffir-Simpson scale. Further details on the methods are available in Annex A.

### 4.6. River flooding

River flooding can cause substantial economic losses, by damaging infrastructure, settlements, and agricultural lands. In terms of total land exposure to river flooding, the most exposed IPAC countries are the Netherlands and Hungary, with around 20% of total area exposed to river flooding (Figure 20). In terms of built-up area exposure, China is the most exposed country with 22% of its built-up area exposed to a 100-year river flood, followed by Latvia (21%), and the Netherlands (19%). In terms of agricultural land exposure, the most impacted IPAC countries are Hungary, the Netherlands, and the Slovak Republic with more than 17% of their cropland exposed to 100-year river flooding.

**Figure 20. IPAC countries are exposed to river flooding to varying degrees**

Built-up area, cropland and total land in 2020 exposed to river flooding with a 100-year return period

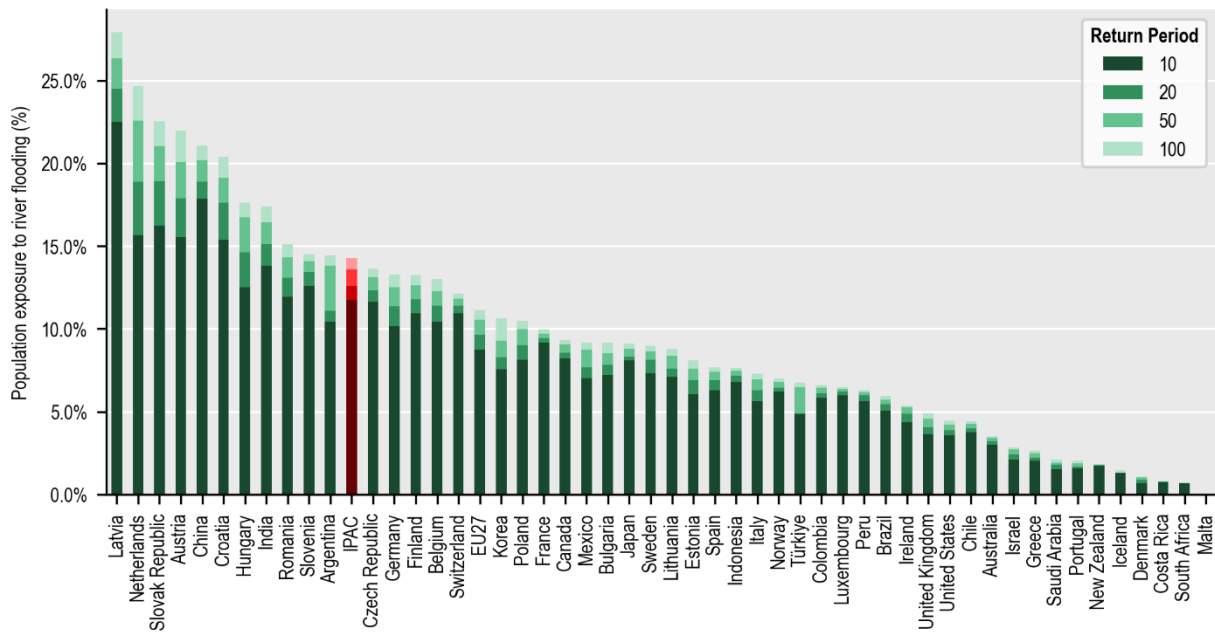


Note: Further details on the methods are available in Annex A.

River flooding can also cause significant human losses. Among the IPAC countries, populations in Latvia and the Netherlands are the most exposed to river flooding with more than 24% of people exposed to a 100-year flood (Figure 21). China and India are also particularly exposed to such hazard with respectively 21% and 17% of their population exposed to a 100-year flood. These two countries also experienced the largest increase in population exposure to river flooding with respectively 3.0 million and 5.3 million additional people exposed in 2015 compared to 2000.

**Figure 21. River flooding exposes many populations in most IPAC countries**

Population in 2020 exposed to river flooding with a 10-, 20-, 50- and 100-year return period



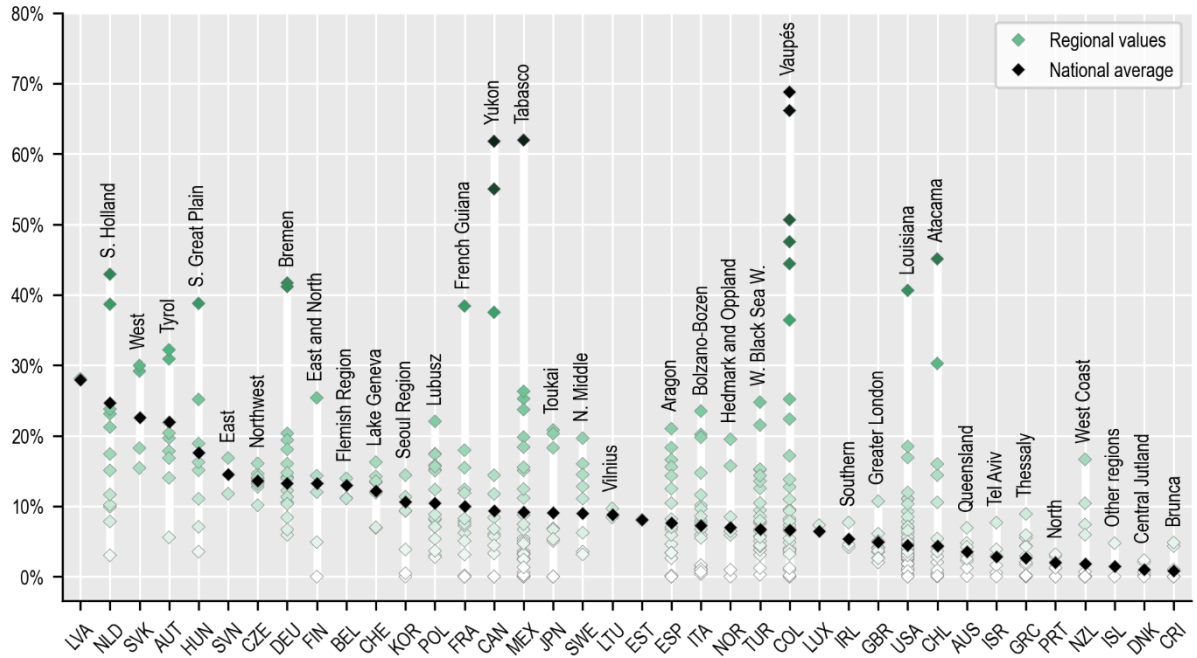
Note: 2020 population data is interpolated from the GHSL 2015 and 2000 population grids. Further details on the methods are available in Annex A.

There are also large subnational disparities in exposure to river flooding. Bremen, South Holland, and Hamburg are the most exposed regions in European OECD countries, with more than 40% of their populations exposed to a 100-year flood (Figure 22). With more than 60% of its population at risk, Rotterdam in the Netherlands is the most exposed OECD metropolitan area of more than 1.5 million inhabitants, followed by Nagoya in Japan and Lyon in France.



Figure 22. Considerable subnational variation in population exposure to river flooding

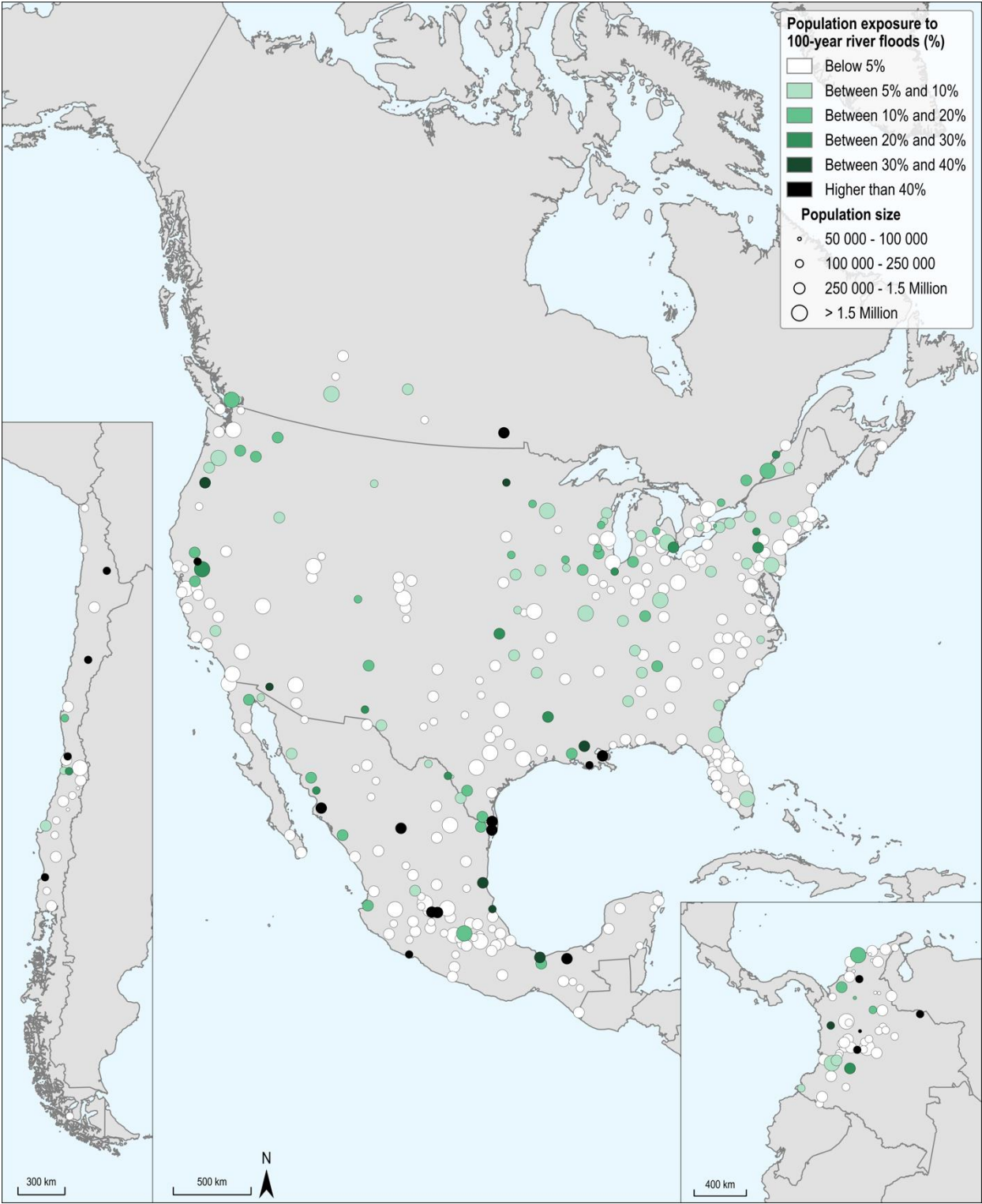
Population in 2020 exposed to 100-year river flooding in OECD large regions (TL2)

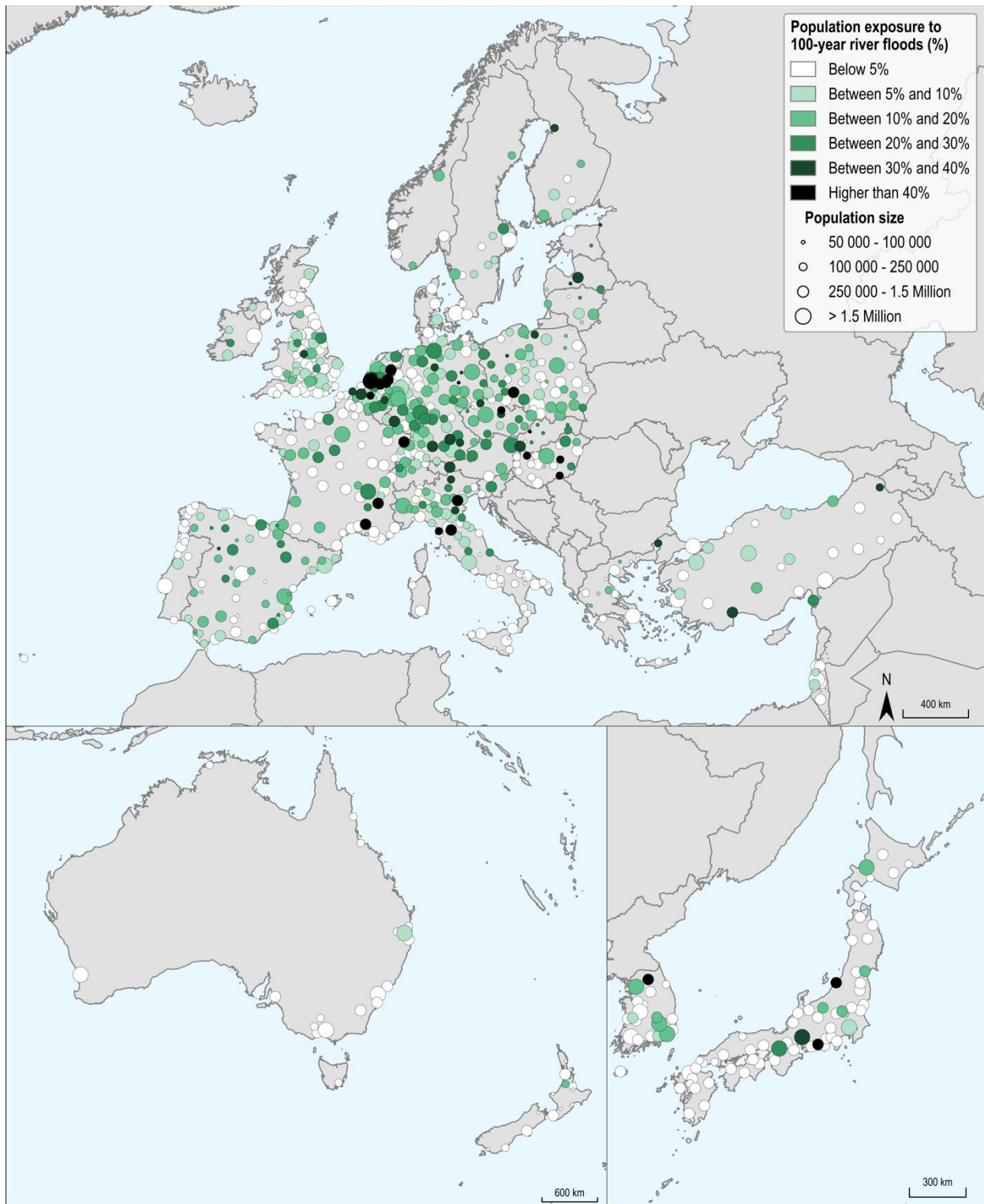


Note: Further details on the methods are available in Annex A.

Figure 23. Considerable city-level variation in population exposure to river flooding

Percentage of population in 2020 exposed to 100-year river flooding in OECD cities





Note: Further details on the methods are available in Annex A.

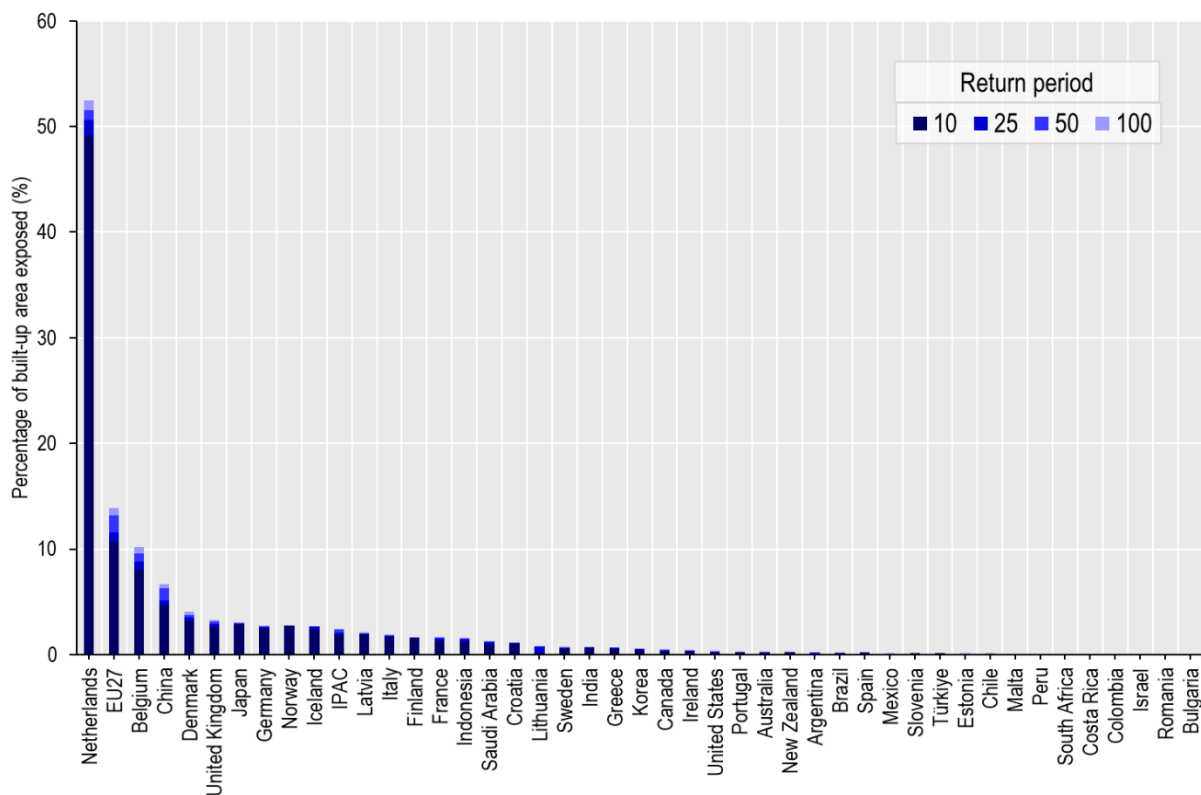
## 4.7. Coastal flooding

Low-lying coastal communities face a range of coastal flooding hazards such as storm surges and coastal erosion. All of these hazards are expected to increase as climate change increases the frequency and severity of coastal floods. In this paper, exposure indicators for coastal flooding hazards are developed using flood hazard maps of storm surges and extreme sea level events. These maps do not account for sea level rise. The most exposed countries are the Netherlands, Belgium and Denmark, of which the Netherlands has approximately 51% of land area potentially exposed to coastal flooding with a 10-year return period, followed by 6.3% and 5.6% for Belgium and Denmark, respectively. These figures should be interpreted with caution because they do not account for existing flood protection measures; nevertheless, they also point to the importance of maintenance of existing protections to prevent future exposures.

In line with previous results, 9 out of 45 IPAC countries have more than 2% of built-up area potentially exposed to coastal flooding with a 10-year return period (Figure 24). The Netherlands is the most exposed with 48.1% of its built-up area potentially exposed to coastal flooding with a 10-year return period, followed by Belgium (7.1%) and China (4.3%) (Figure 24). This reflects the fact that much of the land along the North Sea coast is either below sea level or just slightly above it, exposing a sizeable amount of the land and its built-up areas to coastal flooding hazards (Figure 25).

**Figure 24. A subset of countries has a sizeable part of built-up area potentially exposed to coastal flooding**

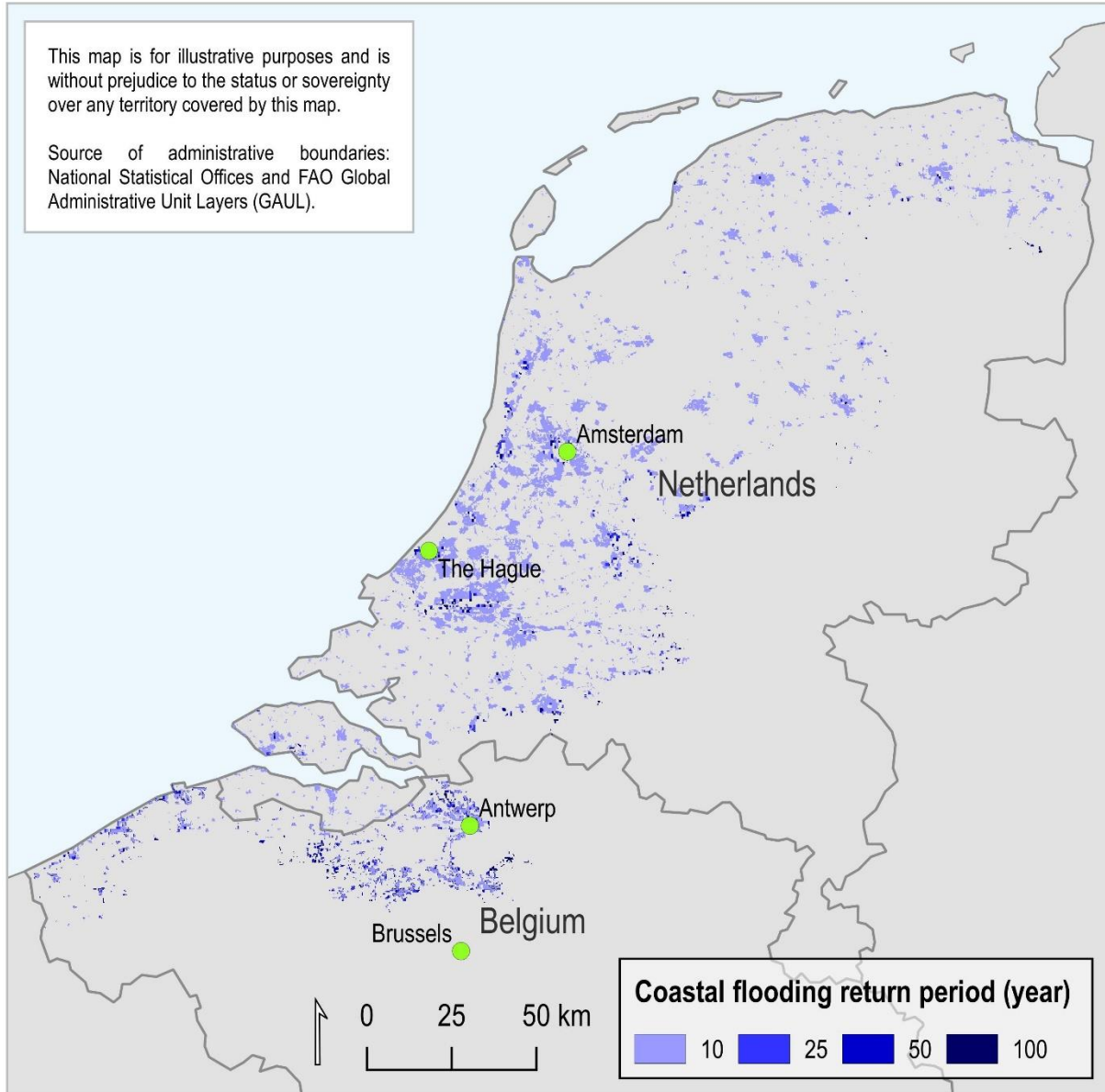
Built-up area in 2020 exposed to coastal flooding with a 10-, 25-, 50- and 100-year return period



Note: Exposure in some countries may be over-estimated because the indicator does not account for flood protection measures. The following countries are not included in the figure because these countries have no coastal zones (i.e. Austria, Czech Republic, Hungary, Luxembourg, Slovak Republic and Switzerland). For details on methods, see Annex A.

**Figure 25. In the absence of coastal protections, large areas of built-up area would be at risk of coastal flooding in Belgium and the Netherlands**

Visualisation of built-up area in 2020 exposed to coastal flooding with a 10-, 25-, 50- and 100-year return period



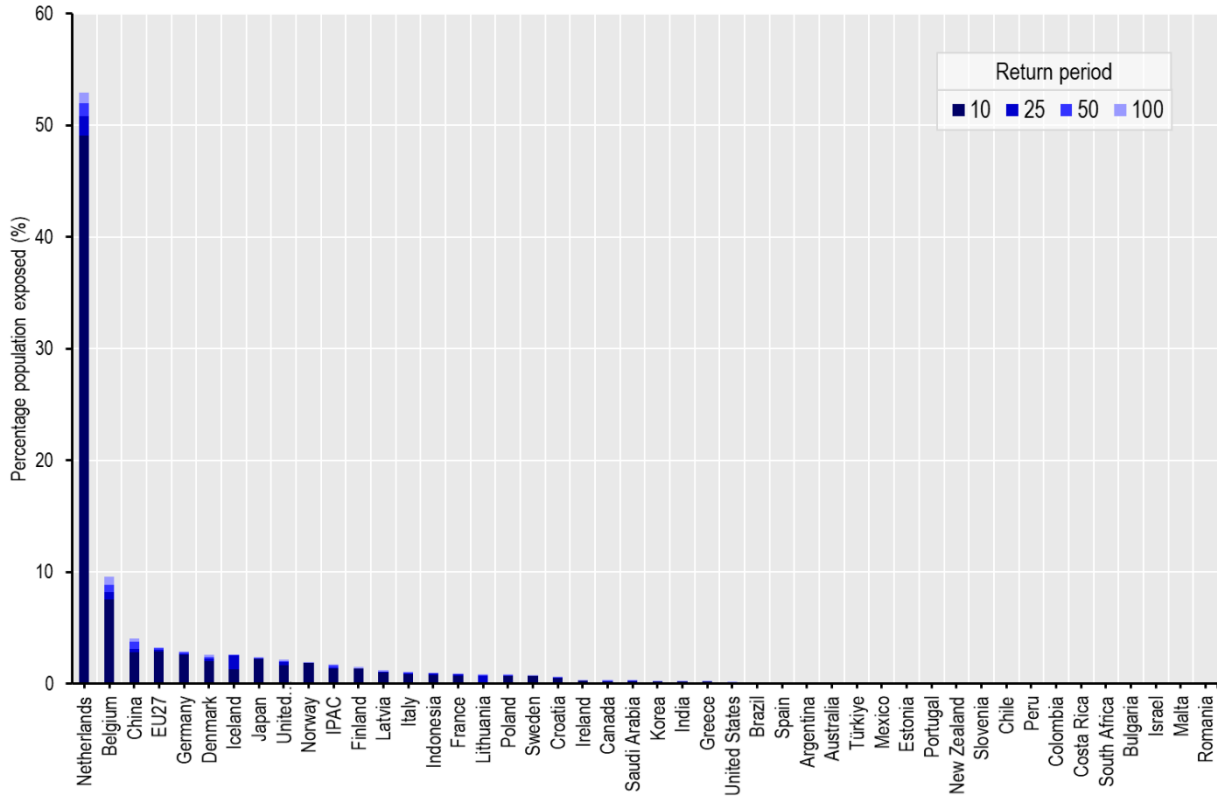
Note: Exposure in some countries may be over-estimated because the indicator does not account for flood protection measures. For details on methods, see Annex A.

Similarly, 7 out of 45 IPAC countries shown here have more than 2% of the population potentially exposed to coastal flooding with a 10-year return period (Figure 26). The Netherlands is the most exposed with 49% of its population potentially exposed to coastal flooding with a 10-year return period, representing approximately 8.2 million people. It is followed by Belgium (7.5% or 0.8 million people), China (2.8% or 39 million people) and the European Union (2.9% or 12.8 million people) (Figure 26).



**Figure 26. A subset of countries has a sizeable part of the population potentially exposed to coastal flooding**

Population in 2020 exposed to coastal flooding with a 10-, 25-, 50- and 100-year return period



Note: Exposure in some countries may be over-estimated because the indicator does not account for flood protection measures. The following countries are not included in the figure because these countries have no coastal zones (i.e. Austria, Czech Republic, Hungary, Luxembourg, Slovak Republic and Switzerland). Population data for 2020 is interpolated from the GHSL 2015 and 2000 population grids and will be updated once 2020 population data is available. For details on methods, see Annex A.

# 5 Discussion

This paper analyses some of the most common climate-related hazards and presents the estimated exposure associated with each hazard. The results suggest that there is considerable exposure of built-up areas, cropland, forests and the population, varying with the climate-related hazard studied. In fact, all countries experience one or more climate-related hazards (Figure 27). Results show significant differences across countries in exposure to different numbers of climate-related hazards with varying degrees of intensities of exposure. This is in line with the literature (Birkmann, 2015<sup>[60]</sup>).

**Figure 27. Most countries experience at least one climate-related natural hazard**

Country ranking from lowest (yellow) to highest (red) exposure to extreme temperature and precipitation, drought, wildfire, wind threats, river and coastal flooding; no exposure is marked green

	Extreme temperature			Extreme precipitation	Drought	Wildfire		Wind threats		River flooding	Coastal flooding
	Hot days	Tropical nights	Heat stress	Cropland exposure	Cropland exposure	Population exposure	Forest exposure	Population exposure	Built-up area exposure	Built-up area exposure	Built-up area exposure
Argentina	3	11	11		5	11	11	34	32	8	30
Australia	6	13	18		3	2	5	26	26	37	30
Austria	28	37	32		24	25	35	19	20	7	NA
Belgium	20	15	38		4	39		6	7	20	2
Brazil	8	6	4	5	9	7	12	44	44	32	30
Bulgaria	18	30	24		15	10	15	42	43	33	
Canada	36	28	34			34	32	21	18	16	24
Chile	35	47	27	13	35	9	20	27	28	27	35
China	4	5	9	13	18	6	18	31	31	1	3
Colombia	27	38	7	3	13	20	21	47	46	22	
Costa Rica	40	8	5	4	36	12	14			50	
Croatia	21	18	21		26	33	23	24	25	5	17
Czech Republic	33	35	36		17	36	31	22	22	15	NA
Denmark		45	46	11	37	29		12	13	49	5
Estonia		43	43		31	40	27	41	41	30	
EU27	23	25	26	13	22	19	22	17	17	18	7
Finland		44	47	13		42		40	40	9	11
France	14	22	29		10	17	19	15	15	14	15
Germany	24	27	35		7	22	29	8	9	19	9
Greece	7	16	14		40	15	10	33	34	42	23
Hungary	13	4	22		30	26	36			6	NA
Iceland					41			1	1	48	10
India	1	1	2			5	8	36	37	13	20
Indonesia	30	10	1	1	33	24	25	45	45	26	12
Ireland			50	7	39			2	2	36	25
Israel	5	19	6			8	2			43	
Italy	16	12	15			21	17	23	23	29	14
Japan	17	14	19	11		44	39	3	3	17	6
Korea	12	7	20		23	27	33	9	10	21	21
Latvia		40	42		21	37		37	35	2	13

Lithuania		42	41		14	41	24	28	30	35	22
Luxembourg	31	41	39		2			10	11	40	NA
Malta		2	25			28	16	13	12		
Mexico	22	33	8	8	19	3	3	35	36	24	29
Netherlands	29	29	40		6	23		4	4	3	1
New Zealand		31	45			35	38	16	14	46	30
Norway		48	49	6				11	5	41	4
Peru	37	32	13	2	32	43	28			25	
Poland	34	36	37	9	16	31	26	38	39	23	19
Portugal	26	24	28		11	4	6	14	16	44	27
Romania	19	26	23		8	13	30	43	42	11	
Saudi Arabia	2	3	3		12	45	1	46		45	16
Slovakia	25	39	31		29	30	34	39	38	4	NA
Slovenia	32	21	30		38	46		30	29	10	
South Africa	11	23	12		1	1	4	29	27	47	
Spain	9	17	17	13	28	18	9	18	19	38	34
Sweden		46	48		27	32	37	25	24	28	18
Switzerland	38	34	33		25			7	8	12	NA
Turkey	15	20	16		20	14	7	32	33	31	28
United Kingdom	39	49	44	9	34	38		5	6	39	8
United States	10	9	10			16	13	20	21	34	26

Note: Countries are ranked for each climate-related hazard through a series of assumptions. Extreme temperature ranking is based on the (1) average annual share of population exposure to hot days ( $T_{\max} > 35^{\circ}\text{C}$ , 2017-21), (2) average annual share of population exposure to tropical nights ( $T_{\min} > 20^{\circ}\text{C}$ , 2017-21) and (3) average annual number of days with strong heat stress ( $\text{UTCI} > 32^{\circ}\text{C}$ , 2017-21). Extreme precipitation ranking is based on the average annual share of cropland exposed to more than 7 days with extreme precipitation events (total precipitation  $> 99^{\text{th}}$  percentile of the reference period [1981-2010]) (2017-21). Drought ranking is based on the average cropland soil moisture anomaly 2017-21 compared to the reference period 1981-2010. Wildfire ranking is based on the average annual percentage of population and forests located in wildfire-prone areas (2017-21). Wind threats ranking is based on population and built-up exposure to a violent storm or worse (wind gusts  $> 28.6$  m/s, 2017-21). River and coastal flooding ranking is based on the percentage of built-up area exposed to a 100-year river or coastal flood (2020). Climate-related hazards not applicable to countries are crossed out. These results are based on national averages and may hide more severe local impacts of climate-related hazards.

Interconnected climate-related natural hazards pose considerable risk to certain countries, meaning that one climate-related hazard may reinforce or undermine other climate-related hazards and hence could exacerbate socio-economic impacts. Interconnected climate-related hazards may result in complex interactions, which are difficult to account for. For example, extreme temperatures are associated with drought conditions (Chikamoto et al., 2017<sup>[61]</sup>) (Karl et al., 2012<sup>[62]</sup>), which in turn can facilitate the occurrence and intensity of wildfires (Littell et al., 2016<sup>[63]</sup>). Similarly, Brazil experiences drought conditions, affecting croplands, suggesting an impact on the food supply. Results show that Brazil has been experiencing an intensification of burning between 2018 and 2020, of which part is caused by human activity mostly through deforestation (Pivello et al., 2021<sup>[64]</sup>). In addition, drought events have been associated with an intensification of fires in Brazil (Cunha et al., 2019<sup>[65]</sup>), illustrating the interconnectedness between climate-related hazards such as drought and wildfires in Brazil. This may have other socio-economic impacts not accounted for in this paper, which could include, for example, serious drought conditions in 2021 that are causing an energy crisis because Brazil is heavily reliant on hydroelectric generation (IEA, 2021<sup>[66]</sup>) (Millard and Chediak, 2021<sup>[67]</sup>). Increased occurrence and intensity of climate-related hazards result in greater food, water, and energy insecurity, highlighting the urgency to address climate change issues.

This paper illustrates a significant impact of extreme heat events across all countries studied, indicating an urgent need to develop evidence-based adaptation plans. In 2017, approximately 30% of the world population was exposed to deadly heat (Mora et al., 2017<sup>[68]</sup>), and an estimated 54% of the world population is expected to be exposed to more than 20 days of dangerous heat a year by 2100 at a  $2^{\circ}\text{C}$  warming (Jay et al., 2021<sup>[69]</sup>). Although air conditioning is becoming more widely available around the world, it remains financially unaffordable for the most vulnerable communities, and is environmentally costly (IEA, 2018<sup>[70]</sup>). The discrepancy between cooling needs and cooling capabilities for households and individuals, also called the cooling gap, is a concern in the policy agenda since the effects from extreme



heat span from increased morbidity and hospitalisations to mental health issues, adverse pregnancy and birth outcomes, increased healthcare costs and political instability. For instance, recent evidence finds that heat extremes are related to increased mental health-related hospital admissions (Hayward and Ayeb-Karlsson, 2021<sup>[71]</sup>) and suicide rates (Burke et al., 2018<sup>[72]</sup>). For example, suicide rates rose 0.7% and 2.1% respectively for a 1°C increase in monthly average temperatures in the United States counties and Mexican municipalities (Burke et al., 2018<sup>[72]</sup>), indicating the urgent need to address issues related to dangerous heat around the world.

The different climate-related hazards selected in this paper also suggest that certain countries are more affected than others. For example, the indicator for extreme precipitation shows countries where considerable impacts are observed for extreme precipitation, suggesting that early-warning policies for extreme precipitation may be important in these countries. Each year severe events are well forecasted but a gap between forecasting and warnings of hydro-meteorological events results in casualties and significant damage to property and infrastructure (WMO, 2015<sup>[73]</sup>). In addition, significant gaps exist in the international exchange of observations on hydro-meteorological events, particularly in Least Developed Countries and Small Island Developing States (SIDS) (WMO, 2021<sup>[74]</sup>). In fact, Latin America and Africa are among the regions least equipped with dense weather station networks in the world (WMO, 2021<sup>[74]</sup>), even though this paper shows that at least five countries in Central and South America experience an extreme number of days with very heavy precipitation.

## 6 Strengths and limitations

This paper proposes a methodology for assessing the hazard prevalence and exposure of people and assets (i.e. built-up areas, cropland, forests) to climate-related hazards on a national and subnational level. It uses data sources with high spatio-temporal resolution to assess the impact of climate-related hazards between countries and within countries.

It is important to highlight that there can be over- or under-estimations of the actual exposure to climate-related hazards. For example, the 2020 global land cover map with a 300 m spatial resolution has an evaluated accuracy of 70.5% on 1344 samples (Defourny et al., 2021<sup>[75]</sup>), while land cover maps with a 100 m spatial resolution have an overall mapping accuracy of just over 80% (80.6% in 2015, 80.3% in 2019) (Buchhorn et al., 2020<sup>[54]</sup>). This meets the statistical validation requirements according to the CEOS Land Product Validation but indicates that a degree of misclassification and differences between this data source and other data sources is likely, which may affect the results of exposure indicators that focus on croplands or forests.

This paper assesses wildfires through three hazard and exposure indicators (Table 4). This includes ex-ante and ex-post data sources to investigate areas that have burned and wildfire-prone areas. In addition, the data sources analysed allow filtering of fires by fire size, making it perfectly feasible to exclude 'small' fires that may be common in certain countries where managed burning is part of the cultural use and management of the landscape. However, the key underlying data of the Global Fire Atlas (i.e. the MODIS MCD614 product) has a pixel size of 25 ha (500 m spatial resolution). Considering that very few managed fires exceed the size of 25 ha, these fire events mostly do not get mapped in the MODIS MCD614 product, strengthening the case that many of these 'prescribed' or 'managed' fires can be excluded for the indicators developed in this paper. Nonetheless, in some countries, larger 'managed' fires are possible such as in Australia and the United States. For example, savannah burning, which occurs in northern Australia, has a long history of indigenous use for land management stretching back for millennia. These practises have exposed ecosystems to frequent fires under such managed fire regimes and traditional land management, and are increasingly re-introduced for Australia's savannah fire management. These practices should be considered when interpreting the results since large 'managed' fires may not be excluded from the wildfire indicators for these countries. In addition, small wildfires, below the remote sensing product resolution, are not represented in this analysis.

# 7 Conclusions and next steps

This paper develops exposure indicators for selected climate-related natural hazards at the national and subnational levels and with global geographic coverage (results shown in this paper are limited to 52 IPAC countries, for ease of presentation). This is achieved by summarising observations at a high spatial and temporal resolution, and combining these with geospatial data sources describing populations, natural assets or built assets. Using global data sources enables the investigation and comparison of the exposure to climate-related hazards within a country and between countries.

Results show that a high proportion of the population in most IPAC countries is exposed to serious extreme heat conditions; this is alarming given that the number of days with extreme heat is expected to increase because of climate change. A majority of cropland in IPAC countries also experience a considerable number of days with above-average precipitation. However, only a small subset of IPAC countries' cropland is exposed to more than 7 days of above-average precipitation. With regards to wildfire, a small subset of countries accounts for the majority of burned area. For example, 20% of burned land globally occurred in ten IPAC countries between 2017 and 2021. Importantly, this empirical evidence is based on observed past conditions and is generally expected to worsen because of climate change.

In terms of possible future work, a similar methodology could be used to develop additional indicators, provided suitable hazard and asset data sources can be identified. The following additions could be explored in the future:

- ▶ **Other hazard types:** Extensions of existing indicators such as identifying more appropriate data sources for assessing forest exposure to drought or cropland exposure to extreme precipitation during the growing season. Other climate-related hazards currently not accounted for in this paper may also become increasingly relevant to monitor, such as lightning strikes, landslides, hailstorm or snowfall events, sea level rise or ocean acidification.
- ▶ **Other asset classes:** For example, % agricultural value added or employment exposed to extreme precipitation, % age groups or livestock exposed to heat stress; sensitive ecosystems, protected areas burned or exposed to wildfire; infrastructure exposed, or exposed GDP or Human Development Index (HDI).

The following directions could also be explored in subsequent work to further refine and expand on the work developed in this paper:

- ▶ **Articulate user needs:** Lack of suitable global data sources hinders the development of indicators for some climate-related hazards. In addition, certain existing data sources may not be ideal for assessing a climate-related hazard.
- ▶ **Vulnerability:** Fully characterising the associated risk would require to also consider vulnerability of the exposed people or assets. Pending the availability of suitable data on vulnerability, this task remains an option for future work. Related work is planned under EPOC's 2023-24 PWB on environmental justice, and related work is also envisaged for the IPAC Climate Action Dashboard.
- ▶ **Projections:** This paper focuses on historical data or hazard maps based on historical events. Exploring climate projection data by Representative Concentration Pathways (RCP) or Shared Socioeconomic Pathways (SSP) would enable to assess the exposure to climate-related hazards under different future scenarios.

# References

- Alfieri, L. et al. (2017), “Global projections of river flood risk in a warmer world”, *Earth’s Future*, Vol. 5/2, pp. 171-182, <https://doi.org/10.1002/2016ef000485>. [46]
- Armstrong, B. et al. (2019), “The Role of Humidity in Associations of High Temperature with Mortality: A Multicountry, Multicity Study”, *Environmental Health Perspectives*, Vol. 127/9, pp. 097007-1-097007-8, <https://doi.org/10.1289/EHP5430>. [77]
- Artés, T. et al. (2019), “A global wildfire dataset for the analysis of fire regimes and fire behaviour”, *Scientific Data*, Vol. 6/1, pp. 1-11, <https://doi.org/10.1038/s41597-019-0312-2>. [82]
- Badgley, G. et al. (2022), “Title California’s forest carbon offsets buffer pool is severely undercapitalized”, <https://doi.org/10.1101/2022.04.27.488938>. [41]
- Balch, J. et al. (2017), “Human-started wildfires expand the fire niche across the United States”, *Proceedings of the National Academy of Sciences of the United States of America*, Vol. 114/11, <https://doi.org/10.1073/pnas.1617394114>. [35]
- Birkmann, J. (2015), “Assessing the risk of loss and damage: exposure, vulnerability and risk to climate-related hazards for different country classifications”, *International Journal of Global Warming*, Vol. 8/2, pp. 191-212, <https://www.inderscienceonline.com/doi/pdf/10.1504/IJGW.2015.071963> (accessed on 2 November 2021). [60]
- Bowman, D. et al. (2020), “Vegetation fires in the Anthropocene”, *Nature Reviews Earth & Environment*, Vol. 1/10, pp. 500-515, <https://doi.org/10.1038/s43017-020-0085-3>. [36]
- Buchhorn, M. et al. (2020), *Copernicus Global Land Service: Land Cover 100m: Version 3 Globe 2015-2019: Product User Manual*, VITO, Geneve, [https://land.copernicus.eu/global/sites/cgls.vito.be/files/products/CGLOPS1\\_PUM\\_LC100m-V3\\_I3.4.pdf](https://land.copernicus.eu/global/sites/cgls.vito.be/files/products/CGLOPS1_PUM_LC100m-V3_I3.4.pdf) (accessed on 14 September 2021). [54]
- Burkart, K. et al. (2021), “Estimating the cause-specific relative risks of non-optimal temperature on daily mortality: a two-part modelling approach applied to the Global Burden of Disease Study”, *The Lancet*, Vol. 398/10301, [https://doi.org/10.1016/S0140-6736\(21\)01700-1](https://doi.org/10.1016/S0140-6736(21)01700-1). [3]
- Burke, M. et al. (2018), “Higher temperatures increase suicide rates in the United States and Mexico”, *Nature Climate Change*, Vol. 8/8, <https://doi.org/10.1038/s41558-018-0222-x>. [72]
- Burke, M., S. Hsiang and E. Miguel (2015), “Global non-linear effect of temperature on economic production”, *Nature*, Vol. 527/7577, pp. 235-239, <https://doi.org/10.1038/nature15725>. [17]

- Burke, M., S. Hsiang and E. Miguel (2015), “Global non-linear effect of temperature on economic production”, *Nature*, Vol. 527/7577, <https://doi.org/10.1038/nature15725>. [81]
- Butry, D., J. Prestemon and D. Thomas (2014), *Investigation of the decline in reported smoking-caused wildfires in the USA from 2000 to 2011*, <https://doi.org/10.1071/WF13146>. [38]
- Chen, C. et al. (2015), *University of Notre Dame Global Adaptation Index: Country Index Technical Report*, University of Notre Dame, <http://index.gain.org/about/reference>. (accessed on 19 July 2021). [15]
- Chikamoto, Y. et al. (2017), “Multi-year predictability of climate, drought, and wildfire in southwestern North America”, *Nature Scientific Reports*, Vol. 7/1, pp. 1-12, <https://doi.org/10.1038/s41598-017-06869-7>. [61]
- Climate Central and Surging Seas (2018), *Areas Vulnerable to Coastal Flooding & Sea Level Rise*. [50]
- Copernicus Climate Change Service (2021), *Changing the reference period from 1981-2020 to 1991-2020 for the C3S Climate Bulletin*, Copernicus Climate Change Service. [79]
- CRED (2019), *Natural Disasters 2019*, Centre for Research on the Epidemiology of Disasters, Brussels, [http://file:///C:/Users/Maes\\_M/Downloads/adsr\\_2019.pdf](http://file:///C:/Users/Maes_M/Downloads/adsr_2019.pdf) (accessed on 6 July 2021). [6]
- Cunha, A. et al. (2019), “Extreme Drought Events over Brazil from 2011 to 2019”, *Atmosphere*, Vol. 10/11, p. 642, <https://doi.org/10.3390/ATMOS10110642>. [65]
- Davies, I. et al. (2018), “The unequal vulnerability of communities of color to wildfire”, *PLoS ONE*, Vol. 13/11, <https://doi.org/10.1371/journal.pone.0205825>. [37]
- Defourny, P. et al. (2021), *Product User Guide Specification: ICDR Land Cover 2016-2020*, European Centre for Medium-Range Weather Forecasts. [75]
- Dorigo, W. et al. (2017), “ESA CCI Soil Moisture for improved Earth system understanding: State-of-the art and future directions”, *Remote Sensing of Environment*, Vol. 203, pp. 185-215, <https://doi.org/10.1016/J.RSE.2017.07.001>. [33]
- Dottori, F. et al. (2021), *River flood hazard maps for Europe and the Mediterranean Basin region*. European Commission, Joint Research Centre, European Commission, Joint Research Centre (JRC). [47]
- EEA (2021), *Europe’s changing climate hazards — an index-based interactive EEA report*, European Environment Agency, Copenhagen. [26]
- EFFIS (2019), *User Guide*, European Forest Fire Information System, <https://doi.org/10.24381/cds.0e89c522>. [88]
- ETC-CCA (2020), *Climate-related hazard indices for Europe*, European Topic Centre on Climate Change, Bologna, <https://www.eionet.europa.eu/etcs/etc-cca/products/etc-cca-reports/climate-related-hazard-indices-for-europe> (accessed on 30 June 2021). [9]
- European Commission (2021), *User Guide General description*, Copernicus Climate Change Service, <https://git.ecmwf.int/projects/CEMSF/repos/geff/browse>. [84]
- FAO (2021), *Statistical Yearbook 2021*, <https://doi.org/10.4060/cb4477en>. [56]

- FAO (2021), *The impact of disasters and crises on agriculture and food security: 2021*, Food and Agriculture Organization of the United Nations, Rome, <https://www.fao.org/3/cb3673en/cb3673en.pdf> (accessed on 19 June 2022). [31]
- FAO (2020), *The State of the World's Forests 2020. Forests, biodiversity and people*. [59]
- Felipe Galizia, L. et al. (2021), "Assessing the accuracy of remotely sensed fire datasets across the southwestern Mediterranean Basin", *Natural Hazards and Earth System Sciences*, Vol. 21/1, <https://doi.org/10.5194/nhess-21-73-2021>. [42]
- Field, R. (2020), "Evaluation of Global Fire Weather Database reanalysis and short-term forecast products", *Natural Hazards and Earth System Sciences*, Vol. 20/4, <https://doi.org/10.5194/nhess-20-1123-2020>. [44]
- Freire, S. et al. (2016), "Development of new open and free multi-temporal global population grids at 250 m resolution", *AGILE*, p. 6, [https://agile-online.org/conference\\_paper/cds/agile\\_2016/shortpapers/152\\_Paper\\_in\\_PDF.pdf](https://agile-online.org/conference_paper/cds/agile_2016/shortpapers/152_Paper_in_PDF.pdf) (accessed on 23 September 2021). [53]
- Global Network Against Food Crises (2022), *Global report on food crises: Joint analysis for better decisions*, Food Security Information Network, [https://docs.wfp.org/api/documents/WFP-0000138913/download/?\\_ga=2.206764691.1871800038.1655125518-95910970.1655125518](https://docs.wfp.org/api/documents/WFP-0000138913/download/?_ga=2.206764691.1871800038.1655125518-95910970.1655125518) (accessed on 13 June 2022). [45]
- Goldammer, J. et al. (2018), *GAW Report, 235. Vegetation Fire and Smoke Pollution Warning and Advisory System (VFSP-WAS): Concept Note and Expert Recommendations*, World Meteorological Organization. [43]
- Gruber, A. et al. (2019), "Evolution of the ESA CCI Soil Moisture climate data records and their underlying merging methodology", *Earth System Science Data*, Vol. 11/2, pp. 717-739, <https://doi.org/10.5194/ESSD-11-717-2019>. [34]
- Hayward, G. and S. Ayeb-Karlsson (2021), "'Seeing with Empty Eyes': a systems approach to understand climate change and mental health in Bangladesh", *Climatic Change*, Vol. 165/1-2, <https://doi.org/10.1007/s10584-021-03053-9>. [71]
- Head, K. et al. (2018), *Web Annex D: Report of the systematic review on the effect of indoor heat on health*, World Health Organization, Geneva, <http://apps.who.int/iris/bitstream/handle/10665/275842/WHO-CED-PHE-18.05-eng.pdf> (accessed on 26 October 2021). [19]
- Hersbach, H. et al. (2018), *ERA5 hourly data on single levels from 1979 to present. Copernicus Climate Change Service (C3S) Climate Data Store (CDS)*. [22]
- Hofste, R. et al. (2019), *Aqueduct 3.0: Updated Decision-Relevant Global Water Risk Indicators*, World Resources Institute, Washington, DC, <https://www.wri.org/publication/aqueduct-30>. (accessed on 1 May 2022). [51]
- Hsiang, S., K. Meng and M. Cane (2011), "Civil conflicts are associated with the global climate", *Nature*, Vol. 476/7361, <https://doi.org/10.1038/nature10311>. [80]

- IEA (2021), *Climate Resilience: Electricity Security 2021*, International Energy Agency, Paris, [66]  
[https://iea.blob.core.windows.net/assets/62c056f7-deed-4e3a-9a1f-a3ca8cc83813/Climate\\_Resilience.pdf](https://iea.blob.core.windows.net/assets/62c056f7-deed-4e3a-9a1f-a3ca8cc83813/Climate_Resilience.pdf) (accessed on 17 June 2022).
- IEA (2018), *The Future of Cooling – Analysis*. [70]
- IEA and CMCC (2022), *Weather for Energy Tracker*, <https://www.iea.org/articles/weather-for-energy-tracker> (accessed on 17 June 2022). [76]
- IPCC (2022), *Climate Change 2022: Impacts, Adaptation and Vulnerability*, Intergovernmental Panel on Climate Change, [2]  
[https://report.ipcc.ch/ar6wg2/pdf/IPCC\\_AR6\\_WGII\\_FinalDraft\\_FullReport.pdf](https://report.ipcc.ch/ar6wg2/pdf/IPCC_AR6_WGII_FinalDraft_FullReport.pdf) (accessed on 10 March 2022).
- IPCC (2021), *Climate Change 2021: The Physical Science Basis. Contribution of Working Group I to the Sixth Assessment Report of the Intergovernmental Panel on Climate Change*, Intergovernmental Panel on Climate Change, Geneva. [1]
- IPCC (2014), *Climate Change 2014: Impacts, Adaptation, and Vulnerability. Part A: Global and Sectoral Aspects. Contribution of Working Group II to the Fifth Assessment Report of the Intergovernmental Panel on Climate Change*, Intergovernmental Panel on Climate Change, Cambridge. [13]
- ISDR (2005), *Hyogo Framework for Action 2005 - 2015: Building the Resilience of Nations and Communities to Disasters*, International Strategy for Disaster Reduction, Hyogo, [14]  
<http://www.unisdr.org/wcdr> (accessed on 21 July 2021).
- Jay, O. et al. (2021), *Reducing the health effects of hot weather and heat extremes: from personal cooling strategies to green cities*, [https://doi.org/10.1016/S0140-6736\(21\)01209-5](https://doi.org/10.1016/S0140-6736(21)01209-5). [69]
- Kaplan, J. and K. Lau (2021), “The WGLC global gridded lightning climatology and time series”, *Earth System Science Data*, Vol. 13/7, pp. 3219-3237, <https://doi.org/10.5194/essd-13-3219-2021>. [89]
- Karl, T. et al. (2012), “U.S. Temperature and Drought: Recent Anomalies and Trends”, *Eos*, Vol. 93/47, pp. 473-474, [62]  
<https://agupubs.onlinelibrary.wiley.com/doi/pdfdirect/10.1029/2012EO470001> (accessed on 2 November 2021).
- Karl, T., N. Nicholls and A. Ghazi (1999), “CLIVAR/GCOS/WMO Workshop on Indices and Indicators for Climate Extremes Workshop Summary”, *Weather and Climate Extremes*, pp. 3-7, [https://doi.org/10.1007/978-94-015-9265-9\\_2](https://doi.org/10.1007/978-94-015-9265-9_2). [21]
- Kirchmeier-Young, M. and X. Zhang (2020), “Human influence has intensified extreme precipitation in North America.”, *Proceedings of the National Academy of Sciences of the United States of America*, Vol. 117/24, pp. 13308-13313, [23]  
<https://doi.org/10.1073/pnas.1921628117>.
- Leverkus, A. et al. (2022), “Tree planting goals must account for wildfires”, *Science*, Vol. 376/6593, pp. 588-589, <https://doi.org/10.1126/SCIENCE.ABP8259/ASSET/8308AAE6-8A6D-42AD-A9EF-C855E50B808C/ASSETS/IMAGES/LARGE/SCIENCE.ABP8259-F1.JPG>. [40]



- Limaye, V. et al. (2018), "Climate Change and Heat-Related Excess Mortality in the Eastern USA", *EcoHealth* 2018 15:3, Vol. 15/3, pp. 485-496, <https://doi.org/10.1007/S10393-018-1363-0>. [18]
- Littell, J. et al. (2016), "A review of the relationships between drought and forest fire in the United States", *Global Change Biology*, Vol. 22/7, pp. 2353-2369, <https://doi.org/10.1111/GCB.13275>. [63]
- Li, Y. et al. (2019), "Excessive rainfall leads to maize yield loss of a comparable magnitude to extreme drought in the United States", *Global Change Biology*, Vol. 25/7, <https://doi.org/10.1111/gcb.14628>. [24]
- Manzanas, R. et al. (2020), *Work Package 6 Deliverable 6.3 Report on the reliability and uncertainties associated with the (hindcast-type) seasonal forecasts of selected sectorial INDECIS indices Seasonal predictability of Fire Weather Index (INDECIS-ISD 128) components over Europe*. [83]
- Marin-Ferrer, M., L. Vernaccini and K. Poljansek (2017), *Index for Risk Management INFORM Concept and Methodology Report — Version 2017*, European Commission Joint Research Centre, Ispra. [10]
- Millard, P. and M. Chediak (2021), "Global Energy Crisis Comes to Drought-Stricken South America - Bloomberg", *Bloomberg Green*, <https://www.bloomberg.com/news/articles/2021-10-03/global-energy-crisis-comes-to-drought-stricken-south-america> (accessed on 2 November 2021). [67]
- Mora, C. et al. (2017), "Global risk of deadly heat", *Nature Climate Change*, Vol. 7, pp. 501-506, <https://doi.org/10.1038/NCLIMATE3322>. [68]
- Muis, S. et al. (2016), "A global reanalysis of storm surges and extreme sea levels", *Nature Communications*, Vol. 7/1, pp. 1-12, <https://doi.org/10.1038/ncomms11969>. [52]
- Munich RE (2022), *Hurricanes, cold waves, tornadoes: Weather disasters in USA dominate natural disaster losses in 2021*, <https://www.munichre.com/en/company/media-relations/media-information-and-corporate-news/media-information/2022/natural-disaster-losses-2021.html> (accessed on 10 June 2022). [4]
- OECD (2022), *OECD Regional Statistics*, OECD Publishing, Paris, <https://dx.doi.org/10.1787/region-data-en>. [57]
- OECD (2022), *Value added by activity (indicator)*, doi: 10.1787/a8b2bd2b-en (Accessed on 01 June 2022). [55]
- OECD (2021), *Adapting to a changing climate in the management of coastal zones*, Organisation for Economic Co-operation and Development, Paris, [https://www.oecd-ilibrary.org/environment/adapting-to-a-changing-climate-in-the-management-of-coastal-zones\\_b21083c5-en](https://www.oecd-ilibrary.org/environment/adapting-to-a-changing-climate-in-the-management-of-coastal-zones_b21083c5-en) (accessed on 2 February 2022). [48]
- OECD (2020), *Common Ground Between the Paris Agreement and the Sendai Framework : Climate Change Adaptation and Disaster Risk Reduction*, OECD Publishing, Paris, <https://dx.doi.org/10.1787/3edc8d09-en>. [7]
- OECD (2019), *Responding to Rising Seas: OECD Country Approaches to Tackling Coastal Risks*, OECD Publishing, Paris, <https://dx.doi.org/10.1787/9789264312487-en>. [49]



- OECD (2017), *Water Risk Hotspots for Agriculture*, OECD Studies on Water, OECD Publishing, Paris, <https://dx.doi.org/10.1787/9789264279551-en>. [30]
- OECD (2016), *Mitigating Droughts and Floods in Agriculture: Policy Lessons and Approaches*, OECD Studies on Water, OECD Publishing, Paris, <https://dx.doi.org/10.1787/9789264246744-en>. [29]
- Perkins, S. and L. Alexander (2013), "On the Measurement of Heat Waves", *Journal of Climate*, Vol. 26/13, pp. 4500-4517, <https://doi.org/10.1175/JCLI-D-12-00383.1>. [20]
- Pesaresi, M. et al. (2017), *Atlas of the Human Planet 2017: Global Exposure to Natural Hazards*, European Union. [87]
- Petroliagkis, T. and A. Alessandrini (2021), *Screening and Selecting Climate Change Impact Parameters as Potential Drivers of Migration*, JRC, <https://doi.org/10.2760/455010>. [25]
- Pivello, V. et al. (2021), "Understanding Brazil's catastrophic fires: Causes, consequences and policy needed to prevent future tragedies", *Perspectives in Ecology and Conservation*, Vol. 19/3, pp. 233-255, <https://doi.org/10.1016/J.PECON.2021.06.005>. [64]
- Price, C. (2009), "Will a drier climate result in more lightning?", *Atmospheric Research*, Vol. 91/2-4, pp. 479-484, <https://doi.org/10.1016/J.ATMOSRES.2008.05.016>. [90]
- Royal Commission (2020), *Interim observations*, Royal Commission into National Natural Disaster Arrangements, Canberra. [58]
- Simpson, N. et al. (2021), "A framework for complex climate change risk assessment", *One Earth*, Vol. 4/4, pp. 489-501, <https://doi.org/10.1016/J.ONEEAR.2021.03.005>. [11]
- So, Haya and Elias (2022), *Voluntary Registry Offsets Database*, Berkeley Carbon Trading Project, University of California, Berkeley. [39]
- Spawn, S. et al. (2020), "Harmonized global maps of above and belowground biomass carbon density in the year 2010", *Scientific Data*, Vol. 7/1, <https://doi.org/10.1038/s41597-020-0444-4>. [85]
- Spinoni, J., G. Naumann and J. Vogt (2017), "Pan-European seasonal trends and recent changes of drought frequency and severity", *Global and Planetary Change*, Vol. 148, pp. 113-130, <https://doi.org/10.1016/j.gloplacha.2016.11.013>. [5]
- The Lancet (2021), "Health in a world of extreme heat", *The Lancet*, Vol. 398/10301, p. 641, [https://doi.org/10.1016/S0140-6736\(21\)01860-2](https://doi.org/10.1016/S0140-6736(21)01860-2). [16]
- UNDRR (2020), *Hazard definition & classification review: Technical report*, United Nations Office for Disaster Risk Reduction, Geneva, [https://www.ria.ie/sites/default/files/undrr\\_hazard-report\\_digital.pdf](https://www.ria.ie/sites/default/files/undrr_hazard-report_digital.pdf) (accessed on 9 July 2021). [8]
- UNDRR (2019), *Global model of cyclone wind 50, 100, 250, 500 and 1000 years return period*, <https://data.humdata.org/dataset/cyclone-wind-100-years-return-period> (accessed on 7 June 2022). [86]
- UNDRR (2015), *Sendai Framework for Disaster Risk Reduction 2015 - 2030*, United Nations Office for Disaster Risk Reduction, New York. [12]

- Wang, W. et al. (2016), "Propagation of drought: From meteorological drought to agricultural and hydrological drought", *Advances in Meteorology*, Vol. 2016, pp. 1-5, <https://doi.org/10.1155/2016/6547209>. [28]
- WMO (2021), *Systematic Observations Financing Facility (SOFF): First Funders' Forum*, World Meteorological Organization, Geneva. [74]
- WMO (2017), *WMO Guidelines on the Calculation of Climate Normals*, World Meteorological Organization, Geneva. [78]
- WMO (2015), *WMO Guidelines on Multi-hazard Impact-based Forecast and Warning Services*, World Meteorological Organization, Geneva. [73]
- Zeri, M. et al. (2021), "Importance of including soil moisture in drought monitoring over the Brazilian semiarid region: An evaluation using the JULES model, in situ observations, and remote sensing", *Climate Resilience and Sustainability*, Vol. 1/1, <https://doi.org/10.1002/cli2.7>. [32]
- Ziese, M. et al. (2014), "The GPCC Drought Index-a new, combined and gridded global drought index", *Earth Syst. Sci. Data*, Vol. 6, pp. 285-295, <https://doi.org/10.5194/essd-6-285-2014>. [27]

## Annex A. Methods for each exposure indicator

This paper does all data processing and statistics to develop exposure indicators in QGIS 2.18.2, Google Earth Engine, Python 3.9.6 via jupyter notebook 6.4.3 and R 4.1.0 via Rstudio using the packages base, doParallel, foreach, gdalUtils, ggplot2, iterators, parallel, purrr, raster, rgdal, sf, sp and ncdf4. All source code to compute these indicators is stored on a Github repository and will be made available upon request.

### B.1. Interpolation of population grids

The GHSL population grids developed by the European Commission Joint Research Centre allow for the estimation of the residential population for target years 1975, 1990, 2000 and 2015 (Freire et al., 2016<sup>[53]</sup>). This is based on data from CIESIN GPWv4.10 and is further disaggregated from census or administrative units into grid cells with a spatial resolution of 250 m or 1 km, depending on the user need (Freire et al., 2016<sup>[53]</sup>). This paper uses the spatial raster dataset depicting the distribution of population, expressed as the number of people per grid cell at a resolution of 250 meters.

Since some of the hazard data sources have annual or monthly data between 1979 and 2021, it is desirable to have population data for all years between 1979 and 2021. However, the GHSL population grids are only available for 4 years as indicated earlier. For this reason, this paper linearly interpolates population data for those exposure indicators where hazard data is available on an annual or monthly level; this includes exposure indicators for extreme temperature, drought, wildfire and wind threats. Linear interpolation of population data is calculated as the below example:

$$POP_{2003} = POP_{2000} + 3 * \left( \frac{POP_{2005} - POP_{2000}}{2005 - 2000} \right)$$

Exposure indicators that include hazard data without a temporal component do not use population data that is linearly interpolated, except for the year 2020, which is based on linear interpolation from 2000 and 2015 population grids. All exposure indicators that use population grids after 2015 will be updated as soon as there is a GHSL release of the 2020 population grid.

### B.2. Percentage of population exposed to extreme temperatures

The Copernicus CDS temperature data (ERA5) is a global gridded product with a 0.25° spatial resolution (~ 27.75 km) containing per pixel information of daily minimum and maximum air temperature at 2 m above the land's surface from 1979 to present (Hersbach et al., 2018<sup>[22]</sup>). This data source is at the basis of OECD and IEA calculations for the development of indicators assessing the number of hot days, tropical nights, icing days, and indicators assessing changing temperatures based on a climatology (IEA and CMCC, 2022<sup>[76]</sup>).

This paper measures temperature extremes based on an absolute threshold through a variety of indices. It measures hot days where the maximum daily temperature exceeds 35°C, tropical nights where the daily minimum temperature exceeds 20°C and icing days where the daily maximum temperature is below 0°C. This paper also measures days experienced as a hot day and a tropical night based on the indices above to develop a combined indicator and identify days that are both hot during the day and night. Finally, this paper also develops a heat stress indicator that accounts for other meteorological variables such as

humidity. There is strong experimental evidence that physiologic stress from high temperatures is greater if humidity is higher; however, large epidemiological models have also found little association of humidity with mortality due to heat stress (Armstrong et al., 2019<sup>[77]</sup>). Nevertheless, this paper includes a fifth indicator based on an absolute threshold to assess intense heat-related events that include other atmospheric variables impacting the human body besides air temperature, i.e. wind, radiation, and humidity. This paper estimates heat stress using the Universal Thermal Climate Index (UTCI). A UTCI value between 32°C and 38°C is considered as strong heat stress, between 38°C and 46°C as very strong heat stress, and above 46°C as extreme heat stress. The UTCI is derived from the Copernicus CDS ERA5 thermal comfort reanalysis (ERA5-HEAT) which provides hourly UTCI since 1979 at a 0.25° spatial resolution (Hersbach et al., 2018<sup>[22]</sup>). A population-weighted average is computed on the number of days per year associated to each heat stress level (strong, very strong, and extreme) using the Global Human Settlement population grids. To estimate the change over time in population exposure to heat stress, this paper compares the average number of days per year corresponding to the different heat stress levels in the last 5 years with the reference period (1981-2010).

This paper also measures temperature extremes based on a relative threshold by assessing temperature changes compared to the reference period (1981-2010). The core aim is to analyse changing temperature over time. For this reason, the paper selects a reference period from 1981 to 2010, which follows WMO guidelines for calculating the standard climatological normal (WMO, 2017<sup>[78]</sup>). The WMO recommends using a rolling 30-year period, updated every 10 years. The WMO recommends using a historical base period (1961-1990) for assessing climate change, as well as the most recent 30-year period, in order to standardise and harmonise across institutions. The commonly adopted 1961-1990 period begins before satellites data was commonly used and thus most datasets do not go back that far in time, including the Copernicus CDS temperature data used in this paper. For this reason, this paper uses the base period from 1981 to 2010. However, since the beginning of 2021, the recommended reference period changed from 1981-2010 to 1991-2020 more recently (WMO, 2017<sup>[78]</sup>) (Copernicus Climate Change Service, 2021<sup>[79]</sup>) but this is not used in this paper because the core aim is to analyse changing temperatures over time as indicated earlier.

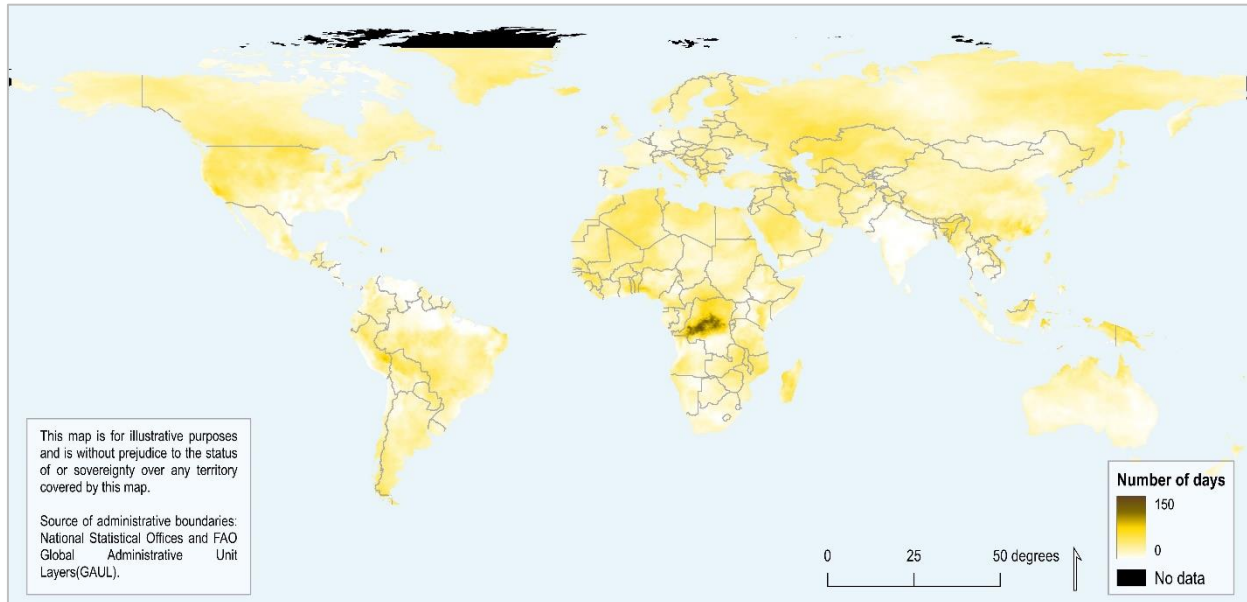
The paper measures days with extreme heat by calculating extremely hot days where the daily maximum temperature<sup>6</sup> exceeds the 95<sup>th</sup> percentile of daily maximum temperature over the whole reference period (i.e. 1981-2010) for a given country (Figure A.1). Similarly, this paper measures days with extreme cold by calculating extremely cold days when the daily minimum temperature is below the 5<sup>th</sup> percentile of daily minimum temperature over the reference period (i.e. 1981-2010). Percentiles are computed on a monthly basis, accounting all days of a specified month in the reference period. As this typically translates into 900 data points per month, the use of a five-day window or other means for reducing the noise is not used here. The indicator thus accounts for seasonal temperature variability, as computing percentile thresholds with all days in the reference period would likely cancel extremely warm days in winter that would in absolute terms be less severe than an average summer day.

---

<sup>6</sup>Daily minimum temperatures and daily maximum temperatures refer to the variables 24 hour minimum and maximum, respectively.

### Figure A.1. Changing temperature extremes across the world

Annual number of days when the daily maximum temperature exceeds the 95<sup>th</sup> percentile of the reference period (1981-2010), 2021.



Note: Areas in high latitudes shown in black have no data.

Recent evidence also suggests that temperature fluctuations cause extreme temperature-related deaths beyond just heatwaves (Hsiang, Meng and Cane, 2011<sup>[80]</sup>) (Burke, Hsiang and Miguel, 2015<sup>[81]</sup>) (Burke et al., 2018<sup>[72]</sup>). For this reason, this paper chooses to measure the number of days with extreme heat and cold instead of extreme temperature waves such as heatwave to keep maximum granularity because the calculation of heatwaves excludes non-consecutive days with extreme heat.

The GHSL population grids developed by the European Commission Joint Research Centre (JRC) allows for the estimation of annual number of persons exposed to the number of days with extreme heat and cold (Freire et al., 2016<sup>[53]</sup>). This is a spatial raster dataset depicting the distribution of population, expressed as the number of people per grid cell at a resolution of 250 meters. By overlaying the analysed temperature data with the population grid data, this paper analyses population exposure to extreme temperature. Populations exposed to zero days of extreme heat and cold are excluded from further analysis in this paper. All data to develop this indicator is freely available online and all source code to compute this indicator is available upon request.

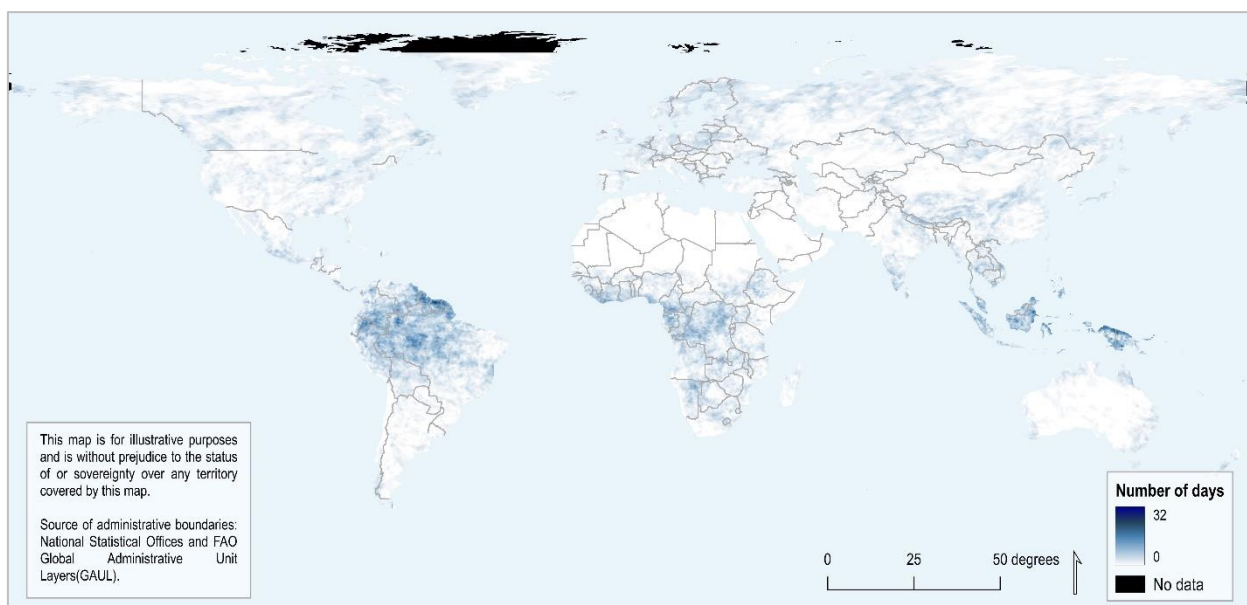
### B.3. Percentage of cropland exposed to extreme precipitation

To develop an exposure indicator for assessing extreme precipitation, this paper uses the Copernicus CDS precipitation data (ERA5), which is a global gridded product with a 0.25° spatial resolution (~ 27.75 km) containing per pixel information of hourly total precipitation amounts from 1979 to present (Hersbach et al., 2018<sup>[22]</sup>). Through OECD and IEA calculations, it measures precipitation extremes based on a relative threshold by assessing precipitation changes compared to the reference period from 1981 to 2010 (IEA and CMCC, 2022<sup>[76]</sup>). The core aim is to analyse the exposure of croplands to changing precipitation amounts, particularly days with extreme precipitation events. To do this, this paper measures the total number of days in a given year where the total daily precipitation amount exceeds the 99<sup>th</sup> percentile of daily precipitation values over the whole reference period (1981-2010) for a given country. Using the 99<sup>th</sup>

percentile instead of a 95<sup>th</sup> percentile allows identifying particularly heavy precipitation events (ca. 4 times per year) and is consistent with the EEA's methodology for assessing the frequency of extreme precipitation events (EEA, 2021<sup>[26]</sup>). Unlike a monthly-approach for extreme temperature, percentiles are computed using all wet days of the reference period (i.e. 1981-2010) because the data sample would otherwise be too small to robustly compute seasonally adjusted percentiles. It defines a wet day as a day where total precipitation is above or equal to 1 mm. Since percentiles are computed using all wet days of the reference period in a given location, this implies a different occurrence frequency between different locations.

### Figure A.2. Changing precipitation extremes across the world

Annual number of days when the total precipitation amount exceeds the 99<sup>th</sup> percentile of the reference period (1981-2010), 2021.



Note: Areas in high latitudes shown in black have no data.

The Copernicus CDS global land cover data allows identifying global cropland cover at 300 m spatial resolution from 1992 to present with a one year delay (Defourny et al., 2021<sup>[75]</sup>). By overlaying the analysed precipitation data with the global cropland data, this paper measures the percentage of cropland exposed to extreme precipitation in days and week categories. All data to develop this indicator is freely available online and all source code to compute this indicator is available upon request.

### B.4. Cropland soil moisture anomaly

Water content in the superficial layers of the soil is important for water supply and vegetation health. Soil moisture anomaly is a suitable indicator for monitoring the intensity of agricultural droughts and shows similar performances in identifying droughts compared to the Standardized Precipitation Index (Zeri et al., 2021<sup>[32]</sup>). This paper measures agricultural droughts in terms of cropland soil moisture anomaly using the Copernicus CDS ERA5-Land monthly average data product. It is a global gridded product with a 0.1° spatial resolution (~ 11.1 km) from 1950 to present, and it provides land variables related to the energy and water cycles over several decades. It contains per pixel information of monthly average volume of water in the surface soil layer of 0 to 7 cm deep, expressed as m<sup>3</sup> water per m<sup>3</sup> soil (Dorigo et al., 2017<sup>[33]</sup>)



(Gruber et al., 2019<sup>[34]</sup>). This data source combines model data with global observations into a complete and consistent dataset and describes how wet or dry the soil is in its topmost layer, providing insights about local precipitation impacts and soil conditions.

To develop an indicator for cropland soil moisture anomaly, this paper omits any soil moisture grid cells not considered cropland. To assess cropland cover, it uses the Copernicus global land cover maps at 300 m spatial resolution for the years 2000 to present (currently available until 2020) (Defourny et al., 2021<sup>[75]</sup>). This paper considers the following land cover classes as cropland: (1) cropland, rainfed; (2) cropland irrigated or post-flooding; (3) mosaic cropland (>50%) / natural vegetation (tree, shrub, herbaceous cover) (<50%); and (4) mosaic natural vegetation (tree, shrub, herbaceous cover) (>50%) / cropland (<50%). Once soil moisture grid cells for each year are selected based on cropland land cover, it measures the cropland soil moisture anomaly based on the reference period (1981-2010) as used throughout the paper. All data to develop this indicator is freely available online and all source code to compute this indicator is available upon request.

## B.5. Wildfires and exposure to areas at very high risk of burning

National inventories of wildfire events exist in many countries, but they do not provide the global coverage and/or the extended record needed for the validation of a fire danger system at a global scale. Satellite observations can supply a valid alternative, especially as they cover remote areas where in-situ observations are sparse. Satellite data have been used to monitor biomass burning at regional and global scales for more than two decades, using algorithms that detect radiative emissions from active fires at the time of satellite overpass, and in the last decade by using burned area algorithms that directly map the spatial extent of the area affected by fires.

### ***Burned area extent***

The Global Wildfire Information System (GWIS) is a joint initiative of the Group on Earth Observations (GEO) and the EU Copernicus work programmes, and is supported by partner organisations and space agencies such as NASA. The GWIS GlobFire database provides information on the occurrence of wildfires (i.e. fire events) during a month or a year and is derived from the MCD64A1 burned area product captured through NASA's MODIS Terra and Aqua satellite system. Since the underlying MODIS MCD64A1 burned area product has a spatial resolution of 500 m (equivalent to a pixel area of 25 ha), it implies that smaller fire events (< 25 ha) are removed from the GlobFire database, indirectly excluding smaller fires such as controlled or prescribed burnings (Felipe Galizia et al., 2021<sup>[42]</sup>). This data source thus excludes small wildfires that may naturally occur or prescribed burnings that are kept small to prevent larger uncontrolled burnings. However, this does not exclude all prescribed fires. In large open territories of Australia and the USA, larger prescribed fires do occur. The GlobFire database defines fire events as a set of burned pixels that are connected within a 5-day window and that have not been burned over the 16 previous days (Artés et al., 2019<sup>[82]</sup>).

In this paper, burned area extent is measured by assessing the total amount of burned land compared to a country's size. Areas that burn twice or more in a given year are counted only once in the total burned area extent. This paper does not measure the total number of fire events because this is not robust over time. The detection of smaller wildfires is dependent on the availability and proper analysis of satellite imagery.

### ***Forest exposure to wildfire danger***

There are three widely used fire risk weather indices, the Canadian Fire Weather Index (FWI), the U.S. Forest Service National Fire-Danger Rating System and the Australian McArthur Mk5 Forest Fire Danger Meter. To assess the risk of wildfires or fire danger, the Fire Weather Index (FWI) System is a meteorologically based index used worldwide for most jurisdictions around the world (Goldammer et al.,



2018<sup>[43]</sup> (Field, 2020<sup>[44]</sup>). The FWI System was developed in Canada and is composed of three moisture codes and three fire behaviour indices. The moisture codes capture the moisture content of three generalised fuel classes, while the behaviour indices reflect the spread rate, fuel consumption and intensity of a fire if it were to start. They are based on an exponential model of moisture exchange. The Fire Weather Index (FWI) is a dimensionless index rating the potential fire line intensity given the meteorological conditions in a reference fuel type (mature pine stands) and level terrain (Manzanas et al., 2020<sup>[83]</sup>). The system is designed to derive the maximum amount of information from the least amount of data and for this reason is easily adaptable to regions outside of Canada (European Commission, 2021<sup>[84]</sup>). The FWI System accounts for temperature, relative humidity, wind speed, and precipitation, each taken once a day at noon.

The Copernicus Land cover gridded maps from 1992 to present allow for the identification of exposed forest areas to areas with a very high (> 5) or extreme (> 6) fire danger based on the FWI Index (Defourny et al., 2021<sup>[75]</sup>).

### ***Population exposure to wildfire danger***

The Global Human Settlement Layer (GHSL) population grids developed by the European Commission's JRC allow for the estimation of the population count present in areas with a very high (> 5) or extreme (> 6) fire danger based on the FWI index. However, only using fire risk weather indices such as the FWI for assessing exposure of the population to wildfire is not good practise because these indices only account for meteorological conditions. Fuel or biomass availability is equally important because areas may have suitable fire conditions but no fuel availability for burning. Accounting for fuel or biomass availability besides meteorological indices is necessary to assess population exposure to wildfire.

Since there are no publicly available global biomass layers that are updated frequently, this paper accounts for fuel availability by calibrating the FWI Fire Danger Rating (FDR) using corresponding historical fire events, assuming frequent historical fire events indicate the presence of flammable fuel. In this paper, the GWIS GlobFire events provide historical data to calibrate the daily FDR as follows:

- ▶ As a preliminary step, the land cover classes (1) cropland, (2) forest, (3) grass and shrubland, (4) water bodies and wetlands and (5) Settlement from the Copernicus Land cover annual gridded maps are used to mask out non-vegetated areas from the daily FDR values ( $FDR_{d_{Q_i}}$ ) for each grid cell  $i$ . The subsequent calibration is applied for the remaining grid cells that were not removed from the daily FDR data.
- ▶ To stratify the vegetated cells, biomass carbon density percentile values are used as calibration parameters. Percentile values were derived from the temporally consistent harmonized global maps of aboveground biomass carbon density for the year 2010 at a 300-m spatial resolution. (Spawn et al., 2020<sup>[85]</sup>). Each cell ( $i$ ) of the daily FDR data is assigned a vegetation-specific carbon density percentile value based on the global distribution of aboveground carbon density (in units of megagrams of carbon per hectare ( $MgC\ ha^{-1}$ )).
- ▶ The GWIS GlobFire fire events data from 2000 to 2020 is used to estimate the likelihood of the stratified vegetated cells to actually burn. The bi-decadal fire events data is disaggregated into quarterly data to account for seasonal effects;
- ▶ For each quarter and grid cell, the number of fire events is measured to get the total number of fire events at a given location during a given quarter between 2000 and 2020;
- ▶ Each grid cell ( $i$ ) is assigned a percentile value for each quarter of the year based on the global quarterly historical distribution of fire events;
- ▶ The percentile value of each cell  $i$  is then further adjusted to account for the mean of (1)  $i$ 's percentile value and (2) the percentile values of  $i$ 's neighbouring cells ( $n=8$ ).

- ▶ Through this process, a quarterly fire ‘climatology’ layer is obtained;
- ▶ The daily FDR values ( $FDR_{d_{Qi}}$ ) for each grid cell  $i$  are calibrated by using these quarterly fire climatology layers to develop a calibrated FDR value ( $FDR'_{d_{Qi}}$ ) as follows:

$$FDR'_{d_{Qi}} = FDR_{d_{Qi}} \times biomass\_carbon\_density_{percentile} \times e^{percentile_{i,Qi}}$$

Calibrated FDR values above a value of 5 are then considered areas at very high risk of burning, accounting for both meteorological variables and calibration based on historical fire events. These areas with a very high risk of burning are then combined with annual population grid data from GHS-POP to estimate the percentage of population exposed to areas at risk of burning.

A key limitation associated with the use of historical wildfire data as a proxy for fuel availability is that wildfires that consume whole forest stands (stand replacing fires) have a recurrence interval between 30-300 years. However, in some regions, the recurrence interval may be shorter. Using historical wildfire data from the past 20 years, as done in this paper, may lead to the omission of certain high-risk areas.

### B.6. Percentage of population and buildings exposed to wind threats

The Copernicus ERA5 dataset provides hourly 10 m wind gust data (in m/s) at a 0.25° spatial resolution (~ 27.75 km) (Hersbach et al., 2018<sup>[22]</sup>). The NOAA wind threat scale allows for the classification of sustained wind speed data into different wind threat categories: (1) low wind threat (20-26 mph), (2) moderate wind threat (26-40 mph), (3) high wind threat (40-58 mph) (Table A.1). The Beaufort wind force scale also allows for the classification of wind threats. Sustained wind is slightly different from wind gusts. A wind gust is defined as the maximum value of the 3-second average wind speed, whereas sustained wind is the average wind speed over a two-minute period. This paper uses the threshold associated to violent storms on the Beaufort scale (64 mph, or 28.6 m/s) on the wind gust data to assess exposure to wind threats. Using the Copernicus wind gust data, an area is considered to be exposed to violent storms or worse if for at least one hour the 10 m wind gust speed is higher than 28.6 m/s.

**Table A.1. Wind scales**

Overlap between the National Oceanic and Atmospheric Administration (NOAA) wind threat scale and the Beaufort wind force scale

NOAA wind threat scale		Beaufort wind force scale		
Wind threat level	Wind speed (mph)	Beaufort class	Wind speed (m/s)	Wind speed (mph)
Extreme	> 57	Class 12: Hurricane	> 32.7	≥ 73
		Class 11: Violent storm	28.5 – 32.6	64 – 72
		Class 10: Storm, whole gale	24.5 – 28.4	55 – 63
High	40 - 57	Class 9: Strong gale	20.8 – 24.4	47 – 54
		Class 8: Fresh gale	17.2 – 20.7	39 – 46
Moderate	26 - 40	Class 7: Moderate gale	13.9 – 17.1	32 – 38
		Class 6: Strong breeze	10.8 – 13.8	25 – 31
Low	21 - 26	Class 5: Fresh breeze	8.0 – 10.7	19 – 24
Very low	20 - 21			
Non-threatening	< 20	Class 4: Moderate breeze	5.5 – 7.9	13 – 18
		Class 3: Gentle breeze	3.4 – 5.4	8 – 12
		Class 2: Light breeze	1.6 – 3.3	4 – 7
		Class 1: Light air	0.3 – 1.5	1 – 3
		Class 0: Calm	< 0.3	< 1

Note: The NOAA wind threat level scale is a scale used to assess the local threat of wind gusts. The modern version of the Beaufort wind force scale consists of 13 classes representing an empirical measure that relates wind speed to observed conditions at sea or on the land.

This paper assesses the exposure to cyclones using GAR 2015 cyclone hazard maps (UNDRR, 2019<sup>[86]</sup>). These maps show cyclone prone areas expressed in terms of wind gust (km/h) for different return periods (50, 100, 250, 500 and 1000 years). In this paper, the return period of 100 years is analysed. The Saffir-Simpson hurricane wind scale estimates hurricane potential property damage based on sustained wind speeds (Table A.2). As the cyclone hazard map shows wind gust speed, the values were readjusted to match the Saffir-Simpson hurricane wind scale by considering that wind gust speed is around 30% higher than sustained wind speed. This readjustment is consistent with the *Atlas of the Human Planet 2017* (Pesaresi et al., 2017<sup>[87]</sup>).

**Table A.2. Saffir-Simpson hurricane wind scale**

Category	Wind speed (m/s)	Wind speed (mph)	Damage intensity
Five	> 70	> 157	Very dangerous winds will produce some damage
Four	59 – 70	130 – 156	Extremely dangerous winds will cause extensive damage
Three	50 – 58	111 – 129	Devastating damage will occur
Two	43 – 49	96 – 110	Catastrophic damage will occur
One	33 – 42	74 – 95	Catastrophic damage will occur

The GHSL population grids developed by the European Commission JRC allows for the estimation of population exposed to wind threats (Freire et al., 2016<sup>[53]</sup>). Similarly, the Copernicus land cover maps allow for the identification of exposed built-up areas, as well as croplands and forests, from 1992 to present (Defourny et al., 2021<sup>[75]</sup>).

## B.7. River flooding

River floods exposure indicators were computed using JRC River Flood Hazard Maps for Europe and the Mediterranean Basin region, and for the World (Dottori et al., 2021<sup>[47]</sup>). The maps depict flood prone areas for river flood events for six different flood frequencies (from 1-in-10-years to 1-in-500-years). Cell values on these maps indicate the water depth (in m). For countries located in Europe and around the Mediterranean Basin, the regional flood hazard maps were used, as the spatial resolution is higher (100 m) than the global maps (1 km). For the remaining countries, the global maps were used. To get flood prone areas, a threshold of 1 cm was applied on the water depth.

Population exposure to river floods at different territorial levels was computed using the Global Human Settlement Layer Population grid linearly interpolated to 2020 based on 2000 and 2015. Built-up and cropland exposure was obtained using the Copernicus Land Cover gridded maps at 300 m resolution.

## B.8. Coastal flooding

Coastal flooding hazard and exposure indicators are developed using the World Bank Global Coastal Flood Hazard maps (Muis et al., 2016<sup>[52]</sup>). The maps present a global reanalysis of storm surges and extreme sea level events based on hydrodynamic modelling. The maps depict coastal flood hazard for nine different frequencies of occurrence (i.e. 2, 5, 10, 25, 50, 100, 250, 500, 1000-year return period). In this paper, exposure indicators for coastal flooding hazards are developed with a 10, 25, 50 and 100-year return period.

Annual values of the amount of land exposed to coastal flooding hazards is measured for each country. Since the coastal flooding hazard maps are not updated, only four values are developed for each country based on the four return periods selected.

The Copernicus Global Land Cover data allows identifying urban areas at a high spatial resolution of 300 m from 2000 to 2020 (Defourny et al., 2021<sup>[75]</sup>). This data source is updated yearly. This paper identifies built-up areas using the urban area classification within the Copernicus Global Land Cover data. By overlaying the coastal flooding hazard maps with the Copernicus urban area data, this paper calculate the percentage of built-up area exposed to coastal flooding hazards for each country between 2000 and 2020.

The GHSL population grids developed by the European Commission Joint Research Centre (JRC) allow for the estimation of the number of persons exposed to coastal flooding hazards per country (Freire et al., 2016<sup>[28]</sup>). The GHSL population grids are updated each epoch and are available for the years 1975, 1990, 2000 and 2015. By overlaying the coastal flooding hazard maps with the GHSL population grids, this paper calculates the percentage of the population exposed to coastal flooding hazards for each country in 1975, 1990, 2000 and 2015. A value for 2020 is developed based on the 2015 population grid, and this will be updated as soon as an updated population grid for 2020 is available. All data to develop this indicator is freely available online and all source code to compute this indicator is available upon request.

## Annex B. Key databases

**Table B.1. Key databases for global environmental data sources on climate-related natural hazards**

Overview of databases containing a variety of global environmental data sources relevant for assessing climate-related natural hazards

Source name	Description
<i>Global Historical Climatology Network (GHCN)</i>	The GHCN is a database of daily/monthly climate summaries from land surface stations. The GHCN contains records from over 100,000 stations in 180 countries and territories. Both the record length and period of record vary by station and cover intervals ranging from less than a year to more than 175 years.
<i>Global Precipitation Climatology Project (GPCP)</i>	The GPCP provides global mean precipitation as monthly means since 1979 and as daily means since 1996 using microwave imagers on polar orbiting satellites and infrared imagers on geostationary satellites.
<i>Global Drought Information System (GDIS)</i>	The GDIS contains several variables and indices useful for climate related hazards, including the Daily Standardised Precipitation Index, the Standardised Precipitation Index, ...
<i>World Resources Institute (WRI) Aqueduct tool</i>	The WRI Aqueduct tool contains a water risk atlas that maps and analyses current and future water risks across locations.
<i>Copernicus Climate Data Store (CDS)</i>	The CDS provides access to a wide range of climate datasets such as mean temperature, total precipitation or snow liquid water equivalent. It contains more than 100 climate variables with 30-km spatial resolution, one-hour temporal resolution and with a temporal coverage of 41 years.
<i>Copernicus Emergency Management Service (CEMS)</i>	The CEMS provides information for selected emergency situations that arise from natural and man-made disasters anywhere in the world. It includes the Global Flood Awareness System (GloFAS) that provides global river discharge data and the Global Drought Observatory that provides global data on drought risk.
<i>Global Wildfire Information System (GWIS)</i>	The GWIS provides data on fire regimes and effects at a global level, including fire danger forecasting, active fire detection and rapid damage assessments. This includes a set of modelled fire danger using historical weather forecasts to provide a complete historical reconstruction of meteorological conditions favourable to the start, spread and sustainability of fires from 1979 to the present (EFFIS, 2019 <sup>[88]</sup> ).
<i>Fire Information for Resource Management System (FIRMS) developed by NASA</i>	FIRMS detect active fires and thermal hotspots through satellite imagery from the Moderate Resolution Imaging Spectroradiometer [MODIS] and Visible Infrared Imaging Radiometer Suite [VIIRS]). It provides a comprehensive data source of active fires including volcanoes and gas flares, and is therefore different from other sources that are based on modelled forecasting.
<i>Global Fire Emissions Database (GFED)</i>	The GFED combines satellite data on fire activity and vegetation productivity to estimate monthly burned area and fire emissions globally from 19978 through to the present.
<i>Emergency Events Database (EM-DAT)</i>	EM-DAT is an international disaster database and contains core data on the occurrence and effects of more than 22,000 disasters in the world from 1900 until now. It covers disasters where more than ten (10) or more people were killed, affected hundred (100) or more people, led to declaration of a state of emergency or led to call for international assistance.
<i>World Wide Lightning Location Network (WWLLN) Global Lightning Climatology and time series (WGLC)</i>	The WWLLN / WGLC repository contains global lightning stroke density and stroke power calculated from georeferenced stroke count data.
<i>Weather for Energy Tracker developed by the International Energy Agency (IEA)</i>	The Weather for Energy Tracker showcases weather-related data useful to understand, analyse and model the energy sector. This includes, for example, data on temperature, precipitation and wind speed (IEA and CMCC, 2022 <sup>[76]</sup> ).
<i>International Best Track Archive for Climate Stewardship (IBTrACS)</i>	The IBTrACS provides a location for tropical cyclone position and intensity information. This includes information on maximum sustained wind speed (knots), minimum central pressure (millibars) and storm centre of circulation (degrees lat/long).
<i>FloodList database</i>	The FloodList database archives over 2,200 flood events from early 2016 to date at a daily and global scale

## Annex C. Excluded domains or subdomains

This section describes in more detail the (sub-)domains that are excluded from the analysis in this paper because (i) the (sub-)domain does not have any global data sources relevant to this analysis or (ii) the identified data sources for this (sub-)domain are not considered appropriate for developing an exposure indicator for the respective climate-related hazard. For example, this paper did not identify appropriate data sources for assessing landslides, with exception of the landslide event variable within the International Disaster database, which does not allow for the development of an exposure indicator for landslide events.

### C.1. Wet and dry

#### *Lightning*

Lightning is a risk to person and property and plays an important role in the Earth system. In addition, it is the key non-anthropogenic cause of wildfire ignitions (Kaplan and Lau, 2021<sup>[89]</sup>). Lightning activity is expected to change due to climate change (Price, 2009<sup>[90]</sup>).

The International Space Station (ISS) Science Data provides data on lightning and lightning density using the Lightning Imaging Sensor (LIS). It detects the distribution and variability of total lightning occurring in the Earth's tropical and subtropical regions but does not cover higher latitudes. The sensor, mounted on the orbiting space station, cannot detect lightning across the entire globe simultaneously. The LIS instrument makes measurements during both day and night with high detection efficiency.

The World Wide Lightning Location Network (WWLLN) provides a global dataset on lightning density, mean, median and standard deviation of stroke power through the Global Lightning Climatology gridded dataset. This data is available at 5 arc-min spatial resolution with daily and monthly temporal resolution from 2010 until 2020. The dataset is updated every year (Kaplan and Lau, 2021<sup>[89]</sup>) and appears to be better than other sensors at detecting lightning when lightning is rare (e.g. during cold seasons or in places with low overall density). This means that the technology behind WWLLN may be appropriate for producing a consistent picture of lightning that is not influenced by sensor proximity. In contrast to satellite-based lightning sensors, a key limitation of the WWLLN dataset is that it is not homogenous in time and space, including when it comes to variations in the density of the WWLLN sensor network.

#### *Landslides*

Landslides are an important climate-related hazard with consequences human settlements and health, resulting in potential environmental and economic damage and loss of human life. Landslides are often accompanied by heavy rains or droughts, which is why it is classified in this paper as part of the domain 'Wet and dry'. Landslides can develop when a mixture of water, rock, earth or other debris mixes in the ground. However, some landslides can also be the result of earthquakes or volcanic eruptions.

The International Disaster Database, also called EM-DAT database, records landslide events (e.g. avalanche of snow, debris, mudflow or rock fall). This data is not georeferenced but does contain the country, region and date of the landslide event. This data source could be used for the development of an estimation of the number of landslide events but is less useful for the development of an exposure indicator because the data is not georeferenced.

## C.2. Snow and ice

### *Snowfall*

Changes in snow conditions because of climate change are important for several sectors including water management and winter tourism. Snowfall is only relevant to particular OECD countries and data is often limited.

The liquid water equivalent (LWE) of snow is the amount of water it contains regardless of its depth or density. LWE reflects how deep the water in snow would be if melted. Thus, LWE allows for easier and more direct comparison between light and heavy snow. This measure gives information about the potential impact embedded by a given snow amount.

### *Hail storm*

Hail storms are damaging climate-related hazards, particularly for agriculture due to damage of crops, and damages to other vehicles, buildings and other infrastructures. Therefore, information on hail storms can be valuable to a wide range of applications.

The International Disaster Database, also called the EM-DAT database, records hail storm events. The category 'convective storm' has a subcategory relevant to hail storms. This data is not georeferenced, but does contain the country, region and date of the hail storm event. This data source could be used for the development of an estimation of the number of hail storm events but is less useful for the development of an exposure indicator because the data is not georeferenced.

## C.3. Oceanic

Climate-related hazards occurring on the coast are often interconnected with broader processes in the ocean (OECD, 2019<sup>[49]</sup>) (OECD, 2021<sup>[48]</sup>). This can include, for example, changes to sea surface temperature, ocean acidification, ocean heat content, ocean salinity and sea level. However, each of the climate-related hazards in oceans has different effects upon society and the economy. For example, changes in ocean sea level can have a direct impact on communities in low-lying coastal regions, while ocean acidification can impact coral reefs and other ocean habitats, resulting in changes in ocean productivity or tourism revenues. In addition, these climate-related hazards originate in oceans, and may not necessarily affect all OECD countries equally.

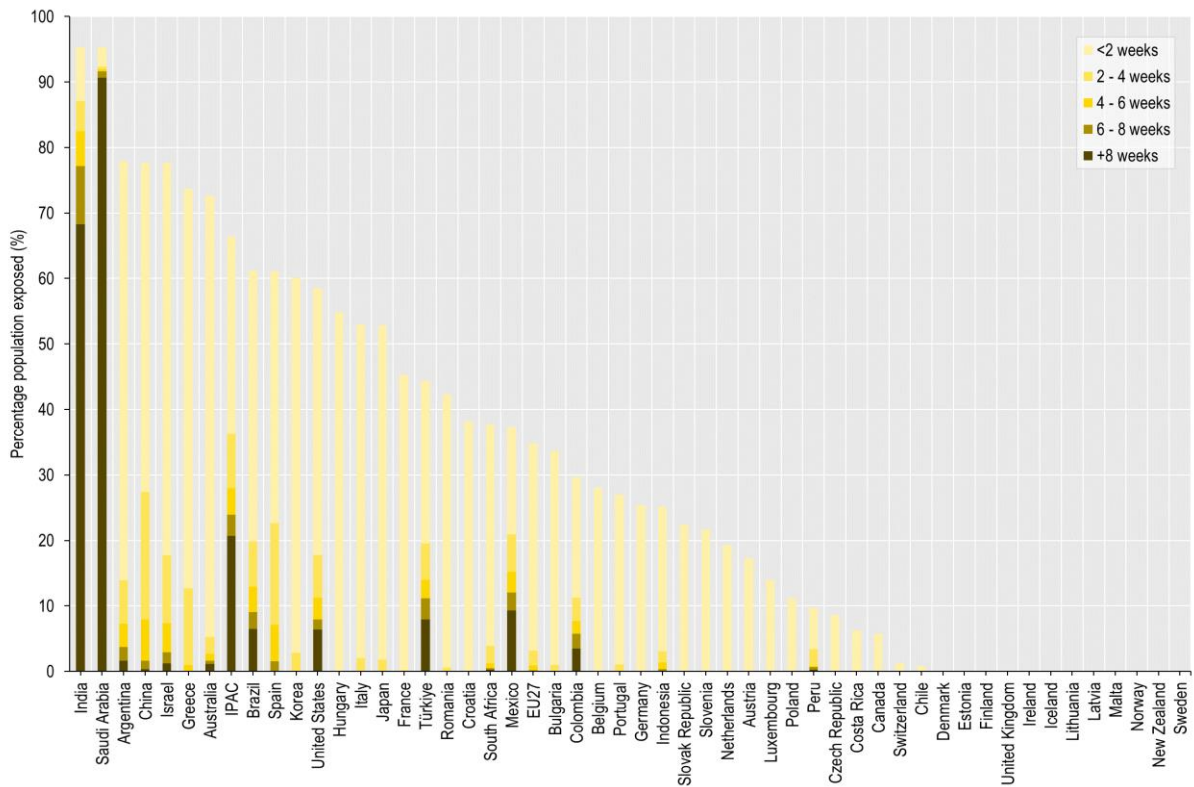
Despite an increasing availability of ocean data from platforms such as the Copernicus Marine Service and the NOAA, data coverage and issues with delineating administrative boundaries in oceans do not yet allow producing representative indicators in ways similar to those developed in this paper.



## Annex D. Additional figures

**Figure D.1. A majority of countries experience some exposure to hot days and tropical nights**

Percentage of population exposed to  $n$  number of days identified as a hot day ( $T_{max} > 35^{\circ}C$ ) and a tropical night ( $T_{min} > 20^{\circ}C$ ) over the years 2017-2021



Note: Countries are ranked according to the share of population exposed to any number of days identified both as a hot day and a tropical night. Further details on the methods are available in Annex A.